Charm Mixing ($D^0 \to K\pi$) With 9 fb^{-1}

Mark Mattson, Paul Karchin, Nagesh Kulkarni
Wayne State University, Detroit, MI
Satyajit Behari
John Hopkins, Baltimore, MD

CDF/ANAL/BOTTOM/CDFR/10914
Version 1.2

September 10, 2012

Abstract

We present a measurement of $R_{\mathcal{B}}(t)$, the time-dependent ratio of the branching fraction for the rare decay $D^0 \to K^+\pi^-$ to that for the Cabibbo-favored decay $D^0 \to K^-\pi^+$. The rare decay will be composed of the doubly Cabibbo suppressed D^0 decay, and $D^0 - \bar{D^0}$ mixing. If $R_{\mathcal{B}}$ changes as decay time increases, this is evidence for charm mixing. We present a method to get the decay time-binned ratio, which is fit to obtain the mixing parameters (R_D, y', x'^2). The results are compared to what is expected if there were no charm mixing, to set a limit on mixing or to make an observation.

This note describes the time-dependent measurement using Two Track Trigger data with 9 fb^{-1} marked good for B physics (in particular, the silicon and COT). We have over 7.7 million CF D^0 decays and 33 thousand DCS/mixing decays from D^* decays.

The best fit for the mixing parameters, assuming no CP violation, is $R_d = xx \pm x.xx(\times 10^{-3}), y' = xx \pm x.xx(\times 10^{-3})$, and $x'^2 = xx \pm x.xx(\times 10^{-3})$. The no-mixing point ($y' = x'^2 = 0$) is excluded with a significance equivalent to xx Gaussian standard deviations.

Contents

List of Figures

List of Tables

1 Introduction

This CDF note describes the analysis method used by the Wayne State University group to measure the mixing parameters for neutral charm meson oscillation, using all available data from Run II (up to period 38). Earlier stages of the analysis are described in the following notes:

- Note 7116 [1], the initial time-independent measurement with data set 0d (0.35 fb^{-1}). The analysis was blessed and resulted in a publication [2].
- Note 8879 [3], the initial time-dependent measurement with data sets 0d/0h/0i (1.5 fb^{-1}). The analysis was blessed and resulted in a publication [4].
- Note 9806 [5], an update of the time-dependent measurement using data up to period 21.

This document will describe the method and try to contain all the information from the previous studies. The blinded analysis method was blessed for the 1.5 fb^{-1} result,

1.1 Brief Theoretical Overview

Since the discovery of the charm quark in 1974, physicists have been searching for the mixing (or oscillation) of neutral charm mesons between particle and anti-particle states. The analogue process was discovered for kaons in 1962 and for B_d mesons in 1987. Charm mixing is so small that the first evidence was not seen until almost twenty years later, in 2006.

In the standard model, the decay $D^0 \to K^+\pi^-$ proceeds through a doubly Cabibbo-suppressed (DCS) tree diagram (see Fig. 1) and possibly through a "mixing" process in which the D^0 changes into a $\overline{D}^0$. (In this section, discussion of a decay reaction implicitly includes the charge conjugate process, unless otherwise noted.) The DCS decay rate depends on CKM factors as well as the magnitude of SU(3) flavor symmetry violation. Mixing may occur through two distinct types of second-order weak processes. In the first, shown in Fig. 2, the D^0 decays into a virtual ("long-range") intermediate state such as $\pi^+\pi^-$, which subsequently decays into a $\overline{D}^0$. The second type, shown in Fig. 3, is a short range process, with either a "box" or "penguin" topology. Short range mixing is negligible in the SM. However, exotic weakly interacting particles could enhance the short range mixing and provide a signature of new physics. Long-range processes can be much larger than short-range perturbative contributions, but are model-dependent.

Current results are consistent with standard model predictions. However, improving the experimental results will allow theorists to exclude certain models for long-range processes. There is still room for improvements in both experiment and theory precision, which will be necessary to see if they are actually in agreement (without new physics).

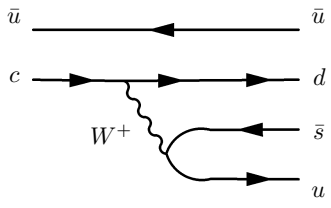

Figure 1: Feynman diagram for doubly- Cabibbo- suppressed decay.

1.2 D^0 Decay Mode

The experimental method we are exploring at CDF exploits the decay chain $D^{*+} \to D^0\pi^+$. The pion from the D^{*+} decay is called the *tagging* pion because its charge identifies the initial state of the neutral D meson as particle (D^0) or anti-particle ($\overline{D}^0$). The subsequent decay $D^0 \to K^-\pi^+$ is Cabibbo-favored (CF) and experimentally well established. We can also have a D^0 decay into $K^+\pi^-$,

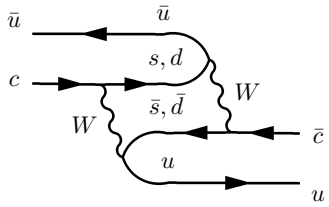

Figure 2: D^0 mixing through a virtual "long-range" intermediate state.

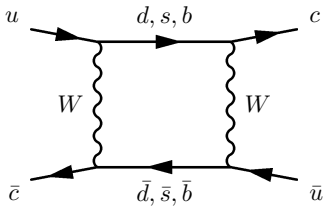

Figure 3: Highly suppressed standard model short-range D^0 mixing via a box diagram.

either by doubly Cabibbo-suppressed decay (DCS), or by mixing. For mixing, the D^0 oscillates to $\overline{D^0}$, and the $\overline{D^0}$ has a CF decay.

For this decay mode, the literature refers to "right-sign" (RS) and "wrong-sign" (WS) decays. For CF decays, the pions from the D^* and D^0 decays have the same charge, and are called right sign. For DCS and mixing decays, the pions have opposite charges, and are grouped as wrong sign.

The D^* tagging pion is also called the *slow pion* because its laboratory momentum is much less than that of the D^0 or $\overline{D}^0$. This kinematic property is a result of the small Q-value (145.4 MeV) of the D^{*+} decay. In the subsequent discussion, the term *right sign* will denote the Cabibbo favored decay, $D^0 \to K^-\pi^+$.

1.3 D^0 Decay Time Dependence

The current value for the charm mixing parameters is a little less than one percent, based on the HFAG fit using all appropriate D^0 decay modes. So we expect the neutral charm mesons to decay well before the time of one oscillation, in sharp contrast to B and K mixing. We can still look for variations in the time-dependece. The ratio $R(t)$ of wrong-sign to right-sign decay rates can be expressed [6] as a simple quadratic function of proper time t under the assumption of CP conservation and small values for the parameters x and y. The parameter R_D is the time-integrated rate of the direct DCS decay relative to the CF decay. The parameter x is defined in terms of the mass difference Δm between the heavy and light mass eigenstates and the parameter y involves the mass width difference $\Delta\Gamma$ between these eigenstates according to,

$$x = \Delta m/\Gamma \quad \text{and} \quad y = \Delta\Gamma/2\Gamma$$

where Γ is the average mass width of the mass eigenstates. Under the assumptions stated above,

$$R(t) = R_D + \sqrt{R_D}y't + \frac{x'^2 + y'^2}{4}t^2. \tag{1}$$

The parameters x' and y' are linear combinations of x and y according to the relations,

$$x' = x\cos\delta + y\sin\delta \quad \text{and} \quad y' = -x\sin\delta + y\cos\delta$$

where δ is a strong interaction phase. While we can't measure the charm mixing parameters directly, we can get information about the amplitude ($x'^2 + y'^2 = x^2 + y^2$). This can be used to exclude the no-mixing hypothesis ($x = y = 0$).

Table 1 summarizes the numerical values of x'^2 and y' provided by wrong sign hadronic decay channel analyses from the recent experiments.

Experiment	R_D (10^{-3})	y' $(10^{-}3)$	x'^2 (10^{-3})	Mixing significance
BaBar	3.03 ± 0.19	9.7 ± 5.4	-0.22 ± 0.37	3.9
Belle	3.64 ± 0.17	$0.6 \pm 4.0 \pm 3.9$	$0.18 \pm 0.21 \pm 0.23$	2.0
CDF (2007)	3.04 ± 0.55	8.5 ± 7.6	-0.12 ± 0.35	3.8

Table 1: Summary of three results from wrong sign hadronic decay channel.

1.4 Experimental Status

The initial CDF analysis resulted in a measurement [2] of R_B, the ratio of branching fractions of wrong-sign and right-sign decays,

$$R_{\mathcal{B}} = \mathcal{B}(D^0 \to K^+\pi^-)/\mathcal{B}(D^0 \to K^-\pi^+) \tag{2}$$

This ratio is given by the ratio of the time-integrals of the corresponding decay rates, yielding,

$$R_{\mathcal{B}} = R_D + \sqrt{R_D}y' + \frac{x'^2 + y'^2}{2}. \tag{3}$$

Thus $R_{\mathcal{B}}$ was sensitive to the three physics parameters R_D, x' and y', but does not provide a separate measure of them. Previous time-dependent measurements have been reported for R_D and had set limits on x'^2 and y'. At the time, experimental results were only precise enough to set upper limits.

At the Moriond Conference on March 13, 2007, the Belle [7] and BaBar [8] collaborations reported evidence for $D^0 - \overline{D}^0$ mixing, using different techniques. The results were published [9, 10].

BaBar saw a direct mixing signal using the same decay chain as studied here. So far, for this decay chain, Belle has reported only limits for x'^2 and y'. Thus, the BaBar evidence remained unconfirmed until the CDF publication with the time-dependent result [4].

It is also worth noting that the evidence for D^0 - $\bar{D}^0$ mixing presented by Belle is based on two methods, both different than the one discussed here for CDF and BaBar. One of the Belle methods is a comparison of the decay time distributions for D^0 to CP-eigenstates K^+K^- and $\pi^+\pi^-$ with the decay time distribution for D^0 to the CP-mixed state $K^-\pi^+$. They measure a non-zero value of y and hence indirect evidence of mixing.

The other method used by Belle is a time-dependent measurement of the Dalitz decay $D^0 \to K^0_s\pi^+\pi^-$ [11]. They report a preliminary non-zero value for x and a value for y consistent with zero. The non-zero value for x constitutes direct evidence for mixing. BaBar confirmed Belle's results [12] shortly after CDF provided the first confirmation of either experiments results.

The $D - \overline{D}$ mixing is now fairly established. The HFAG group has combined all charm meson decays and experimental results, including earlier results by CLEO [13] and FOCUS [14], to determine the world average [15]. As of 2010, the overall fit excludes the no-mixing hypothesis at the 10 sigma level. However, no single result has reached the level of observation (5σ).

1.5 General Notes On This Analysis

One adventage for this analysis is that all RS and WS signal events start as a D^*, and involve a decay of D^0 to $K\pi$. We are not comparing particles of different mass or different final states. We do not have to worry about relating two different triggers, for example.

CDF has a substantial number of CF D^0 and D^*, with relatively little background. Fig. 4 shows the $K\pi$ mass distribution. With looser cuts, the number of D^* would be around 16 million. We decided to use the CF D^* to determine mass and other kinematic distributions.

Other than the decay time distribution, the WS D^* should have the same kinematic distributions as the RS D^*. Both decays involve a particle with the same mass decaying into a kaon and pion. We are assuming no CP violation for this measurement. We are including the charge-conjugate decay for both RS and WS. The only way the WS distributions would be different from the RS distributions is if there are differences between the particle and anti-particle distributions. This would cause problems with virtually every CDF analysis (including this one), and there is no evidence that such a problem exists. (There are subtle differences in the detector efficiency that result in a negligible systematic error, as described later.)

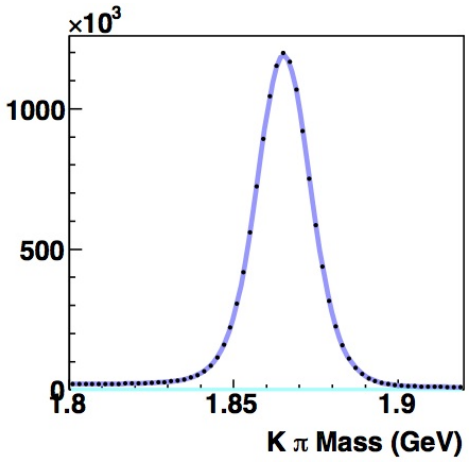

Figure 4: Right-sign D^0 mass distribution. This plot is for illustrative purposes only. Events are required to pass all basic selection criteria (see section 2.5) and have a mass difference consistent with a D^*. Black dots are data. The light blue line (near the x-axis) is the background fit. The dark blue line is signal + background.

We do not make a decay time fit for the RS and WS samples separately, only with the ratio WS/RS. There are many systematic effects which will cancel in the ratio.

We avoided using Monte Carlo directly for most this analysis, as we can use the very clean CF D^* sample. It would be prohibitive to make a full (PYTHIA) MC sample several times larger than our data sample, which is the most common use for MC. We have used a full MC sample generated by another charm analysis (see http://www-cdf.fnal.gov/ dicanto/internal/bmc.html), as a guide for the general behavior of partially reconstructed charm. We have also made toy MC of the mass distributions, to test alternative background and signal models.

The basic ideas for this analysis method had not changed since the last publication and blessing, but the CDF B-Group membership has. We had previously aimed to update the analysis with more data (up to period 21), but members unfamiliar with the previous blessing were confused when we described what had changed (without going into the details of the previous blessed analysis). There were also requests for more checks and validations.

2 Data Sample

This section describes the data being used for this analysis, including selection and cuts applied. Basically, what was done before the first mass plots were made.

For convenience, we want to define a few quantities which will be used later.

- Decay length significance for a particle is defined as

$$L_{xy} = \frac{\vec{r} \cdot \vec{P_T}}{P_T}$$

  where **r** is the distance between the primary and D^0 vertex and P_T is the transverse momentum vector of the D^0. In our analysis we sometimes use decay length significance L_{xy}/σ_{xy}, where σ_{xy} is the uncertainty on L_{xy}.

- Impact parameter for a particle is related to the distance of the closest approach from the primary vertex in the transverse plane and is defined as

$$d_0 = \frac{\hat{z} \cdot (\vec{r} \times \vec{P_T})}{P_T}$$

  where $\hat{z}$ is the unit vector along z-axis.

- Mass difference (ΔM) is the difference in the mass between the D^* candidate and the D^0 and π^* candidates

$$\Delta M = M_{K\pi\pi^*} - M_{K\pi} - M_{\pi^*}$$

  The use of π^* is to distinguish between the soft momentum pion used to form the D^* candidate, and the trigger track pion used to form the D^0 candidate. The mass difference is used instead of the D^* mass because many of the detector uncertainties will cancel when subtracting the D^0 mass, resulting in a narrower mass (difference) peak.

2.1 CDF Detector

The detector components relevant to this analysis are the silicon vertex detector (SVX), Intermediate Silicon Layer (ISL), silicon Layer zero (L00), and the drift chamber (COT) surrounded by a superconducting magnet producing a magnetic field of 1.4 T. These components together provide the physics quantities required to reconstruct wrong sign and right sign events. The other detector parts, like the silicon vertex tracker (SVT), Extremely fast tracker (XFT), and Cherenkov luminosity counter (CLC), were used during online data taking, but do not directly affect how we reconstruct the events.

2.2 Data Sets

Table 2 lists the "hadronic" data sets we are using from the Bstntuple area. For comparison with other CDF analyses, we will quote an integrated luminosity of 9.3 fb^{-1} for this data set, which is the value quoted by the analysis for CPV asymmetries with charmless bottom hadrons [16]. The initial time-independent result used period 0 data only. The previous blessed result (CDF note 8879) used data up to period 10. The previous CDF note (9806) went to period 21.

The two track trigger is described in other CDF notes, but key points will be repeated here. The data were collected by a three-level trigger system, aimed at selecting detached heavy flavor decays with at least two decay tracks. At level 1, COT tracks are reconstructed in the transverse plane by a hardware processor (XFT). Two opposite-charge particles are required, with reconstructed transverse momenta $p_T(1), p_T(2) > 2GeV/c$, the scalar sum $p_T(1) + p_T(2) > 5.5GeV/c$, and an azimuthal opening-angle $\Delta\varphi < 135°$. At level 2, the silicon vertex trigger (SVT) [18] combines XFT tracks with SVX hits to measure the impact parameter d_0 (distance of closest approach to the beam line) of each track with 45 μm resolution. The requirement of two tracks with $0.1 < d_0 < 1.0$ mm reduces the light-quark background by two orders of magnitude while preserving about half of the signal. A tighter opening-angle requirement, $20° < \Delta\varphi < 135°$, preferentially selects twobody B decays over multibody decays with 97% efficiency and further reduces background. Each track pair is then used to form a heavy flavor candidate, which is required to have an impact parameter $d_0(B) < 140\mu$m and

Data set	Periods	Run range	Dates	Name
hadr-80/xbhdid	0	138425-186598	2002.02.09-2004.08.22	x0d
cdfpbnt/xbhdih	1-4	190697-203799	2004.12.16-2005.09.04	x0h
cdfpbnt/xbhdii	5-10	203819-233111	2005.09.05-2007.01.30	x0i
cdfpbnt/xbhdij	11-13	233133-246231	2007.01.30-2007.05.13	x0j
cdfpbnt/xbhdik	14-17	252836-261005	2007.11.04-2008.04.16	x0k
cdfpbnt/xbhdfm	18-28	261119-289197	2008.04.18-2010.02.25	x0m
cdfpbnt/xbhdfp	29-38	289273-312510	2010.02.25-2011.09.30	x0p

Table 2: Bstntuple "hadronic" data sets and corresponding date ranges.

to have travelled a distance $L_{xy} > 200\mu$m in the transverse plane. At level 3, an array of computers confirms the selection with a full event reconstruction.

For the blessing of the 1.5/fb result the B-Group agreed with us that the trigger (and specifically "volunteers") will not affect our WS/RS ratio, except for K+/K- and pi+/pi- detector efficiency (which we include as a systematic error calculation later) and any volunteers that involve the third track (soft pion) passing the trigger. We will later impose a cut on the soft track p_T to remove this possibility. (We don't have the full conversation handy, but do have an e-mail by Kevin Pitts where he mentions, "Provided that the kinematics of the RS and WS decays are identical, I don't immediately see another way in which volunteers can bias your analysis.") This is largely due to our signals including the charge conjugate decay, the identical kinematics of RS and WS D^*, and using the ratio.

2.3 Ntuples

To speed up processing, we are using the BStNtuple files [17]. These are the B-Physics ntuples built from the production StNtuples, with an emphasis on quantities used in heavy flavor physics analyses. The BStNtuple files provide a common track reconstruction and vertexing for all heavy flavor analyses, but we still need to make our own ntuple files with quantities specific to this analysis. The procedures to generate the local tuples are listed on an internal CDF web page (MarkMattson/analysis).

We select the "$B \to \pi\pi$" block. This makes a vertex from the oppositely charged TTT trigger tracks. The events in this block are required to have the decay vertex with $L_{xy}/\sigma_{xy} > 4$, but there is no mass selection. All available D^0s will be in the BStNtuple files, after changing the two tracks to be $K\pi$. For the two tracks that form the B candidate, we try both $K\pi$ and πK particle assignments for the tracks. If the two-track mass is within the range 1.78-1.95 GeV/c^2 for either interpretation, that candidate is accepted as a possible D^0. The "pion" track block is used to get extra pions, which are combined with the D^0 candidate to form a D^* candidate. The mass difference ($\Delta m = m_{K\pi\pi^*} - m_{K\pi} - m_{\pi^*}$) can be anywhere from 0 - 2 GeV, for a D^0 and any random pion in the event. We only retain candidates with $\Delta m < 40$ MeV, which will retain all possible D^* decays, and provide enough sideband events to observe the background distribution. These mass windows are deliberately wide, in case we wanted to make changes after the ntuples were processed. In practice, we only look at (RS or WS) $K\pi$ mass from 1.80 - 1.92 GeV, and ΔM below 30 MeV.

At the time we started this analysis, the BStNtuple had reconstructions for D^0 and D^*, which we could not use as the selections were for RS D^*, which are biased against WS D^*. It was pointed out that the $B \to \pi\pi$ block would contain all the D^0 that we were looking for, and could be used to make the RS and WS D^*.

These are the older "v80" tuples. For future studies, such as measuring CP violation, we are considering switching to the "v90" tuples, which will be ready for winter 2012 analyses. The good run list (v31) selection was applied after the ntuples were written to disk.

Table 3 lists the approximate number of RS D^0 found in each data set, using a simple time-integrated $K\pi$ fit. This is not used in the analysis, but was part of the checks that the code was running correctly. For the 0p set, about 35 out of 108 CAF jobs failed. Since they were clustered together, the likely explanation is a problem with some CAF nodes on the day it was running. We are considering working on recovering those events, but that process was complicated by a computer hard disk failure that had the working ntuple-generating code.

Fig. **??** shows the p_T and d_0 of the trigger tracks, and L_{xy} of the D^0.

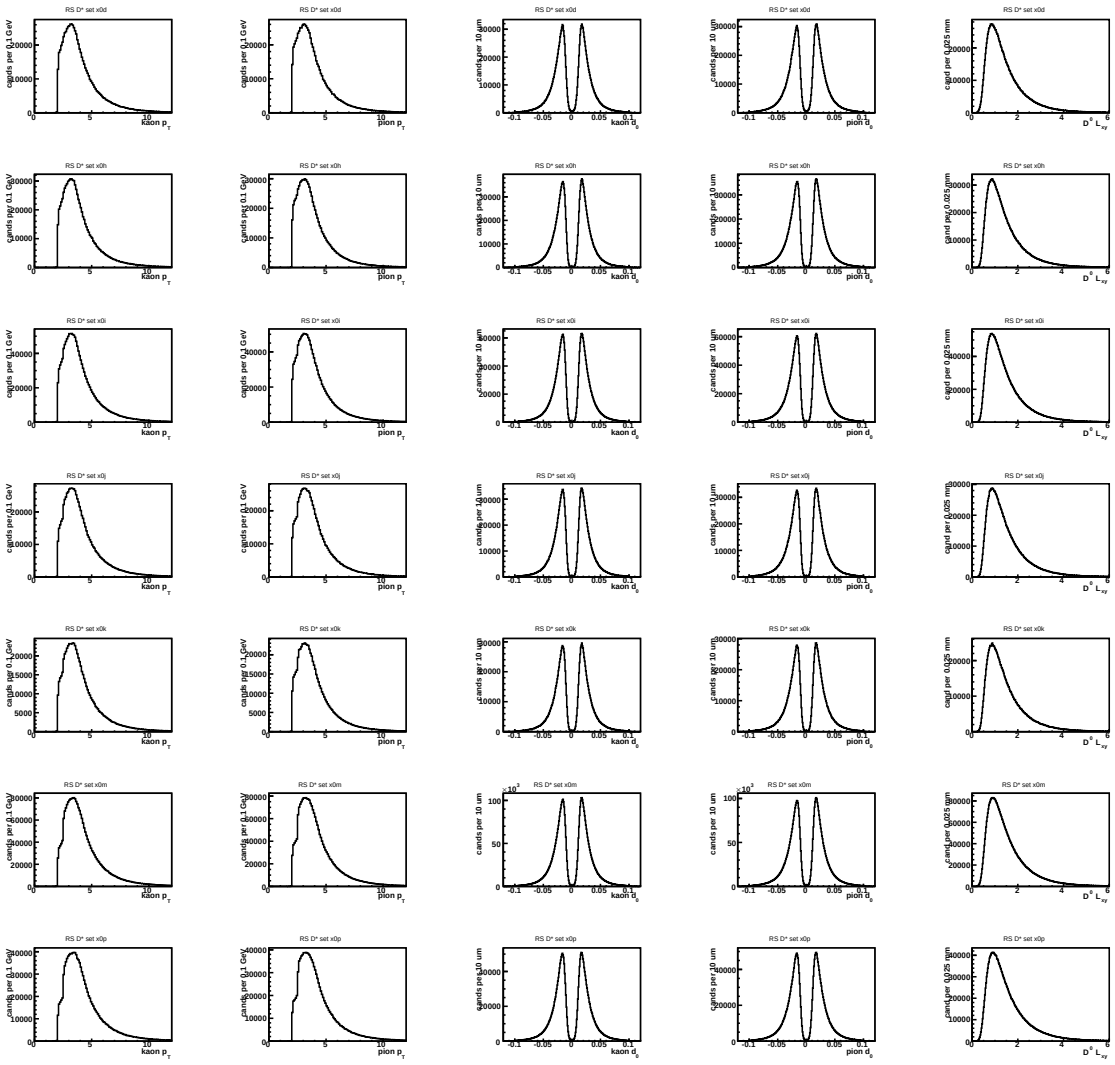

Figure 5: Variables from the BStNtuples
The p_T and d_0 of the trigger tracks, and L_{xy} of the D^0, from the post-processed BStNtuple output. A cut on the (RS) $K\pi$ mass and the mass difference, consistent with being a D*, is used to reduce background. Left to right: kaon p_T, pion p_T, kaon d_0, pion d_0, and L_{xy}. Top to bottom: set x0d, x0h, x0i, x0j, x0k, x0m, x0p. (The PDF figures can be zoomed in, to be read.)

Data set	Luminosity (fb^{-1})	D^0 (millions)
x0d	0.38	1.5
x0h	0.39	1.7
x0i	0.87	3.0
x0j	0.40	1.6
x0k	0.50	1.4
x0m	3.19	5.1
x0p	3.14	2.5

Table 3: Approximate D^0 yield per data set, from the BStNtuples. The luminosity is the online value for "all good". Since this analysis does not use the calorimeter or the muon detectors, this is only to set a scale for the size of the sets.

2.4 Signals and Backgrounds

Before describing the additional selection cuts used for this analysis, it is useful to give an overview of the classes of events that will be important for this analysis:

- Prompt D^* (signal) - RS or WS D^* that are produced at the primary vertex. The D^* signal peaks at 5.85 MeV in the mass difference, and 1.8645 GeV for $K\pi$ mass (PDG values).
- "B-decay" D^* (signal) - D^* that are produced at a secondary vertex. We expect these to come from B-decays. These are still potentially good D^*, but will have the wrong decay length (unless the primary vertex is not used). On the order of 10% of the RS D^* are from B decays. These candidates will have a different impact parameter (d_0) distribution compared to prompt D^*.
- D^0 plus random pion - A correctly reconstructed D^0 combined with an unassociated pion to get a fake D^* tag. This will form a D^0 peak in the $K\pi$ fits, but have a broad distribution for the mass difference.
- D^0 misidentification - A real D^0 decay where the kaon and pion assignments are swapped (double particle misidentification). The mass distribution in the $K\pi$ plot is about 10x wider than for correctly reconstructed D^0.
- Single misidentification - A real $D^0 \to KK$ or $\pi\pi$ decay which has one of the tracks misidentified, to form a $K\pi$ candidate. Those candidates will have a $K\pi$ mass that is low for both RS and WS interpretations, or high for both.
- Other charm decays - Other D^0 decay modes that might fall in our $K\pi$ mass window.
- Combinatorial background - Candidates formed from a random selection of tracks, which happens to pass our selection criteria. This is a well understood phenomena in any physics analysis. The mass plots from this background are featureless (beyond statistical fluctuations), and the $K\pi$ distribution can be modeled by a linear or simple polynomial fit.

Figure 6 shows candidates plotted with both RS and WS interpretations, from a very early study with a small sample of x0d events. The real RS D^0s, which appear as a broad distribution along the WS axis, dominate the plot. The plot also has clustering of events in the high mass (upper right) and low mass (lower left) regions. These are due to $D^0 \to KK, \pi\pi$ events. When transforming the data candidates into those mass plots, peaks at the D^0 mass are clearly shown, as seen in figure 7. These candidates are distinct from both the RS and WS $K\pi$ signal. Excluding these events is the primary reason for restricting the $K\pi$ mass range to 1.80-1.92 GeV. An additional complication below 1.80 GeV are charm decays involving π^0, which adds more complications in attempts to fit in that region.

2.5 Basic Selection Cuts

We apply some modest selection cuts, to reduce the combinatoric background slightly. Since they affect RS and WS events equally, there is no systematic effect on the ratio. There will be selections

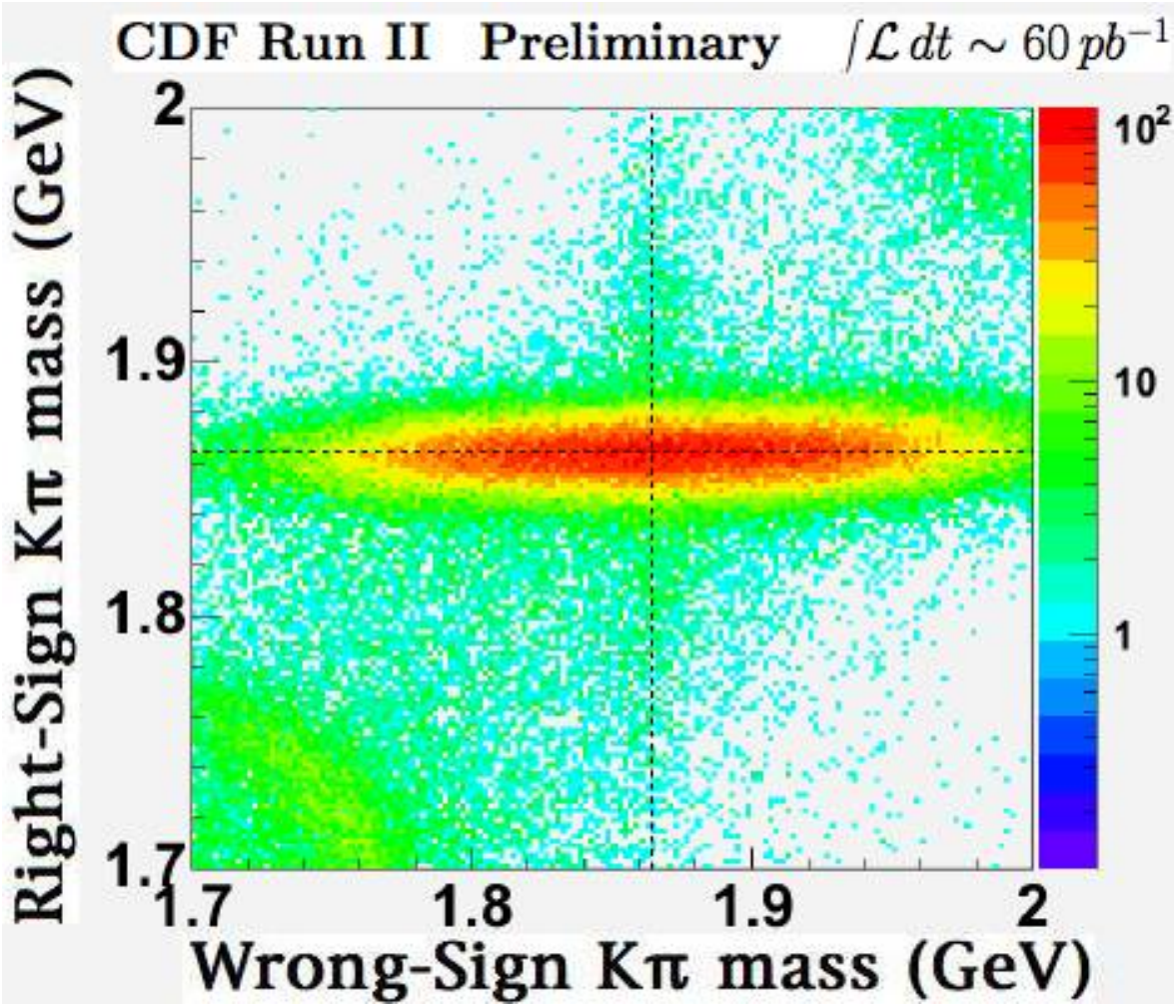

Figure 6: $K\pi$ mass For RS Versus WS
Candidates from a 60 pb^{-1} subsample are plotted with both RS and WS interpretations. The dashed lines are the PDG D^0 mass of 1.8645 GeV. A cut requiring a good (WS) D* tag is used to reduce background. The bins are 3 MeV wide, along each axis.

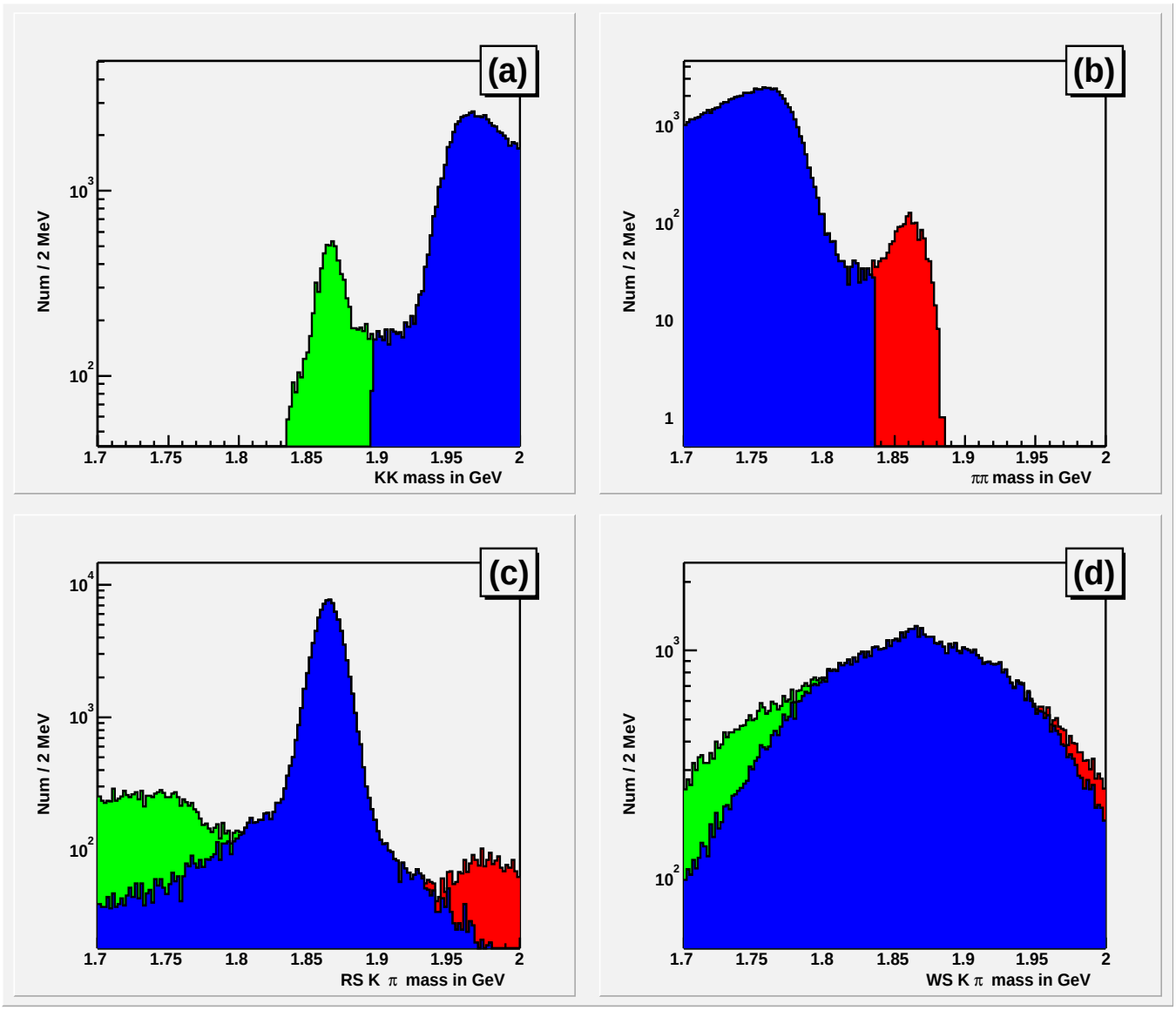

Figure 7: Candidates Reconstructed as KK and $\pi\pi$.
Data events from a 60 pb^{-1} subsample have their invariant mass recalculated, assigning the tracks as KK (a) or $\pi\pi$ (b). Events within 30 MeV of the D^0 mass in (a) are colored green. Events within 30 MeV of the D^0 mass in (b) are colored red. All others are colored blue. Those events are then shown as cumulative distributions for RS $K\pi$ candidates (c) and WS $K\pi$ candidates (d).

to distinguish RS and WS interpretations, but that will be described in the next section. These cuts were optimized from the earliest sample, as described in CDF note 7116.

The last round of cut optimization used our analysis method to get the time-integrated number of D^*, as described in the next chapter. We want to improve the significance of the number of WS D^* to the uncertainty on that number, which will behave like $S/\sqrt{S+B}$. We used the number of RS D^*, and scaled it by $R_D \approx 1/250$ to give the estimate of the number of WS D^*. We use the WS D^* fit uncertainty, but do not look at the value of the number of WS D^*, to keep the procedure "blinded". Since that fit uncertainty is approximately $\sqrt{S+B}$, a script computes for B (without revealing the value of S), then substitutes the scaled RS signal S' to get the blinded uncertainty $\sqrt{S'+B}$. The expected WS significance $S'/\sqrt{S'+B}$ is plotted for a range of cut variables and values, and we look for any improvements. The original procedure is described in CDF note 7116, and updated for the time-integrated result.

The cuts have not been modified since that time. Projecting from the local ntuples into histograms for this cut study took hours when we only had the 0d set. Such a study now would probably take days to run the code, independent of the time required for someone to look through several dozen pages of cut variables. A recent effort was made to use a neural network, as described in CDF note 9806, but the improvement was slight enough that we decided to retain these simple cuts.

Fig. 8 shows an example of the cut optimization that was done for the previous ($1.5/fb$) result. Most of the variables that kept in our local ntuples do not improve over what comes from the BStNtuples. Fig. 9 shows the one variable that had a clear improvement, the impact parameter of the soft pion. Another variable, Z_0 of the soft pion, does not show a clear maximum value, but the background distribution had long tails, extending well past where most of the signal and background events are distributed. A soft cut for this variable was chosen to exclude these "outliers".

These are the basic selection cuts we use:

- The two tracks that form the D^0 must have dE/dX information.
- The pion coming from the D^* vertex must have (unsigned) d_0 less than 600 microns.
- The reconstructed D^0 candidate must have an (unsigned) impact parameter d_0 less than 500 microns.
- The pion coming from the D^* vertex must have a point of closest approach to the primary vertex less than 1.5 cm along the Z axis.
- The pion coming from the D^* vertex must have p_T less than 2 GeV.

The impact parameter of the D^0 has the best expected WS significance around 100 μm. However, that cut also reduces the number of D^* coming from B-decays. We actually need enough of those events, at impact parameter values up to 500 μm, to get a reasonable measurement of how many of those events are in our data sample.

There was some question about how "spectators" would affect our result. From an e-mail exchange with Kevin Pitts, the only contribution that might affect our result is if the soft pion (from the D^*) were swapped with the pion from the D^0. We put in the p_T cut on the soft pion, which makes it impossible for both of the pions to pass trigger requirements. This affected less than 1% of the events.

We investigated using a dE/dX cut on the soft pion. While we cannot distinguish π from K at low momentum, we could exclude protons and hyperons. This cut was removed, as the current blessed dE/dX calibrations have not been calibrated at low momentum. The background reduction was small, but might be worth exploring in the future (along with using the time-of-flight particle ID).

2.6 Selection Cuts to distinguish RS and WS

For events in the generated ntuple, every D^* candidate has both a RS and WS interpretation (by switching the K and π particle assignments). The mis-assigned interpretation has a $K\pi$ distribution much wider than a correctly reconstructed D^0. However, we have $R_D \approx 250$ times as many RS D^* as WS D^*, which means that any real WS signal will be sitting on top of background from mis-assigned RS events.

To reduce mis-assigned background, we use what we refer to as "opposite assignment" mass cuts. When looking at WS $M_{K\pi}$, we remove candidates consistent with a RS $M_{K\pi}$ consistent with a D^0,

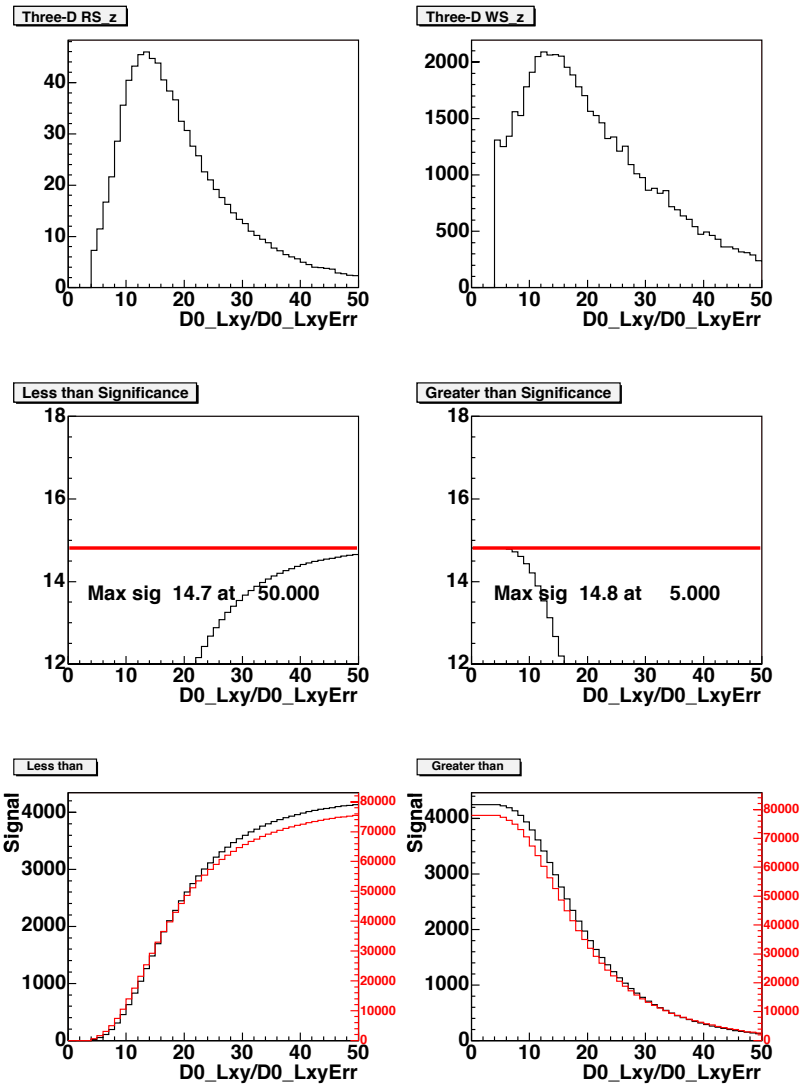

Figure 8: Cut optimization using L_{xy}/σ_{xy} of the D^0 candidates.
The upper left plot is an illustrative distribution, using sideband subtracted event near the D^0 mass. The upper right plot uses events from the sidebands. The middle left plot shows the expected WS signal/background significance, keeping events less than a particular cut value. The middle right plot shows the expected WS signal/background significance, keeping events greater than a particular cut value. The red line shows the WS significance if no cut on this variable is applied. The bottom plots show the expected signal S' (in black) and background B (in red) for the possible cut values.

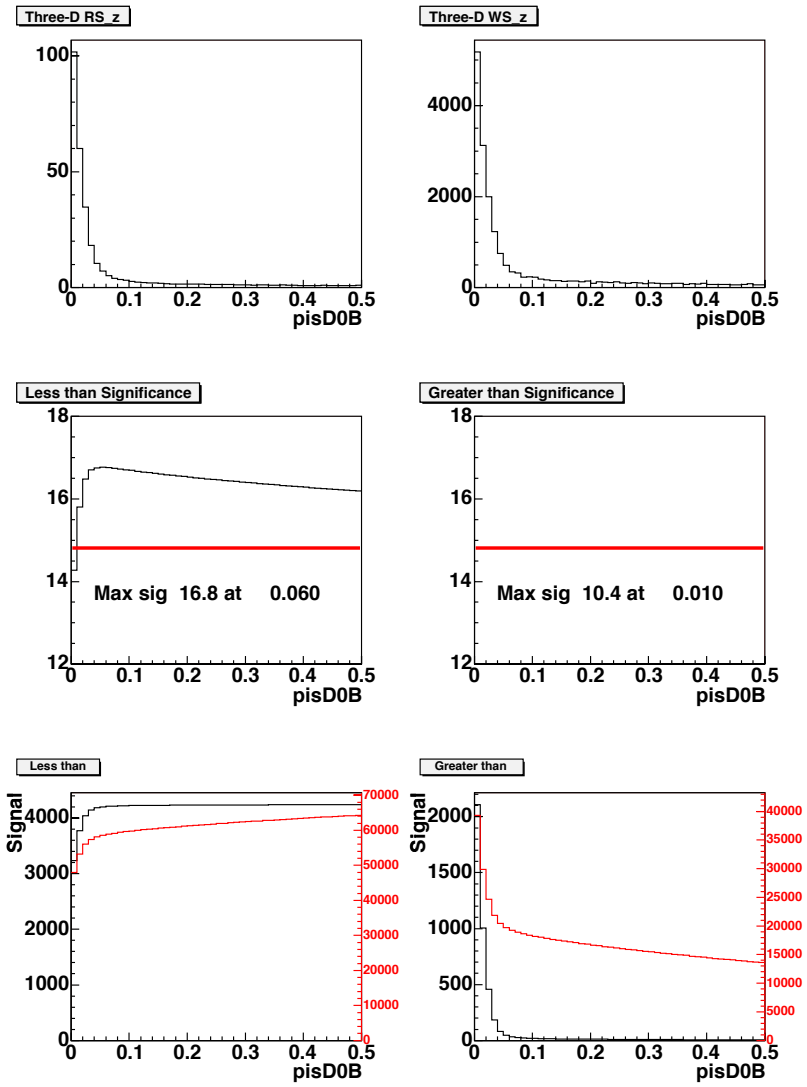

Figure 9: Cut optimization using the impact parameter of the soft pion.
The upper left plot is an illustrative distribution, using sideband subtracted event near the D^0 mass. The upper right plot uses events from the sidebands. The middle left plot shows the expected WS signal/background significance, keeping events less than a particular cut value. The middle right plot shows the expected WS signal/background significance, keeping events greater than a particular cut value. The red line shows the WS significance if no cut on this variable is applied. The bottom plots show the expected signal S' (in black) and background B (in red) for the possible cut values.

$|M_{K\pi} - M_{D^0}| < 20MeV$. This cut is illustrated in Fig. 10. WS D^0 are similarly removed when looking at the RS $M_{K\pi}$ distribution, to have the same systematic effect for both interpretations. The improvement by making this cut is illustrated in Fig. 11.

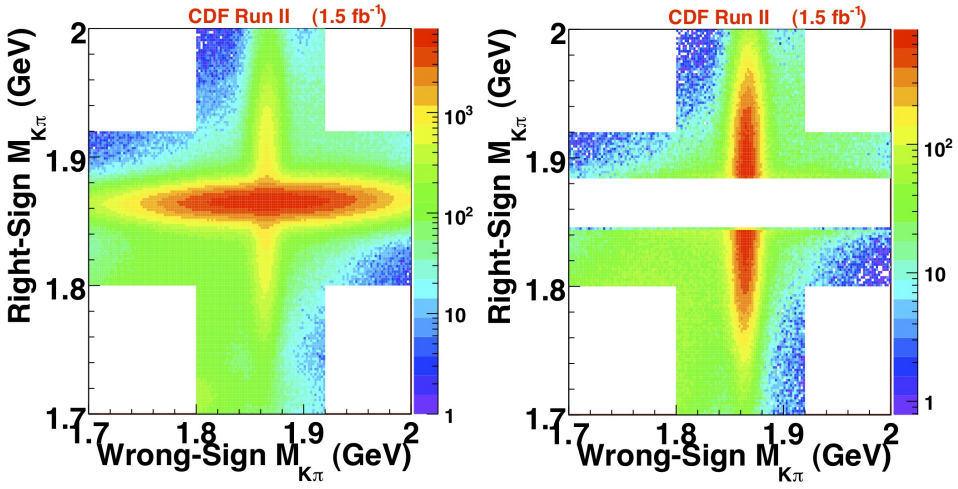

Figure 10: Plots from CDF note 8879, to illustrate the mass cut to exclude RS D^0 that are mis-assigned as WS background. The left plot shows the RS and WS mass interpretations for the events. The right plot shows the cut to exclude events consistent with being RS D^0.

To make sure that we understand the WS plot, we constructed a toy model. A particle with the D^0 mass decays to a kaon and a pion in the rest frame, with the track directions known. The daughter tracks are boosted to the lab frame. The kaon and pion assignments are swapped, and the new invariant mass is calculated. The difference in mass is shown in Figure 12. The kaon and pion will be boosted differently, when transforming from rest to lab frame. The largest difference in mass will occur when the kaon decays parallel or anti-parallel to the direction of the D^0 momentum. In figure 13, a scatter plot of the data is shown, with the toy model prediction drawn in red. The data is dominated by RS decays. At any particular decay angle of the kaon, the mass distribution is determined by the detector resolution. It is the sum over all decay angles which causes the integrated RS D^0s to have a broad distribution when reflected into the WS mass plot.

We also use dE/dX, which refers to the ionization energy loss as particles pass through the COT. (The details of how dE/dX is done are too complicated for this note, but are described in other papers[18, 19].) Rather than using particle identification for each track, we look at which two track interpretation ($K^-\pi^+$ or π^-K^+) is more likely, and only keep that interpretation.

The dE/dX variable which is expressed as $dE/dX = \log(dedx_{measured}/dedx_{predicted})$. For a correct hypothesis, the $Z = (dE/dX)/\sigma_{dE/dX}$ distribution is a unit gaussian centered at zero. For an incorrect hypothesis, the distribution is shifted away from zero. This is illustrated in Fig. 14. With $Z_{K(\pi)}(1)$ being the dE/dX value for the first track with a kaon (pion) hypothesis, and $Z_{\pi(K)}(2)$ being the dE/dX value for the second track with a pion(kaon) hypothesis, we compare $(Z_K^2(1) + Z_\pi^2(2))$ to $(Z_\pi^2(1) + Z_K^2(2))$ and only accept the more probable hypothesis (the one closer to zero).

Currently, we only accept the lower of those two interpretations, so each D^* candidate will only show up in either the RS or the WS plots. It is possible (in the future) to make a different selection, such as keeping both interpretations (if both PID values are small) or excluding both interpretations (if both are large).

The mass cut to removed mis-assigned background was optimized simultaneously with the dE/dX PID cut, as both cuts reduce the same background source. The mass cut is more effective than the PID cut (separately), but the combined effect is better. The optimal mass cut would be wider (30 MeV) if we did not use PID. This optimization was done for the time-integrated result, and has not changed since then.

The blinded (scaled RS signal) technique that was used to optimize the "basic" selections is also used here. The dE/dX cut variable is required to be less than (greater than) a given cut value, for the RS (WS) distributions. (A negative value means the RS interpretation is favored over the

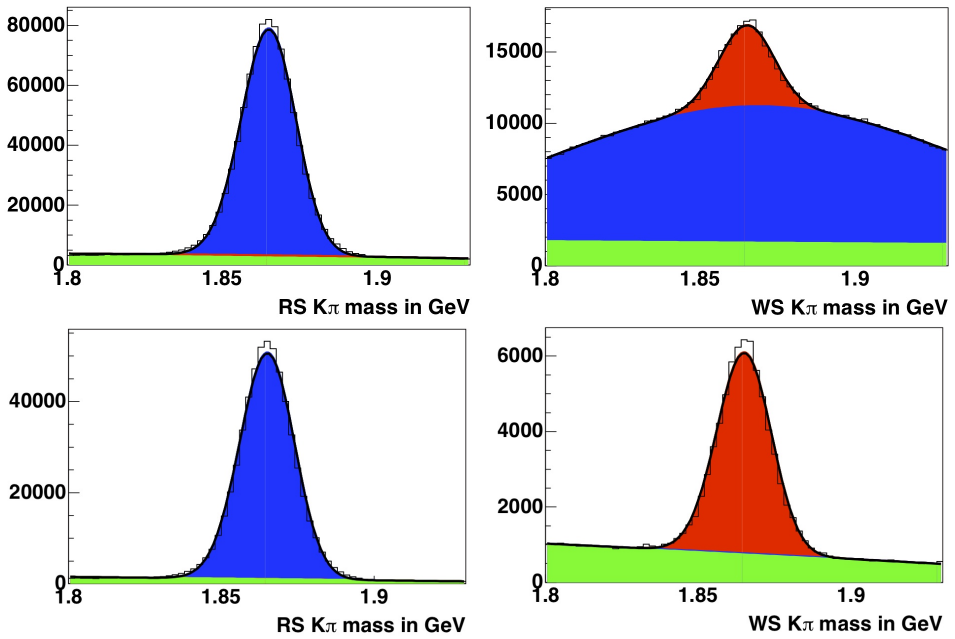

Figure 11: Plots from CDF note 8879, to illustrate the effect of the opposite assignment mass cut. The top two plots are before appying the cut, the bottom plots are after the cut. The left plots shows the RS $M_{K\pi}$ distribution, the right plots shows the WS $M_{K\pi}$ distribution The blue events are consistent with being correctly reconstructed as RS, the red events consistent with WS, and green is the combinatoric background level. The red events will be a combination of WS D^* and fake WS D^* candidates that are formed by a real D^0 and a random pion from the primary vertex. These plots are not used in the analysis, and were only generated to show visually the effectiveness of the opposite assignment mass cut.

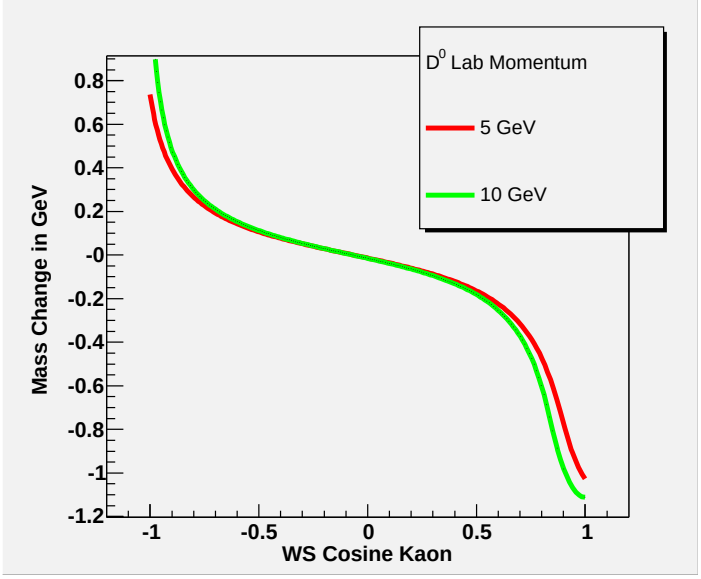

Figure 12: Mass Difference From Alternate Particle Assignment
The plot is the change in mass, when the kaon and pion tracks from a simulated RS D^0 having its mass assignments switched. The cosine kaon is the cosine of the angle of the WS kaon in the rest frame of the WS D^0, with respect to the D^0 direction. The red curve is a D^0 with 5 GeV of momentum in the lab frame, the green curve is a 10 GeV D^0.

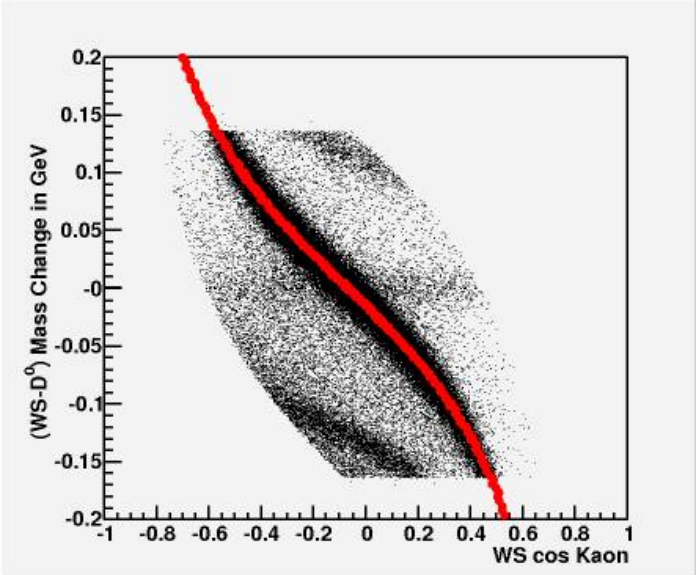

Figure 13: Mass Change Prediction Compared to Early 0d Data
This is a data scatter plot of the WS mass (in GeV) with the mean fit D^0 mass subtracted. The $K\pi$ mass is limited to the range from 1.7 to 2.0 GeV. The cosine kaon is the cosine of the angle of the WS kaon in the rest frame of the WS D^0, with respect to the D^0 direction. The red line uses the same model as figure 12, with 7 GeV momentum.

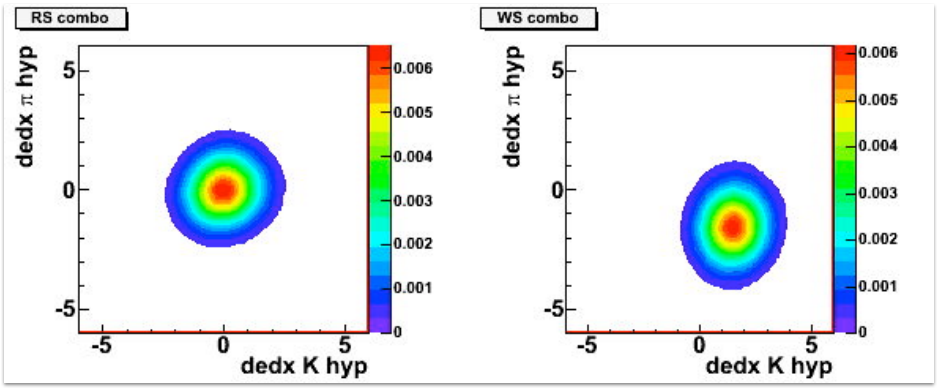

Figure 14: D^0 dE/dX distributions for correct and incorrect interpretations
dE/dX distributions for events consistent with RS D^0 and D^* mass, from the $1.5/fb$ result. The left plot is the RS interpretation for the track assignments. The right plot is the WS interpretation, swapping the K and π tracks. This is not directly used in the analysis, and is for illustrative purposes only.

WS interpretation.) The opposite assignment mass cut is then chosen, to find the expected WS significance. The mass cut value was changed, until a maximum significance is found.

Table 4 summarizes the results of the cut optimization. While there is some overlap between the two cuts, a combination of OAM and dE/dX cuts is stronger than either of them alone. The OAM cut value will be set at 20 MeV, and the dE/dX cut at 0. These are convenient, round numbers that are very close to the maximum significance. An advantage of having the dE/dX cut at zero, is that an event that passes the RS cut will fail the WS cut, and vice versa. Any other cut value will have events that could pass both the RS and WS dE/dX cuts, or fail both cuts.

dE/dX Cut Value	Max Significance	OAM Cut Value
-3.0	14.1	19
-2.5	14.5	19
-2.0	14.7	20
-1.5	14.9	20
-1.0	15.0	20
-0.5	15.1	22
0	15.1	22
+0.5	15.0	22
+1.0	14.9	23
+1.5	14.8	23
+2.0	14.7	25
+2.5	14.6	25
No dE/dX	13.0	28 MeV

Table 4: Optimization for OAM and dE/dX Cuts
The blinded yield technique is used to get the WS signal significance for dE/dX and OAM cut values. The dE/dX cut is fixed at a value, while the OAM cut is scanned (in steps of 1 MeV) to find value with the highest significance. The dE/dX cut is then changed by half a unit, and the procedure repeated.

In the next chapter, we will need to compute the number of RS D^* that show up as mis-assigned background in the WS mass plots. This will require knowing the efficiency of the opposite mass and (dE/dX) PID cuts we applied. (The other selection cuts have the same efficiency for both RS and WS events, so won't affect our measurement.)

Suppose that we start with N_{D^*}, the number of RS D^* before we apply the opposite mass and PID cuts. The number of RS D^* that we measure will be

$$N_{RS} = N_{D^*} f_k(RS \to RS) f_p(RS \to RS)$$

where $f_k(RS \to RS)$ is the efficiency for RS D^* to pass the mass cut to make it to the RS plots, and $f_p(RS \to RS)$ is the efficiency for RS D^* to pass the PID cut to make it to the RS plots. The number of mis-assigned background events will be

$$N_{MRS} = N_{D^*} f_k(RS \to WS) f_p(RS \to WS)$$

where $(RS \to WS)$ are the cut efficiencies for a RS D^* to make it to the WS plots. Combining the two gives:

$$N_{MRS} = N_{RS} \frac{f_k(RS \to WS)}{f_k(RS \to RS)} \frac{f_p(RS \to WS)}{f_p(RS \to RS)}, \tag{4}$$

We measured $12.93 \times 10^6 \pm 4.57 \times 10^4 D^*$ before the PID cut, and $10.97 \times 10^6 \pm 4.20 \times 10^3 D^*$ after the PID cut (using fitting techniques described in the next chapter). Using the formula for the efficiency uncertainty [20], we have $f_p(RS \to RS) = 84.86 \pm 0.13\%$ and $f_p(RS \to WS) = (1 - f_p(RS \to RS))$.

To get the "failure rate" of the OAM cut, we fit the D^0 signal peak, and calculate how much of the fit function is more than 20 MeV away from D^0 mass. The fit function parameter uncertainties are used to get the uncertainty on the number of events outside the OAM cut. After the PID and opposite assignment mass cuts are applied, we measured $8.481 \times 10^6 \pm 3.61 \times 10^4 D^*$. These give us $f_k(RS \to RS) = 77.30 \pm 0.17\%$ and $f_k(RS \to WS) = 3.58 \pm 0.02\%$.

This means we can expect $N_{MRS} \approx N_{RS}/118$.

2.7 Multiple candidates per event

Although multiple candidate events are unlikely to harm our result, it is difficult to explain that to an audience in a quick and easy manner, so the solution was to remove those events. After the basic selection cuts, opposite assignment mass cut, and dE/dX were applied, any event with more than one D^* candidate (RS or WS) was excluded.

The events with multiple D^* candidates are, almost exclusively, a single D^0 candidate with more than one soft pion available to form a D^* candidate. This is not surprising, considering how many tracks are coming from the primary vertex. Combining a random pion with a D^0 will form a D^* candidate with a mass difference between 0 (no opening angle) and about 2 GeV (opposite directions). That is one reason why requiring the D^* makes such a clean D^0 signal, as the mass difference width of the signal peak is very small compared to the phase space from D^0 plus random pion.

We would expect those candidates to add to the background, but not affect the prompt D^* signal. At the November 3, 2009 BMLCPV meeting, we showed that the number of multiple candidate events is consistent with a model assuming that each event has a 6.5 % chance of having a 2nd candidate (with 6.5 % of those events having a third candidate), and that the extra candidate was equally likely to be from π^+ as π^-.

Another option, that was not used, is to tightening selections that would reduce the likelihood of multiple D^* candidates, like reducing the mass difference window to less than 30 MeV. This will reduce the number of multiple candidate events, but no studies have been done yet to find an optimal value. (Making the mass difference window smaller will increase the uncertainty on the fit for the background.)

3 Analysis of Data

This chapter gave the analysis method to determine the number of D^*, using the events that passed the selection criteria explained in the previous chapter.

Our goal is to have WS/RS ratio versus decay time R_i in time bins i, and fit that distribution with a quadratic formula to get the three mixing parameters in Eq. 1 (reprinted here for convenience):

$$R_{\mathcal{B}}(t) = R_D + \left[y'\sqrt{R_D}\right] t + \left[\frac{1}{4}(x'^2 + y'^2)\right] t^2$$

where t is the proper decay time in units of the D^0 lifetime.

The measurement for D^0-$\bar{D}^0$ mixing for this analysis will be reconstructing D^* events coming from the primary vertex. The reasons for using those events are:

- The charge of the soft pion coming from the decay $D^* \to D^0\pi^*$ will tag whether the charm meson started out as a D^0 (for π^+) or a $\bar{D}^0$ (for π^-).
- The charge of the pion from the $D^0 \to K\pi$ decay, along with the charge of the π^*, determines what type of candidate the event is. "Right-Sign" (RS) events, where both pions have the same charge, are candidates for Cabibbo-Favored charm decays. "Wrong-Sign" (WS) events, where the pions have opposite charge, are candidates for DCS decays and mixing.
- D^*s decay strongly. For D^*s produced at the primary vertex, we can use the distance from the primary vertex to the $K\pi$ secondary vertex to obtain the D^0 decay time.
- Although the Two-Track Trigger was optimized for beauty decays, CDF has a copious amount of $D^0 \to K\pi$, with a large signal-to-background. Requiring a D^* improves the signal purity.

We will be using what we call the "yield" technique. This is basically a 2-dimensional (binned) histogram fit, with a difference. We fit slices of "x" (for example), and use the results of those fits to make a 1-D histogram for the "y" variable. For example, when fitting the D^* mass peak, we will use the D^0 yield versus mass difference distribution. We are using the fact that $M_{K\pi}$ and ΔM are independent variables. We can get the number of D^0 by fitting the $M_{K\pi}$ distribution for a particular range of ΔM. By making multiple fits for the D^0 at different values of ΔM, we get the D^0 yield versus ΔM. The amplitude of the D^0 signal is allowed to be independent for every $M_{K\pi}$ fit. The advantage of this technique, compared to an unbinned likelihood fit, is that we don't need to know the distribution of non-D^0 events (like combinatoric background) versus ΔM.

Right-Sign (RS) and Wrong-Sign (WS) candidates are handled in separate binned fits. The following fits are done in succession, with the signal (and uncertainty) from the previous fit being used as the yield distribution for the next fit.

- Number of candidates vs. $K\pi$ mass: The result is the number of D^0.
- Number of D^0 vs. Δ mass difference: The result is the number of D^*.
- Number of D^* vs. impact parameter d_0: This information will be used to distinguish prompt D^* (produced at the primary vertex) versus D^* produced in secondary (beauty) decays.
- Ratio of WS to RS prompt D^*s vs. proper decay time: The fit for this distribution will provide the estimate of the charm mixing parameters.

Along the way, we will be using studies with the clean, high-statistics RS D^* to determine signal distributions. However, the WS D^* is almost 300 times smaller, which means the analysis often has to use coarser binning than the examples we are using in the studies.

3.1 $M_{K\pi}$ fits

Each histogram of $M_{K\pi}$ has 60 bins with a mass range from 1.80 - 1.92 GeV. As mentioned in the previous chapter, there are significant, complicated backgrounds above and below this mass range. The signal shape for correctly reconstructed D^0 should be independent of decay time, ΔM, d_0, and RS/WS. We make a time-summed RS $K\pi$ mass plot to get larger statistics for the D^0 signal shape.

The fit to that plot is shown in Fig. 15. The signal shape parameters (except the amplitude) are fixed to the values from this fit, for every $M_{K\pi}$ after this one. The same is true for the shape of the "lump" Gaussian.

We use the ROOT fit with options "L" (log-likelihood, so zero bins are used in the fit), and "E" (improved error estimates compared to the default MIGRAD). The fit function has 13 parameters

- 6-parameter double Gaussian for correctly reconstructed D^0. The means of the Gaussians are allowed to be different, as the signal shape is very slightly asymmetric.
- 3-parameter 2nd-order polynomial for the combinatoric background, which is assumed to be non-increasing and nearly linear.
- 3-parameter Gaussian for the "lump" background near 1.830 GeV. The amplitude is set to zero for WS plots.
- 1-parameter amplitude of the Gaussian for the mis-assigned RS D^* background. This is set to zero for RS plots, and is a fixed calculated value for the WS plots

For the time-summed $M_{K\pi}$ fit (in Fig. 15), the χ^2 is slightly high, but this is due to a high statistics distribution being fit with a simple function. During the time-independent blessing, the B-Group pointed out that this is a known trait of high statistics data samples, and was okay for this analysis as long as the integral of the function gave the correct number of events. We studied this for the previous blessing (CDF note 8879), and the high-low fluctuations in the pull-distribution average out.

The double-Gaussian signal shape has the following 5 parameters, fixed from the time-summed fit:

- The number of events in the 2nd Gaussian is 37.6 % of the total (for this function)
- 1st Gaussian mean is 1.86525 GeV
- 2nd Gaussian mean shifted relative to the 1st mean by -0.33 MeV
- 1st Gaussian width is 7.29 MeV
- 2nd Gaussian width is 1.60 times larger than the 1st width

We need to consider background events in the mass plot, most of which are where one or both tracks do not belong to a $D^0 \to K\pi$ decay. An earlier study of D^0 mesons by CDF (see CDF note 6391) used a linear (decreasing) function to model this background. We used the same function for the previous time-independent measurement, but allowed the parameters to float for each fit, rather than assuming a particular slope. The data from the $1.5 fb^{-1}$ analysis shows that we need to use a quadratic function for the WS background, as shown in Fig. 16. (To be consistent, we use the same functional form for RS and WS $K\pi$ fits.) A fit for the WS $K\pi$ plot in that figure has a chisquare per degree of freedom of 7.79 with a linear background fit, which changes to 1.28 for a quadratic fit. The combinatoric background is forced to be flat or concave down, otherwise the fitter might try to absorb the signal peak with the parabola.

During the $1.5/fb$ analysis, we tried to improve how well the fit matched data, and discovered that adding an extra Gaussian ("lump") greatly decreased the chi-square of the RS $K\pi$ fit, as shown in Fig. 17. With the parameters floating, the ROOT fitter put the Gaussian around 1.83 GeV, with a width of 10 MeV. A fit for the Right-Sign $K\pi$ plot has a chisquare per degree of freedom of 24.2 with a quadratic background fit without an additional gaussian, which changes to 1.89 when the lump is added to the fit . The lump in the RS plot is about two orders of magnitude smaller than the signal amplitude; it looks larger when using a log scale.

For the analysis, we allow RS fits to have a floating parameter for the lump amplitude, and do not use the lump in WS fits (zero amplitude). We tried fitting both RS and WS distributions with the extra lump, with the amplitude floating. The WS fits are compatible with zero amplitude for the extra lump, and incompatible with the RS lump amplitudes. The WS fit pull distribution in figure 16 does not indicate any deviations at 1.83 GeV. This suggests that the extra lump is not a part of the D^0 signal distribution, as it would be present for both RS and WS plots.

We tried to search the cause of the extra lump through some realistic Monte Carlo simulation studies. One idea was to test semileptonic $D^0 \to Kl\nu$ decay. For a quick look we generated 3000

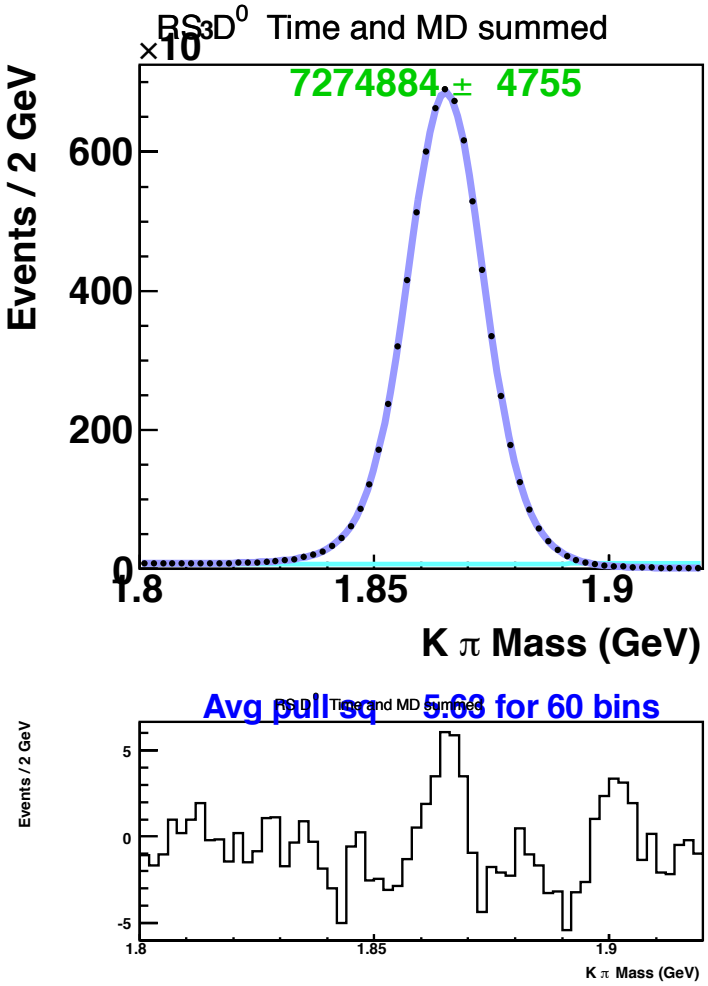

Figure 15: Time-summed $M_{K\pi}$ plot for events with $4.5 < \Delta M < 8$ MeV (D^* peak region) and $d_0 < 60\mu$m. Light blue is the fit to background, dark blue is signal + background.

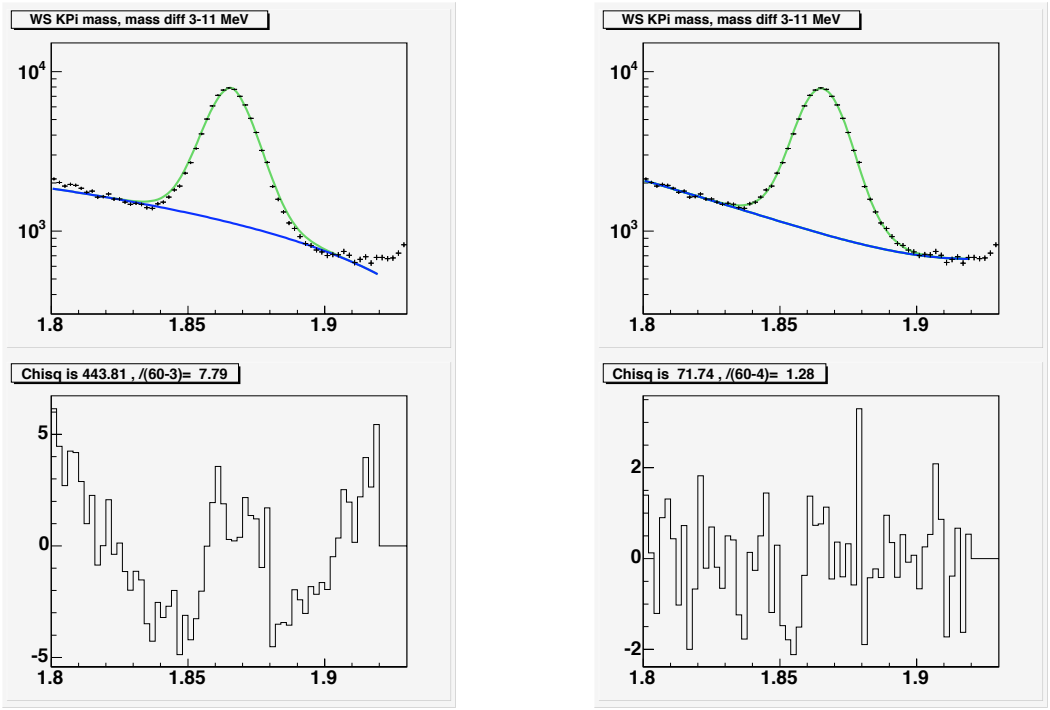

Figure 16: WS candidates from period 0-10 data are plotted as a function of $K\pi$ mass (top plots). The blue line is a fit to the background, the green line is signal plus background. The left plots use a linear background function, the right plots have a quadratic background. The pulls (difference between the data points and the fit, divided by the square root of the number of events in the bin) are in the bottom plots. A D^* mass difference cut of $3 < \Delta m < 11$ MeV is applied to improve signal purity. No selection on decay time is made. The signal shape is fixed from a fit to the RS time-summed $K\pi$ distribution.

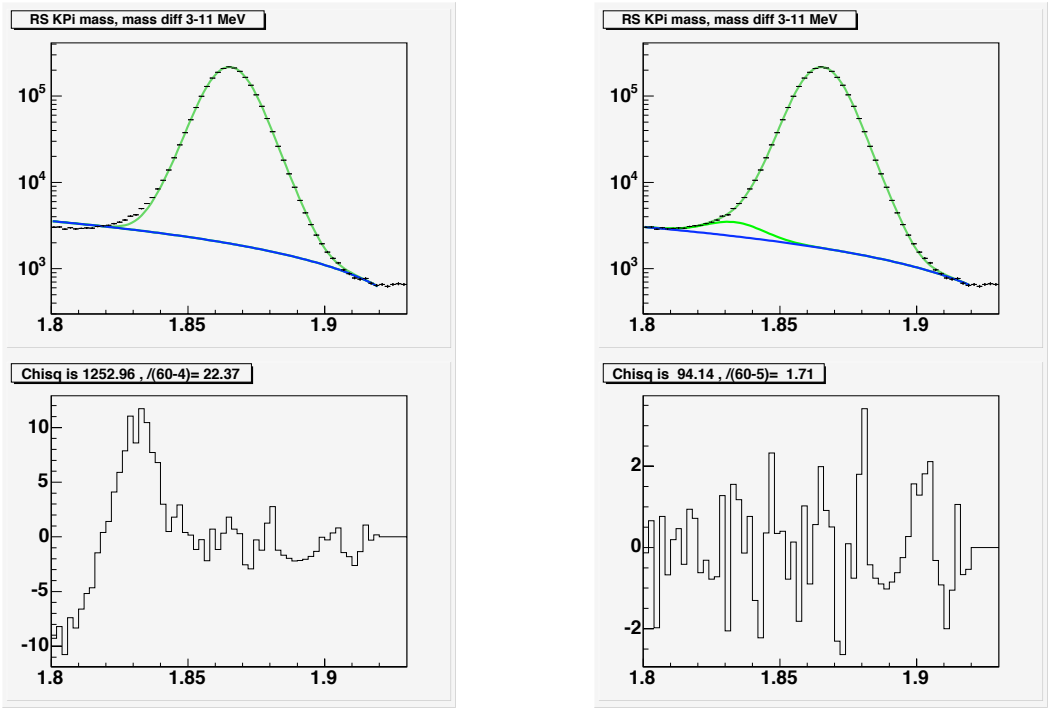

Figure 17: RS candidate $K\pi$ mass, similar to the WS plots in Fig. 16, with a quadratic function for the background. The right plot has an additional Gaussian background lump added to the fit. The lump is at 1.832 GeV (determined from the fit). The titles of the pull plots have the wrong number for the degrees of freedom, since it does not account for the D^0 signal shape parameters, which are determined from these fits. The left plot should be χ^2/dof = 24.6, the right plot is χ^2/dof = 1.96.

$K\pi$ mass Fit	χ^2 /ndf for Period 0 to 16 data	χ^2 /ndf for Period 0 to 21 data
Without Gaussian	852.65/50 = 17.05	983.5/50 = 19.67
With Gaussian	129.60/48 = 2.70	137.59/48 = 2.86

Table 5: χ^2 /ndf for with and without extra Gaussian for the old and the new data.

$D^* \to D^0\pi^+$, $D^0 \to K^+\mu^+\nu_\mu$ simulated events using Pythia model. We find that the D^0 mass reconstructed from this decay falls below 1.8 GeV and after applying mass difference cut, it cannot cause a lump at 1.83 GeV where it was found in the real RS D^0 data. Similar results found in other decay chains we tried. None of them had mean invariant mass close to 1.83 GeV. The cause of the extra lump is still a mystery.

We conducted another study of the lump with data up to period 21. We fit the RS $K\pi$ mass distribution with and without extra Gaussian for period 0 to 16 data and for period 00 to 21 data separately. Table 5 lists the χ^2 /ndf for both the data sets.

Figure 18 shows the RS and WS time-integrated fit for "good" D^0s. RS fit has 9 free parameters: 6 for the double Gaussian signal, and 3 for the (quadratic) background. The WS fit has 4 free parameters: 1 for the signal amplitude, and 3 for the background. The WS signal shape is determined from the RS fit. The RS fit, besides having an enormous χ^2, shows structure in the pull distribution.

To improve the RS $K\pi$ fit, we added an additional Gaussian. The parameters for that "lump" Gaussian are a mean of 1.83 GeV, width of 10 MeV, and an amplitude of 0.6 % compared to the signal Gaussian. Figure 19 shows the RS and WS fits when this "lump" is determined from the RS fit, and treated as part of the signal Gaussian. (The WS fit has no additional parameters, because the signal shape is determined from the RS fit.) The improvements in the RS fit pull distribution and χ^2 are compelling reasons for including the extra Gaussian in the $K\pi$ fit.

We also tried a fit where the extra Gaussian is treated as a background term. The mean and width are the same for both RS and WS, but the amplitudes are allowed to float. Figure 20 shows those RS and WS fits. The WS fit χ^2 has improved by 25.4 units with the addition of a parameter for the "lump" amplitude (independent of the RS). This excludes the hypothesis that the "lump" is signal, at the 5.0σ level. In fact, the WS fit put the amplitude to zero. (The ROOT fit was not allowed to have a negative amplitude.) When looking at the WS $K\pi$ fits divided by mass difference or decay time, the "lump" amplitude was always consistent (within errors) with zero. This confirmed the decision to not have the "lump" in the WS $K\pi$ fits, and to have the lump amplitude be an independent background parameter for RS $K\pi$ fits.

After determining the D^0 signal distribution from the fit to the time-integrated RS $K\pi$ plot, we proceed to fit the 4800 time-dependent $M_{K\pi}$ plots (60 bins of mass difference, 2 d_0 regions, RS/WS, and 20 time bins). The distributions are fit with a function that includes the following components:

- Correctly reconstructed D^0, which has a fixed shape.
- Combinatoric background, which has a non-increasing, nearly linear distribution
- A small empirical "lump" background near 1.830 GeV, which only appears in the RS plots
- Mis-assigned RS D^* background, which has a broad distribution in the WS plots

In the previous chapter, we gave the calculation for the number of RS D^* that are mis-assigned as WS background, given the number of RS D^* that we observe in the RS plots. We would like to correct for that background, so it is necessary to find the distribution in (WS) $M_{K\pi}$ and (WS) ΔM. In CDF note 7116, we did studies that showed we understand the mathematics of the distributions, but the exact values are determined from data.

We use the yield technique, plotting the number of (time-summed) RS D^* as a function of WS $M_{K\pi}$ and WS ΔM. This is shown in Fig. 21. A single Gaussian is used for the WS $M_{K\pi}$ distribution, which matches the data distribution well. For the WS ΔM shape, we subtract off the calculated fit background from the histogram. Once we have measured the number of RS D^* that we observe in the RS plots, and calculated the total number of mis-assigned background events, we can distribute them as a function of WS ΔM and WS $M_{K\pi}$ (to get the overall normalization correct).

Fig. 22 shows the χ^2/dof for those fits. It would be impractical to show all the plots in this note. With 4 plots to a page, that would make this note over 1200 pages and several hundred MB in file size.

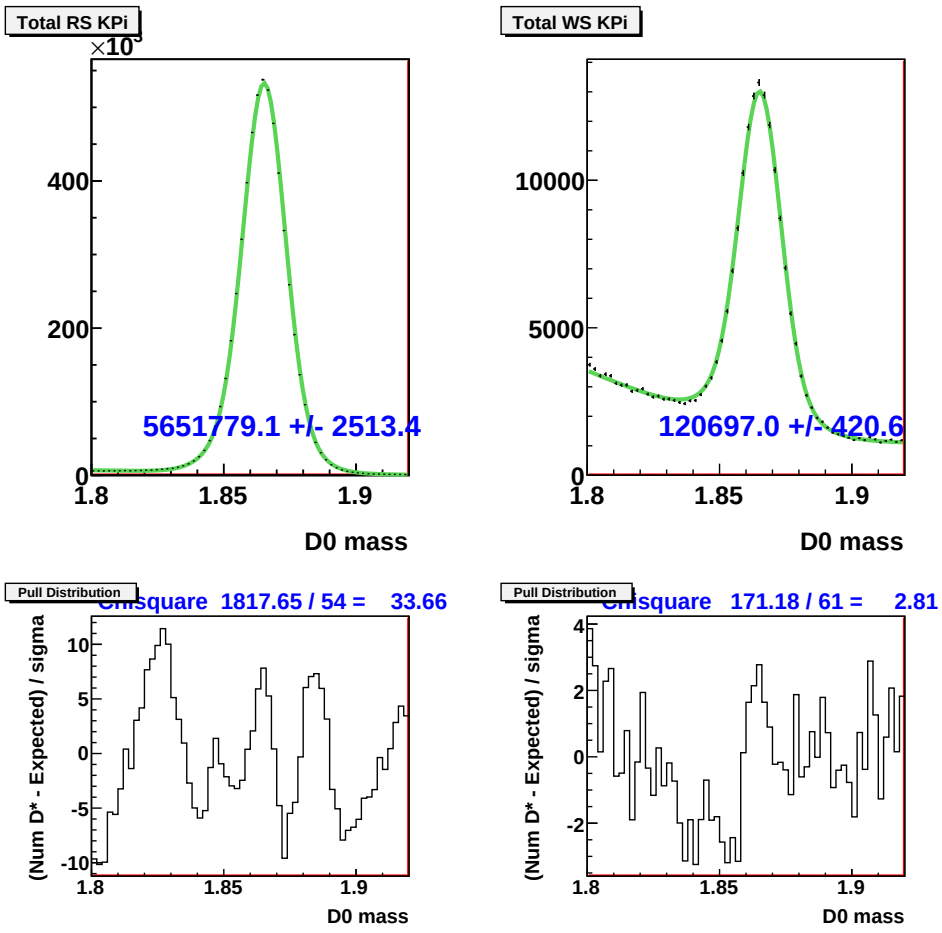

Figure 18: $K\pi$ mass for "good" RS (left) and WS (right) candidates, fit without an extra Gaussian (lump).

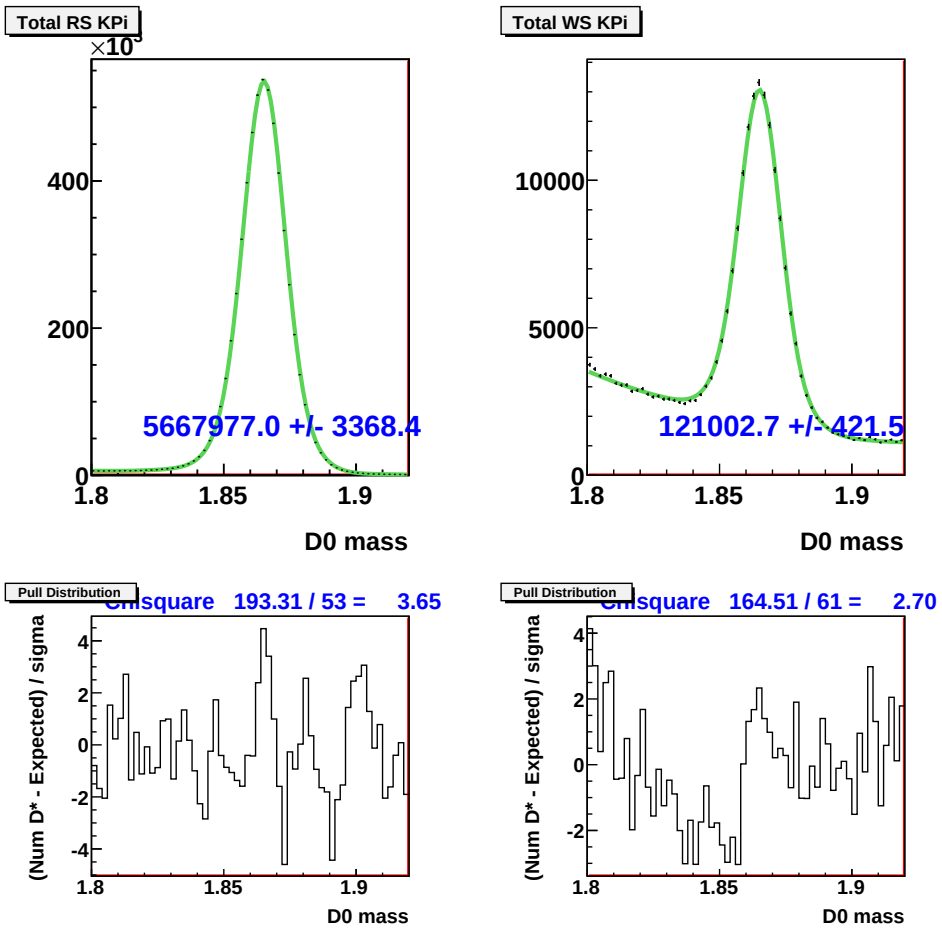

Figure 19: $K\pi$ mass for "good" RS (left) and WS (right) candidates, fit with an extra Gaussian (lump) that is treated as part of the signal shape.

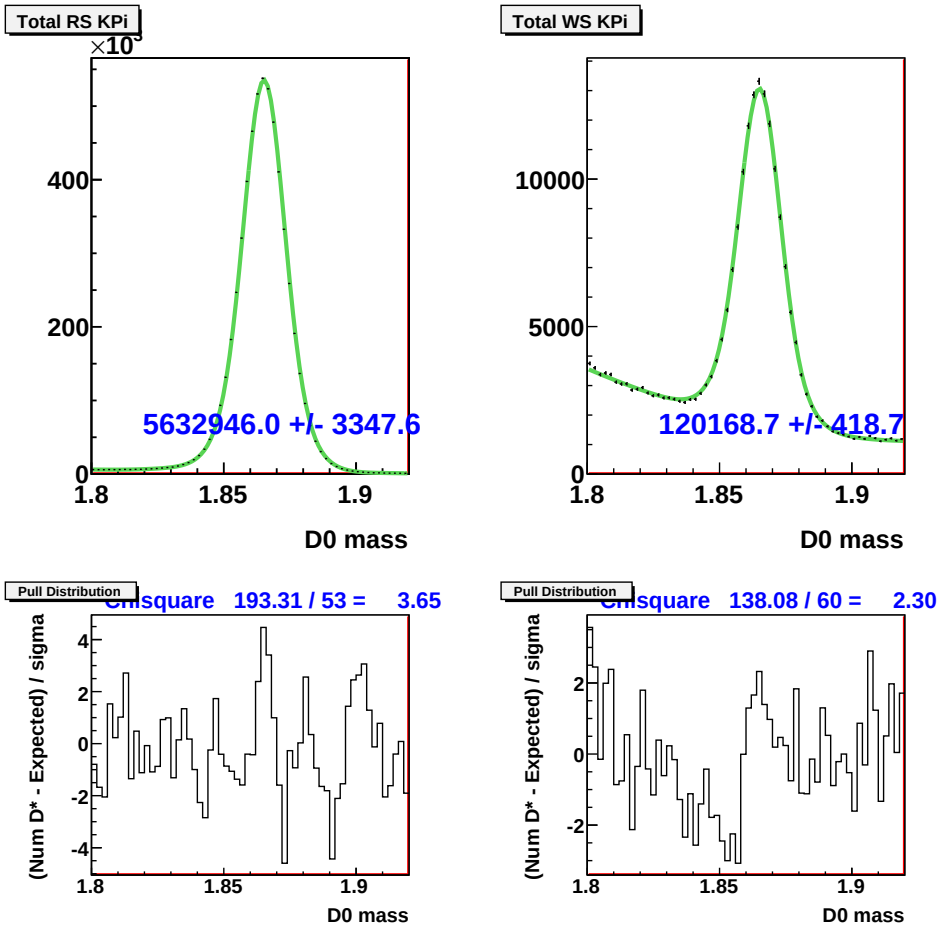

Figure 20: $K\pi$ mass for "good" RS (left) and WS (right) candidates, fit with an extra Gaussian (lump) that is not considered signal. The RS and WS fits have independent amplitudes for the extra Gaussian, although they have the same mean and width. The WS fit resulted in zero for the "lump" amplitude.

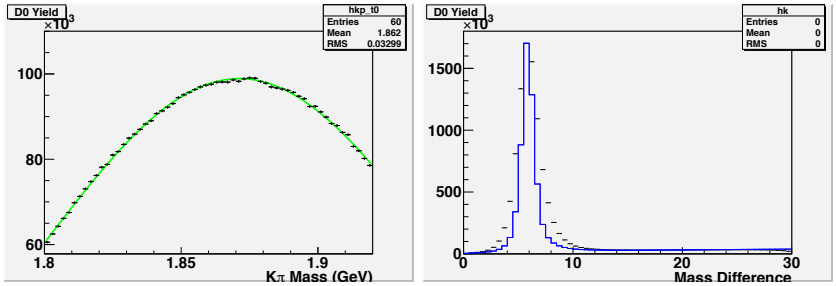

Figure 21: The distributions of mis-assigned RS D^* for WS $M_{K\pi}$ (left) and WS ΔM (right). The green curve is a single Gaussian fit. The blue curve is the signal shape for correctly reconstructed D^*, which is narrower than the mis-assigned distribution. The single Gaussian used in Fig. 21 has a mean of 1.8715 ± 0.0009 GeV and a width of 72.87 ± 0.17 MeV. The χ^2/dof for that fit is 90/54.

(The plots are stored on Wayne State computers at CDF, so are available on demand.) In appendix A, we have included the time-independent (all time bins summed) 60 RS and 60 WS $M_{K\pi}$ fits.

3.2 ΔM fits

The results from the $M_{K\pi}$ fits are used to make distributions of the D^0 yield as a function of ΔM Each histogram of ΔM has 60 bins with a mass range from 0 - 30 MeV. Every point on the ΔM yield plot is the result of a $M_{K\pi}$ fit, for the number of D^0 and the uncertainty on that number. So these plots have correctly reconstructed D^0. The only question is if the D^* candidate is signal, or a D^0 with a random pion attached. The distribution is fit with a function that includes the following components:

- D^* signal, which have a narrow distribution
- Background from D^0 plus a random track assigned to form the D^* candidate

The function used for the signal was obtained by empirically (trial and error), by trying to minimize the chi-square of the fit and to avoid features in the pull distributions. The signal function is a gaussian plus an additional pseudo-Gaussian asymmetric function. With seven parameters $(A, B, C, D, \mu_1, \mu_2, \sigma)$ and the mass difference Δm, for $\Delta m < \mu_1$ the signal function is: For $\Delta x < \mu_1$

$$A\left[\exp\left(B(\Delta m - \mu_1)\right) + C\exp\left(-(\Delta m - \mu_2)^2/\sigma^2\right)\right] \tag{5}$$

and for $\Delta x > \mu_1$

$$A\left[\exp\left(D(\frac{\mu_1}{\Delta m} - 1)\right) + C\exp\left(-(\Delta m - \mu_2)^2/\sigma^2\right)\right] \tag{6}$$

The function for the background is ΔM raised to a power. It is similar to a square root function. The pseudo-Gaussian signal shape has the following 6 fixed parameters (in MeV) from the RS time-summed fit: $B = 1.475, C = 0.5378, D = 10.184, \mu_1 = 5.911, \mu_2 = 5.854, \sigma = 0.8031$. The RS background power term is 0.4504, and the WS background power term is 0.4436.

Both the signal and background shapes should be independent of decay time and d_0. The signal shape should also be the same for RS and WS. We make a time-summed RS ΔM plot to get larger statistics for the D^* signal shape, which will lead to smaller relative uncertainty due to statistical fluctuations. The fit to that plot is shown in Fig. 23. The signal shape parameters (except the amplitude) are fixed to the values from this fit, for every ΔM fit after this one. The power parameter for the RS (WS) background shape is determined from the RS (WS) ΔM fit.

We expect the RS and WS background shapes to be similar, but not necessarily the same. For example, a charm quark has a $+2/3$ charge. If a charm quark is produced at the initial reaction and hadronizes to a D^0, the "jet" of particles should have a positive charge, making it slightly more likely that a random π^+ (as opposed to a π^-) will be available to form a (fake) D^* candidate.

We have 80 $M_{K\pi}$ plots (2 d_0 regions, RS/WS, and 20 time bins). Fig. 24 shows the χ^2/dof for those fits. Appendix B has the 20 RS and 20 WS ΔM yield fits, for $d_0 < 60\mu$m. Appendix C has the 20 RS and 20 WS ΔM yield fits, for $d_0 > 60\mu$m.

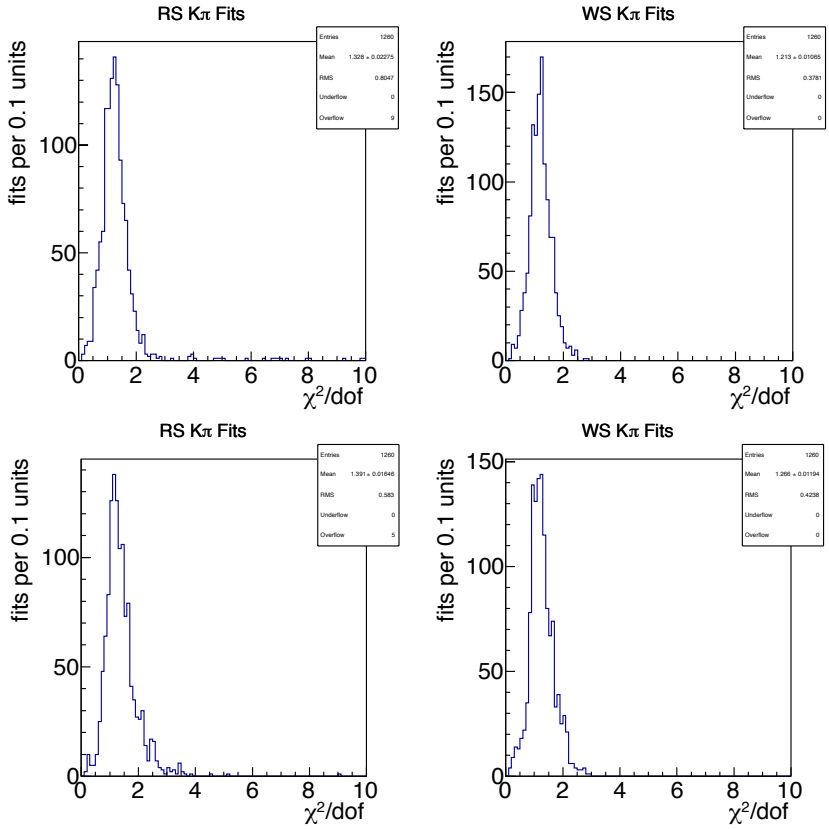

Figure 22: χ^2/dof distribution for the 4800 $M_{K\pi}$ fits The top plots are for candidates $d_0 < 60$, the bottom plots for $d_0 > 60$. The left plots are for RS, the right plots for WS. Each plot has 1200 entries (60 bins of ΔM, 20 bins of time).

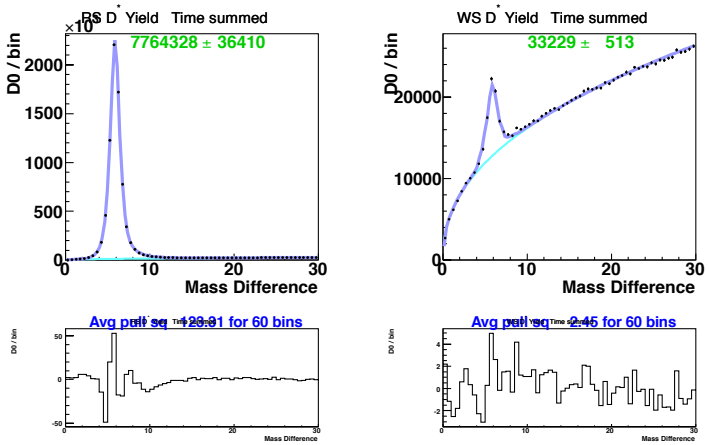

Figure 23: Time-summed $M_{K\pi}$ plot for events with $4.5 < \Delta M < 8$ MeV (D^* peak region) and $d_0 < 60\mu$m. Light blue is the fit to background, dark blue is signal + background.

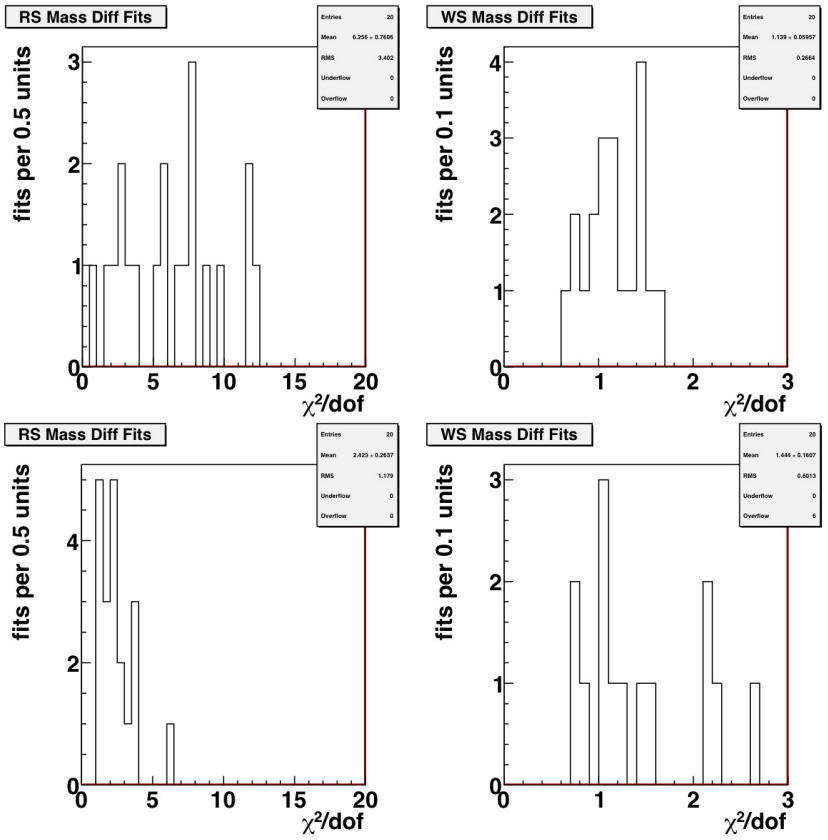

Figure 24: χ^2/dof distribution for the 80 ΔM yield fits The top plots are for D^* candidates $d_0 < 60$, the bottom plots for $d_0 > 60$. The left plots are for RS, the right plots for WS.

3.3 Impact parameter fits

The results from the ΔM fits gives us the number of D^*. We would like to distinguish prompt D^* (produced at the primary vertex) from secondary decay D^* (like $B \to D^* X$). Since we are measuring decay times using the length from the primary vertex to the D^0 decay, the non-prompt events will not have the correct decay time.

The impact parameter of D^* coming from secondary decays will be different from prompt D^*, as illustrated in Fig. 25. Ideally, we would make yield plots of D^* as a function of d_0. However there is a limit to how often the data can be segmented before the WS $M_{K\pi}$ fits become unreliable due to low statistics.

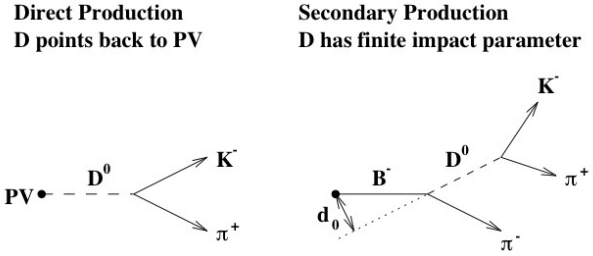

Figure 1: The impact parameter of direct and secondary charm in the $r - \phi$ plane.

Figure 25: Impact parameter diagrams taken from CDF note 5996 [21].

The normalized distribution as a function of d_0 should be the same for both RS and WS. (After the D^* is produced, its location will be independent of how the D^0 decays.) We do have several million RS D^* to work with. We make an independent study of the distribution of RS D^* versus d_0 for each time bin. We then calculate the fraction of D^* expected with $d_0 < 60\mu$m and $d_0 > 60\mu$m. Those fractions, combined with the results from the RS and WS ΔM fits, allow us to calculate the number of prompt D^*.

The prompt distribution should be time-independent, based on studies done for CDF note 5996 [21]. We use a double Gaussian, which has the same parameters (except for amplitude) for all twenty time bins. It has four parameters (2 widths, 1 relative amplitude for the second Gaussian compared to the first, 1 overall amplitude), since the means of the Gaussian are zero.

We used trial-and-error to get the functional form of the non-prompt background. For the previous result with $1.5/fb$, we used a single Gaussian. CDF note 8879 shows those IP fits in Appendix C. On June 18, 2009, Nagesh gave an analysis update at the BMLCPV meeting. On slides 27-30, he compared a single Gaussian fit to B-generator MC events he made. The chi-square was reasonable, given the low statistics. However, the single Gaussian had problems for the short lifetime bins, where the non-prompt shape should converge towards the (double Gaussian) prompt shape. It also seemed to underestimate the tails of the distribution. Switching the non-prompt shape to a double Gaussian helped empirically, as shown in Fig. 26.

Appendix D has the distribution of RS D^* versus d_0 for the twenty time bins. The number of D^* in the fit function is constrained to be the number of D^* in the histogram (for each time bin). The relative number of prompt to non-prompt D^* is allowed to float independent of the time bin, and is only used to help the fit converge.

For the $1.5/fb$ analysis, initially we had a cut at $|d_0| < 100\mu$m, to exclude most of the non-prompt D^*, but we were unable to estimate the number of non-prompt D^* that survived that cut. Thomas Kuhr also pointed out that the signal distribution might have tails past the IP cut. Although this fraction is small, at short times the prompt signal is large enough that those tails are comparable to the amount of non-prompt events. Next, the events were separated into $|d_0| < 100\mu$m and $|d_0| > 100\mu$m. The problem arose that WS fits for $|d_0| > 100\mu$m had very low statistics, which led to large uncertainties. This lead to moving the dividing point to 60μm, to increase the statistics for the larger impact parameter region.

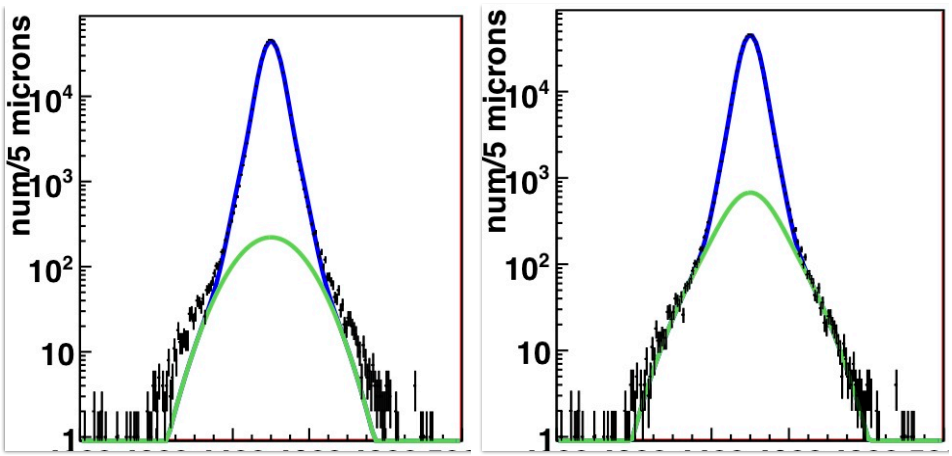

Figure 26: Impact parameter diagrams for the time-bin 1.75-2.0 lifetimes, for data from p0-16. The left plot is a single Gaussian fit for non-prompt distribution. The right plot uses a double Gaussian. This was presented at the BMLCPV meeting on 11/24/2009.

3.4 Correction For Non-prompt D^*

The study presented in the previous section used RS D^* to determine the prompt and non-prompt distribution shapes for impact parameter. For the analysis, we are concerned with how those events are distributed into two I.P. bins. We want to know the fraction of the non-prompt distribution f_i with $d_0 \leq 60\mu$m, and the fraction $g_i = 1 - f_i$ with $d_0 > 60\mu$m. (The subscript i is for each time bin.) We also have the fractions f_p and g_p for the prompt distribution. The fractions are shown in table 7, which is after the plots in Appendix D.

The yield technique described earlier in the chapter is used to get the number (n_i) of RS D^* with $d_0 \leq 60\mu$m, and (o_i) for D^* with $d_0 > 60\mu$m. The unknown variables are the number of prompt (N_i) and non-prompt (P_i) D^*.

However,

$$n_i = N_i f_p + P_i f_i$$

$$o_i = N_i g_p + P_i g_i$$

A little linear algebra allows us to solve for:

$$N_i = (n_i\, g_i \; - \; o_i\, f_i)/(f_p\, g_i \; - \; f_i\, g_p)$$

$$P_i = (o_i\, f_p \; - \; n_i\, g_p)/(f_p\, g_i \; - \; f_i\, g_p)$$

4 WS to RS Ratio Time Distribution

The last chapter described how we obtain the number of prompt D^* for any particular decay time bin. The data was divided into the following 20 time bins:

- 13 bins of a quarter D^0 lifetime width, for decay times from 0.75 - 4.0 D^0 lifetimes
- 4 bins of a half D^0 lifetime width, for decay times from 4.0 - 6.0 D^0 lifetimes
- 2 bins of a D^0 lifetime width, for decay times from 6.0 - 8.0 D^0 lifetimes
- 1 bin of two D^0 lifetimes width, for decay times from 8.0 - 10.0 D^0 lifetimes

The bin sizes are not optimized, but a by-hand attempt to balance sufficient WS statistics with a simple scheme. We have > 80 WS D^*s in the longest decay time bin (with $d_0 < 60$), which has the smallest number of signal events. There are very few events beyond 10 lifetimes. There are no events below half a lifetime. To be cautious, we do not use events below 0.75 lifetimes.

4.1 Monte Carlo

For the previous $1.5/fb$ blessing, there was a desire to see Monte Carlo validation of some of the analysis methods. However, despite two people certain that there was reliable D^* samples, when we followed up, it turned out that those samples were either gone or otherwise no longer usable. Fortunately, for this analysis we have a few tools available.

The first is B-Generator level MC, like Nagesh used to investigate non-prompt impact parameter distributions. This was statistics limited (compared to data), and it may not model actual results closely, since it doesn't include detector resolutions that sculpt and smear the distributions.

The second is a full (Pythia) MC, generated by Angelo DiCanto, Paola Garosi, and Paola Squillacioti. Some useful information is on the web page: http://www-cdf.fnal.gov/ dicanto/internal/bmc.html. This sample of $D*$ is allowed to decay to all (known) decay modes. It is also statistics limited (compared to data), but has the advantage of being run through detector simulation and written out in BStNtuple form, so it should be closer to actual data. This sample was used during the investigation on partially reconstructed charm backgrounds in our $K\pi$ plots.

The last is a toy MC to make simulated mass distributions. The results from our fits to data are used to estimate the amounts and distributions of all signals and backgrounds (that were included in the fit). This template is then used to generate mass plots, which can be fed into our normal analysis code. The advantage here is that very specific changes can be made, like to the charm mixing parameters or the signal distributions, to see what effect it has on the analysis output. The disadvantage is that we need to be confident that the analysis is dividing the various signals and backgrounds properly, and that fit distributions are close enough to the real thing to be useful. This toy MC was used during studies of the systematic effects, and to validate that the analysis code was working as expected.

Fig. 34 shows the output of 400 toy MC events. No changes were made to the simulation, so the analyzed results should be very similar to the simulation input values. The choice of 400 simulations was arbitrary; getting sqrt(N)/N = 5% requires about half a day of computer processing. The results of the twenty time bin fits (with $d_0 < 60$) are used to obtain $\Delta R/R$, the relative difference in the WS/RS ratio of the analyzed simulation compared to the seed values. For this example, the shift in the ratio distribution (which would indicate a systematic effect) is within 1 sigma of zero.

4.2 Systematic Uncertainties

Before we fit the prompt WS/RS D* ratio versus decay time, we add a few additional systematic uncertainties (in quadrature) to the results for the number of prompt D^*. We then make the distribution of the ratio of WS to RS prompt D^* in our time bins. We then consider how to interpret the results of the mixing fit to that distribution.

This section lists the systematic uncertainties for this result. The CDF Statistics Committee [22] points out that a fit to data includes some uncertainty about the fit shapes, as long as those parameters are floating. For that reason, the errors returned from the fitter are (stat. + syst.). Occasionally, we are asked if we tried alternate functions for the background (for example), to get a systematic

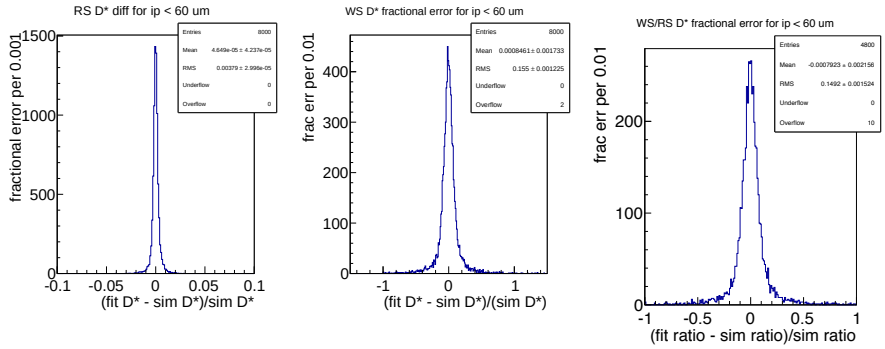

Figure 27: Generated 400 toy MC events. The results of the twenty time bin fits (with $d_0 < 60$) are used to obtain $\Delta R/R$, the relative difference in the WS/RS ratio of the generated simulation signal compared to the results when the simulation is analyzed like data. The left plot is RS D^*, the middle plot is WS D^*, and the right plot is the ratio. For all three plots, the distributions centered within 1 sigma of zero.

uncertainty for the shape. Since the fitter already includes some uncertainty from the shape, adding more uncertainty to the function shape would be a form of double counting. This is different from analyses that use Monte Carlo, where the function shape parameters are fixed beforehand. The uncertainty from having the wrong functional form is more tricky to handle, but that question ("is that the right shape?") is true for all analyses, even when MC is used.

4.2.1 Signal Shapes

The true distribution of the D^0 and D^* signal shapes is complicated, but well matched by the simple signal functions we have chosen. The true signal distributions are the same for RS and WS, since they have identical kinematics. We use the same signal shapes for RS and WS. If we wanted to report the RS or WS signal yield separately (like for a lifetime fit), we would need to account for the systematic uncertainty on the signal shapes, which we are fixing from the time-summed fits. However, we only use the WS to RS ratio. The systematic effect is a common multiplicative factor for both WS and RS, and will mostly cancel in the WS/RS ratio.

Fig. 34 shows the output of 400 toy MC events, with the D^0 signal shape in the simulation altered to use the signal shape from CDF note 8484 [23], which includes a radiative tail. The radiative tail accounts for about 2% of the signal events. Since the analysis code has not been modified, we expect to undercount the signal compared to what was put into the simulation. Most of that cancels in the ratio. We still see a shift of $|\Delta R/R| = 0.40\%$, which will be used as the systematic uncertainty for the signal shape.

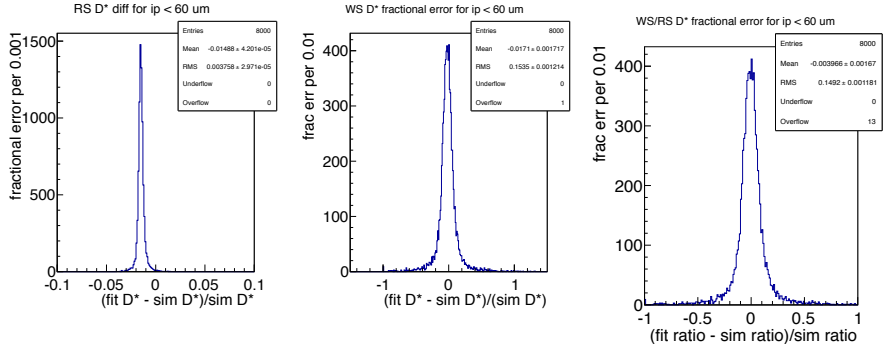

Figure 28: Generated 400 toy MC events. The D^0 shape in the simulation was modified to use the signal shape from CDF note 8484 [23], which includes a radiative tail. The left plot is RS D^*, the middle plot is WS D^*, and the right plot is the ratio.

4.2.2 $K\pi$ Background

We expect an effect due to uncertainty in the background shapes for the $K\pi$ plots. Since the signal-to-background ratio is different for WS and RS, the ratio could be affected as well. However, since we allow the quadratic polynomial parameters to float for every $K\pi$ fit, the systematic uncertainty is already included in the signal uncertainty returned by the fitter. (The signal uncertainty is larger than a similar unbinned likelihood fit, or binned fits where the background shape is fixed a priori.)

Another point to consider is that we can't have an alternate background function as a cross-check. We are using a quadratic polynomial to fit the background. The $K\pi$ fits agree with the data points, with an average χ^2/dof of 1. Any differences between our distribution and the "true" background from data must be small. Any difference in shape could be treated as a Taylor expansion, which would also make it a polynomial, which we are already using in the fit. We have tried including a third order term to the polynomial (in CDF note 8879). There was no noticeable changes in the signal yields, and all fits that we looked at had the third order term set to zero.

We made two studies to investigate partially reconstructed charm background. The first was for $D^+ \to K\pi\pi$. The first two tracks form the D^0 candidate, while the second pion is treated as the D^* tag. These events fall outside of the RS mass window, but swapping the K and π particle assignments can cause a mass shift which puts these events in the WS mass window. Fortunately, we can see a clear D^+ peak when we knew what to look for, as shown in Fig. **??**. We obtain the number of D^+ background in bins of WS $K\pi$ mass, similar to our normal yield technique. The study showed 0.274% WS background, per RS $K\pi$. That background fit is well described by an exponential fit. Fig. 30 shows the WS and RS scatter plot, and the fit for the D^+ background.

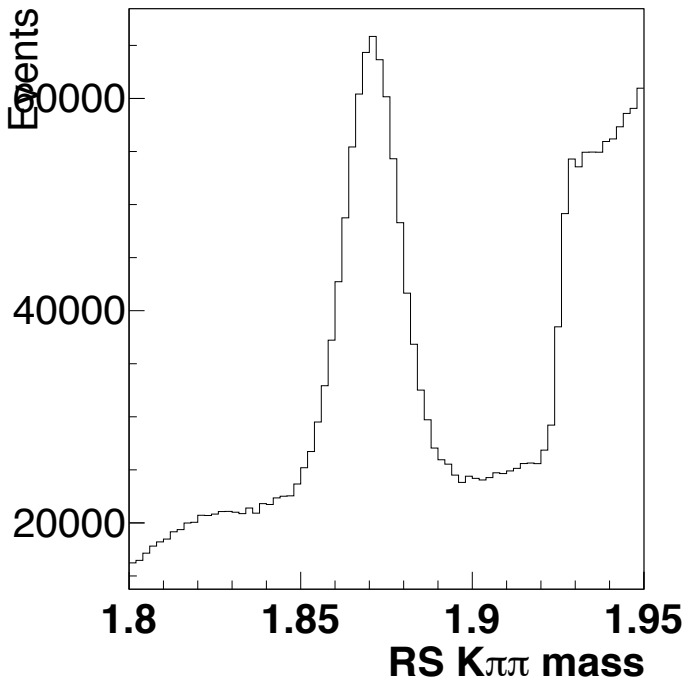

Figure 29: D^+ signal peak for the three-track RS mass plot. The climb in the background above 1.92 GeV is due to the event selection for this study, which is also related to the cross structure in the RS-WS scatter plot.

The B-Group pointed out that the D^+ background will have a different lifetime distribution than the D^0. We measured the number of D^* for each time bin, as shown in Fig. 31, for use in the Toy MC. Fig. 32 shows the output of 400 Toy MC events, where we replace the appropriate amount of the (WS) combinatorial background (quadratic fit) with the exponential distributions of the D^+. We still see a shift of $|\Delta R/R| = 0.28\%$. The systematic bias might be zero, but to be conservative, we will add this value in quadrature to the current errors. The study of the individual time bins (to look for time-correlated systematic effects) is not completed, but the first impression is that this systematic

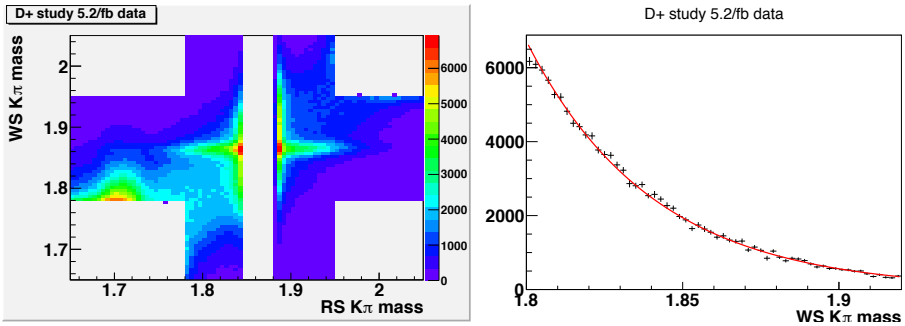

Figure 30: D^+ background in WS $K\pi$ mass plots. The left plot shows an excess of events at RS $m_{K\pi} = 1.7$ GeV, which can spill into the WS mass window used for the analysis. These events formed a clear mass peak when reconstructed as $D^+ \to K\pi\pi$. The right plot shows the D^+ versus WS $m_{K\pi}$ yield plot, with a red line for an exponential fit.

effect is negligible.

While it is possible to impose a lower limit on the RS $K\pi$ mass that would eliminate this background, it would also cut away signal. (The WS signal has a wide distribution when plotted with RS $K\pi$ mass.) Depending on how hard a D^+ cut is applied, around 5% of the signal would be lost. Since the assigned systematic error for this background is small (and might actually be zero), we decide not to apply that cut.

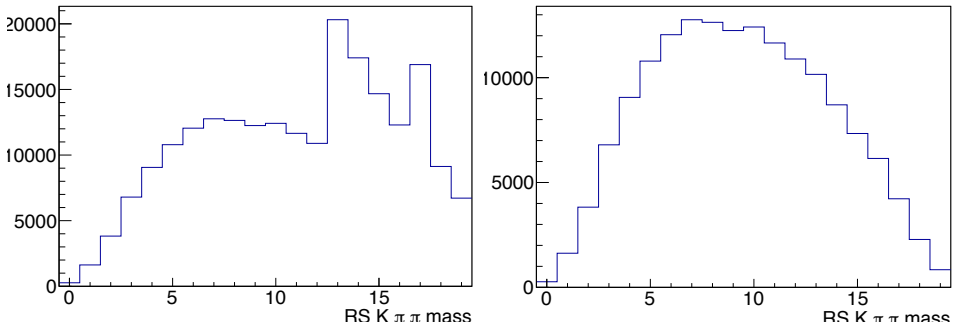

Figure 31: Fit number of D^+ for the twenty time bins used in the analysis. The left plot are the "raw" numbers per bin, the right plot is normalized for the varying width of the time bins.

The second was for D^0 that decay to modes other than $K\pi$. The used the full MC made by Angelo, Paola, and Paola. We obtain the number of background events relative to the RS $D^0 \to K\pi$ (which is also in that MC). This MC sample had 1.39% RS background and 2.35% WS background, per RS $K\pi$. We also get the distributions for the RS and WS mass plots. Those background fits are well described by an exponential fit. Fig. 33 shows the WS and RS scatter plot, and the fit for the D^+ background.

Fig. 34 shows the output of 800 Toy MC events, where we replace the appropriate amount of the combinatorial background (quadratic fit) with the exponential distributions from the partially reconstructed charm studies. We still see a shift of $|\Delta R/R| = 0.09\%$, consistent with zero. To be conservative, we will add this value in quadrature to the current errors.

4.2.3 $K\pi$ Lump at 1.83 GeV

Since we cannot currently explain the source of the "lump" in the RS $M_{K\pi}$ fits, the B-Group would prefer that we include a systematic uncertainty in case this "lump" is actually present in the WS fits. We observe a change in the number of RS events of $\Delta R/R = 0.34\%$ when the extra lump background is fixed to zero (instead of floating for all $K\pi$ fits). A systematic uncertainty of the same amount was added to the WS D^* yields for each time bin.

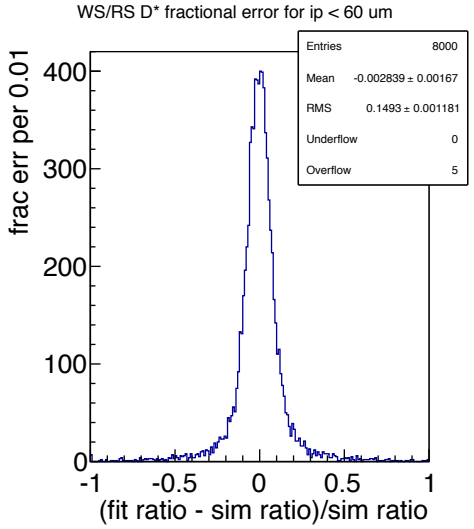

Figure 32: Generated 400 toy MC events, with entries for all 20 time bin ratios. The comparison is between the generated amount of signal in a particular simulation, and the analyzed value for that simulation. Based on the D^+ data studies, we replace an appropriate amount of the combinatorial background (quadratic fit) with the exponential distributions for $m_{K\pi}$.

4.2.4 Mass Difference

We do assign an additional uncertainty due to fixing the mass difference background power term from the time-summed fit. As a check, we changed the power term by $\pm 1\sigma$, based on the fit to the time-summed data, and then observed the change in the WS/RS ratio in each time bin compared to the best fit power term. The RS background caused a negligible change in the ratio, in particular because the signal-background is so high. The WS change in the ratio was on average $\Delta R/R = 0.80\%$. For the fit to the time-summed data, the ratio change was roughly a quarter of the uncertainty returned by the fitter.

4.2.5 Mis-assigned Background Correction

There is no additional systematic uncertainty due to correcting for mis-assigned RS D^*s that show up as background in the WS plots. Our kinematic and particle identification cuts greatly reduce this background, and the $K\pi$ mass distribution for this background only has slight curvature under the signal. The number of WS D^* (time-summed, $d_0 < 60$) for this analysis is 26276 ± 450. We set the MRS amplitude to zero for the WS $M_{K\pi}$ fits, and obtain 26772 ± 442. This is a difference of 496 events, or $\Delta N/N = 0.01888$. The uncertainty on that correction is about 1%, which is negligible compared to the (stat.+syst.) uncertainties from our fits.

4.2.6 Non-prompt D^* Correction

We do not assign any additional uncertainty due to correction for non-prompt D^*. The uncertainties in the fractions of the IP distributions, for $d_0 < 60$ and $d_0 > 60$, are included and propagated when we calculate the number of prompt D^*.

4.2.7 Detector charged track asymmetries

In CDF note 6391 [24], they measure the charge asymmetry in the detector. This will result in a difference in the efficiency of finding the charged pions used to tag the D^*. On page 26, they quote the charge asymmetry as being $A = \frac{N_+ - N_-}{N_+ + N_-} = 1$ % (within errors). So if we started with equal number of positive and negative tracks, we expect to reconstruct $N_- = \frac{1.01}{0.99} N_+$.

Also, the charged kaons and pions have different nuclear interactions. On page 75 of CDF note 8464 [23], the ratio of the efficiencies to reconstruct $K^+\pi^-/K^-\pi^+ = 1.0166$. Our measured WS/RS

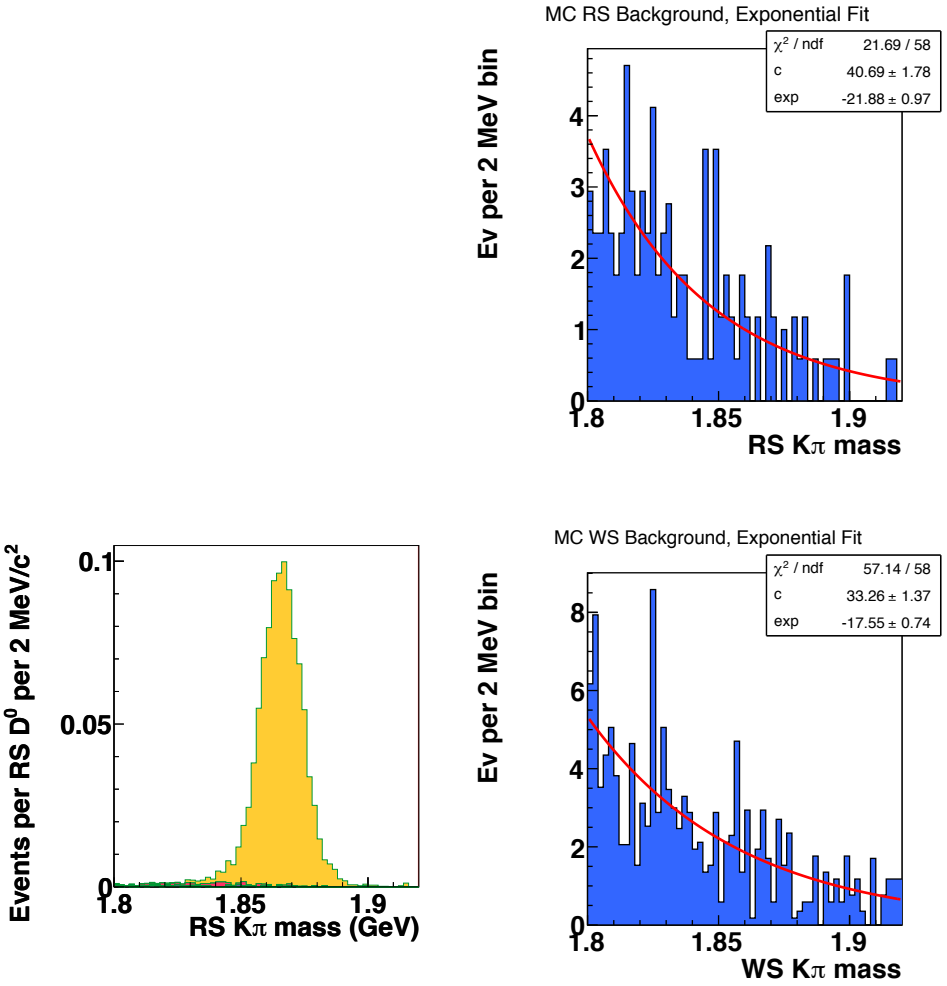

Figure 33: Partially reconstructed charm background from full MC. The left plot shows the RS D^0 signal (yellow) compared to the partially reconstructed charm background (all other colors, near the x-axis). The right plot shows the exponential fit to the RS and WS $K\pi$ background distributions.

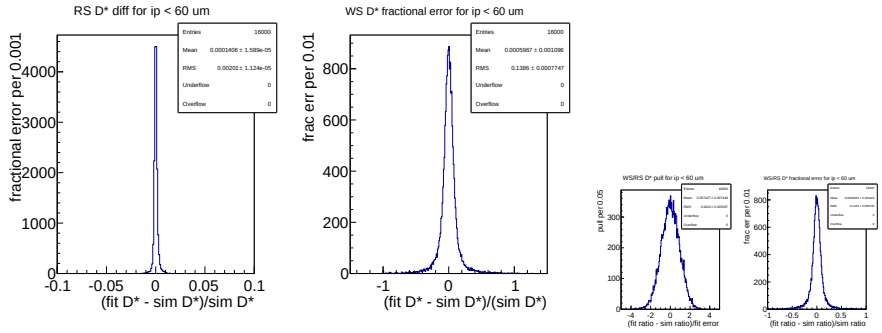

Figure 34: Generated 800 toy MC events, with entries for all 20 time bin ratios. The comparison is between the generated amount of signal in a particular simulation, and the analyzed value for that simulation. Based on the partially reconstructed charm studies, we replace an appropriate amount of the combinatorial background (quadratic fit) with the exponential distributions. The left plot is RS D^*, the middle plot is WS D^*, and the right plot is the ratio.

ratio is

$$R = (N_{D^{*+},D^0\to K^+\pi^-} + N_{D^{*-},D^0\to K^-\pi^+})/(N_{D^{*+},D^0\to K^-\pi^+} + N_{D^{*-},D^0\to K^+\pi^-})$$

If we assume that we started with equal numbers of mesons and anti-mesons, then

$$\Delta R/R = (1.0166 + \frac{1.01}{0.99})/(1 + (1.0166)(\frac{1.01}{0.99})) - 1 = -0.016\%$$

This systematic is added for each ratio uncertainty, but is negligible compared to the other systematic errors.

4.3 Time-Dependent Ratio

The ratio of WS to RS decays as a function of time is given in Eq. 1. Fig. 35 shows the distribution and the fits. The fit parameters are summarized in table 6. Keep in mind that the mixing parameters are heavily correlated, so don't use the parameter uncertainties without considering the covariance. The best fit point has an unphysical value for x'^2 but it is within statistical uncertainty with 0.

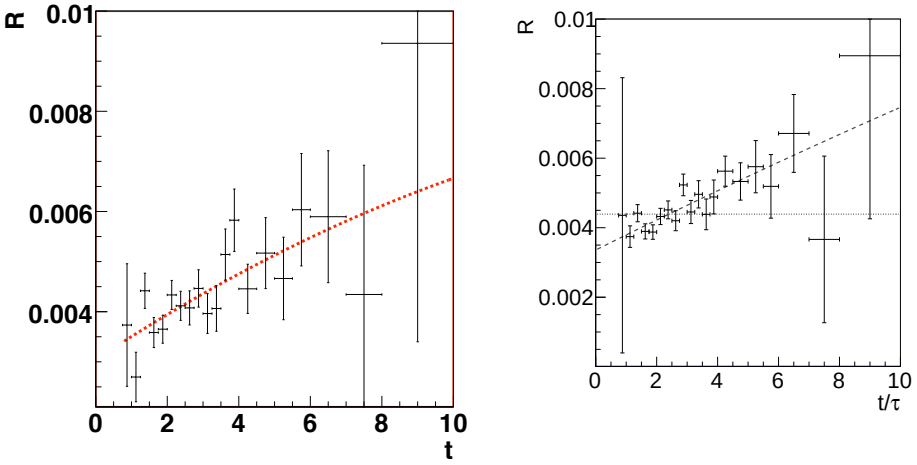

Figure 35: The decay time dependence of the WS/RS ratio of prompt D^*, for the previously published 1.5/fb result (left) and the full data set (right). The dotted horizontal line is the best fit assuming no-mixing. The dashed line is the best fit to data, using Eq. 1 and allowing $x'^2 < 0$.

Experiment	$R_D(10^{-3})$	$y'(10^{-3})$	$x'^2(10^{-3})$	Fit χ^2
Best fit (old)	3.04 ± 0.55	8.54 ± 7.55	-0.11 ± 0.35	19.17
Physical (old)	3.22 ± 0.23	6.02± 1.4	0	19.30
No-Mix (old)	4.15 ± 0.10	0	0	36.77
Best fit	3.36 ± 0.43	7.52 ± 5.60	-0.067 ± 0.270	17.40
Physical	3.46 ± 0.17	6.13± 1.08	0	17.46
No-Mix	4.39 ± 0.08	0	0	47.56

Table 6: Mixing parameters from the ratio fit. The values at the top of the table are the previous blessed numbers with $1.5fb^{-1}$. The values at the bottom of the table are now. The correlation between y' and x'^2 is -0.982.

4.4 Interpretation of the results

We can ask if the results are consistent with the hypothesis that there is no mixing. We will use three different measures. They are described in more detail in CDF note 8879. The different methods came

up with approximately the same significance for no-mixing for the previous blessed result, so we use all three as a cross-check.

4.5 Bayesian contours

We calculate the Bayesian probability that a particular set of values for (y', x'^2) are consistent with our ratio plot. We use the χ^2 of the fit, integrate over the mixing parameter R_D (as a nuisance parameter), and assume a prior uniform for y' and x'^2. We then generate contours containing the highest probability points, such that the region enclosed corresponds to n Gaussian σ

Fig. 37 shows the Bayesian contours for the most recent result. (Fig. **??** shows the Bayesian contours for the published 1.5/fb result.) In the left plot, the highest probability contour that excludes the no mixing point is equivalent to $5.xx\sigma$. In the right plot (restricted to the physically allowed values), no mixing is excluded at $5.xx\sigma$.

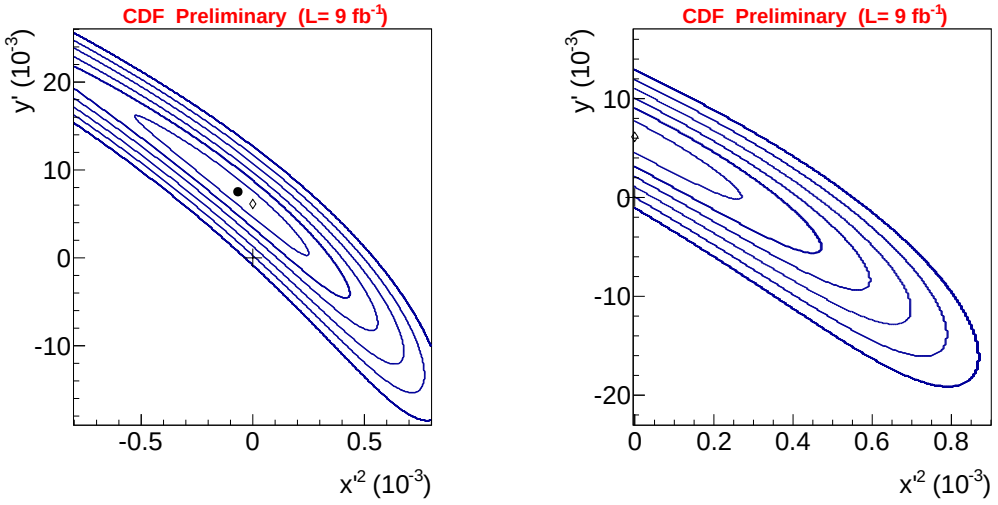

Figure 36: Bayesian contours from data, the posterior probabilities equivalent to 1 through 6 Gaussian sigmas (line contours). The left plot has the $y' - x'^2$ parameter space, the right plot is restricted to the physically allowed region ($x'^2 \geq 0$). The black dot is the best fit. The open diamond is the best fit point in the physically allowed region. The cross shows the no-mixing point.

4.6 P-Value

During the process to write the previous paper [4], the Godparent committee approved a procedure to test the Frequentist p-value. A toy model is made of our final ratio plot for prompt D^*. The generated ratio points are assumed to have a Gaussian distribution, with the width equal to our data error bars, and a mean at the (best data fit) no-mixing value. For each toy model generated, we make mixing (quadratic) and no-mixing (constant value) fits. The difference in χ^2 between those fits is calculated. We then determine how many of those models have $\Delta\chi^2$ greater than or equal to what we observe with data.

(This test has not been completed at the time of the pre-blessing, and will take time to finish. We plan to get the plot ready before the blessing.)

4.7 χ^2 difference

The last check we make is to use the difference in χ^2 between the no-mixing point and the best fit (or the best fit in the physically allowed region). This technique to used often in other analyses, but usually without a description of the method.

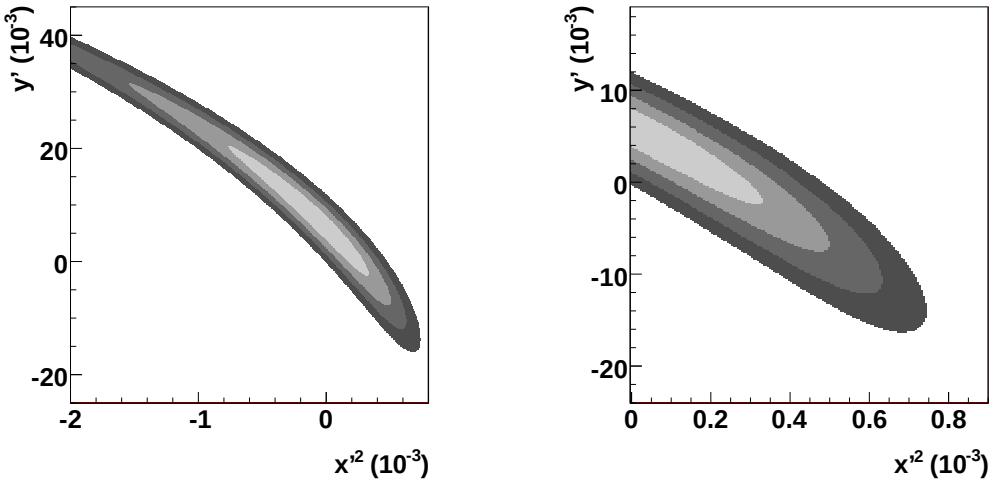

Figure 37: Bayesian contours from the 1.5/fb result. he posterior probabilities equivalent to 1 through 4 Gaussian sigmas (shaded regions) are drawn. The left plot has the $y' - x'^2$ parameter space, the right plot is restricted to the physically allowed region ($x'^2 \geq 0$). The black dot is the best fit. The open diamond is the best fit point in the physically allowed region. The cross shows the no-mixing point.

If we have two fit functions which are similar, and differ by n additional parameters, we assume that the difference in χ^2 has a χ^2 distribution with n degrees of freedom. The statistical contribution to the χ^2 will be the same for both fits, and cancel in the difference, leaving the systematic difference of the two functions. For this analysis, the no-mixing fit is a constant, while the best fits is a 2nd order polynomial. We can then compute the probability that a χ^2 distribution with 2 degrees of freedom will have a value the same or worse than the measure $\Delta\chi^2$.

Looking at table 6, $\Delta\chi^2 = 30.16$ for the best fit, and $\Delta\chi^2 = 30.10$ for the best fit in the physically allowed region. This corresponds to $5.xx\sigma$ and $5.xx\sigma$, respectively. (To reach the 5σ "observation" level, we would need $\Delta\chi^2 \geq 28.8$.)

4.8 Future plans

There were some suggestions made by the B-Group during the Full Status review and the pre-PreBlessing.

- A study of systematic effects versus time needs to be completed. If there is correlation between time bins, the errors will need to be adjusted to account for that.
- Currently we are using the center of the time bins. The suggestion is to use the event-weighted position for each time bin.
- For the 0p data set, there were a number of data files that were not processed, due to various errors. After some investigation, it may be possible to recover these events before the blessing. A rough estimate is that we may have up to 50% more data for the x0p set.
- Still a few places where numbers need to be updated. For example, the no-mixing significance is over 5 sigma, but we want to get the actual number. (That will depend if we recover more 0p data, as we will have to rerun parts of the analysis.)
- In general, would be useful to go over this CDF note a few more times, for clarity.

In the future, we want to make the measurement allowing CP violation. This will most likely require making two distinct ratio fits, by separating the charge-conjugate decays. Differences in the

mixing parameters for the two fits would be a signal for CP violation. This will require correcting for any detector asymmetries for charged kaons and pions. Subtle effects, like the trigger or various backgrounds, will need to be investigated.

All current experimental results are consistent with no CP violation for neutral charm mesons.

We are considering processing the more recent v90 BStNtuples for the CP violation analysis.

A Time-Independent $M_{K\pi}$ Fits

This appendix shows the time-summed $M_{K\pi}$ fits, for events with $d_0 < 60\mu$m. The dark blue curve is the signal + background fit, the light blue is background. "Time 0" means the time-summed histograms. Each bin of "MD" is 0.5 MeV window of ΔM.

The signal shape is the same for all plots, although the amplitude is a floating variable.

Appendix A: Time-independent $M_{K\pi}$ Distributions

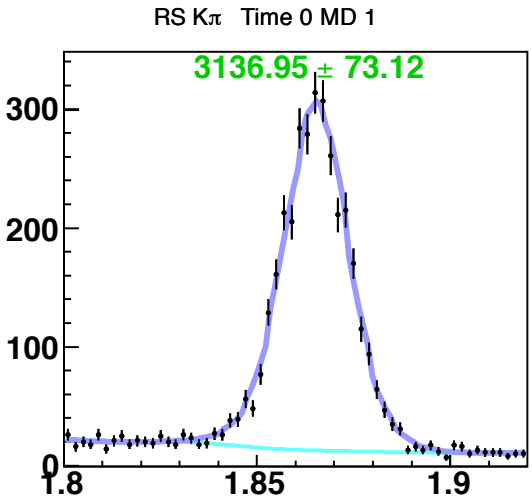

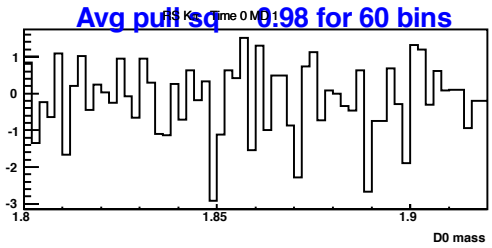

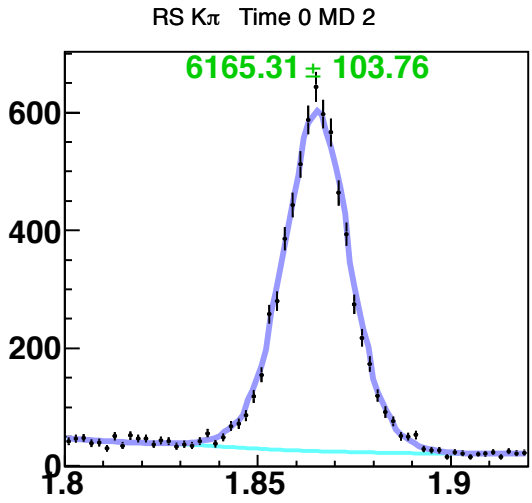

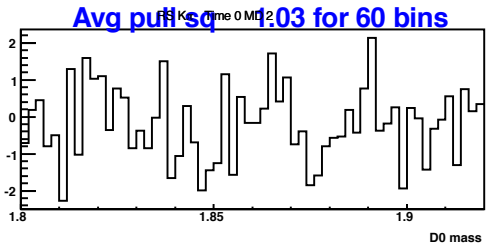

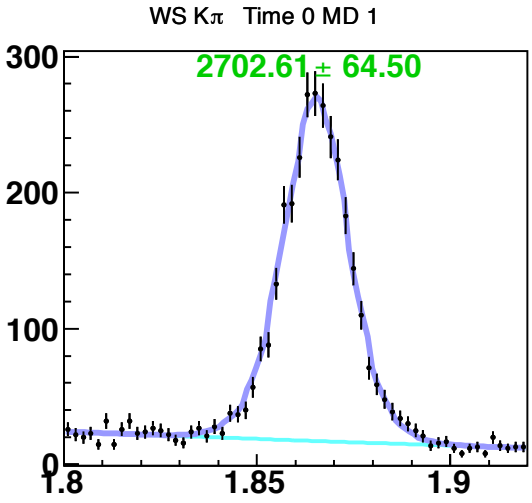

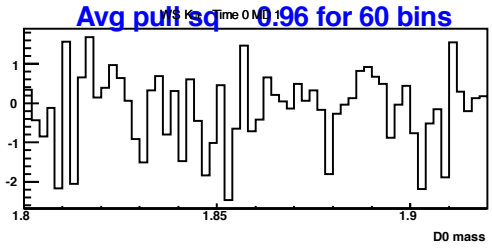

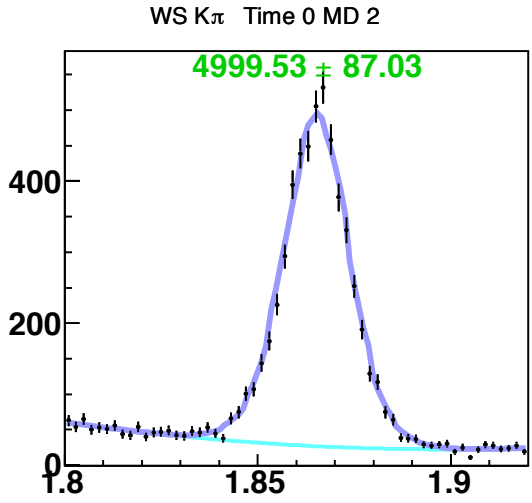

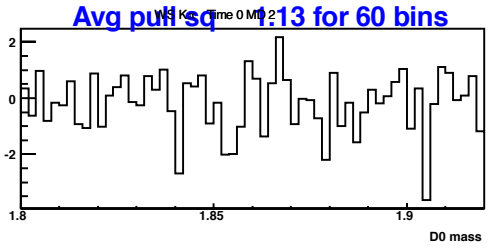

Appendix A: Time-independent $M_{K\pi}$ Distributions

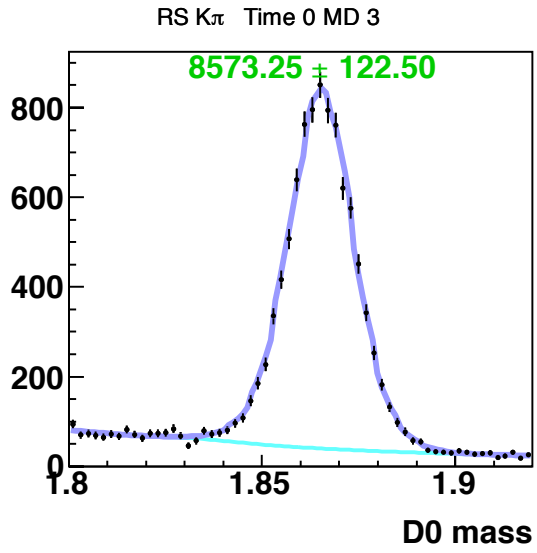

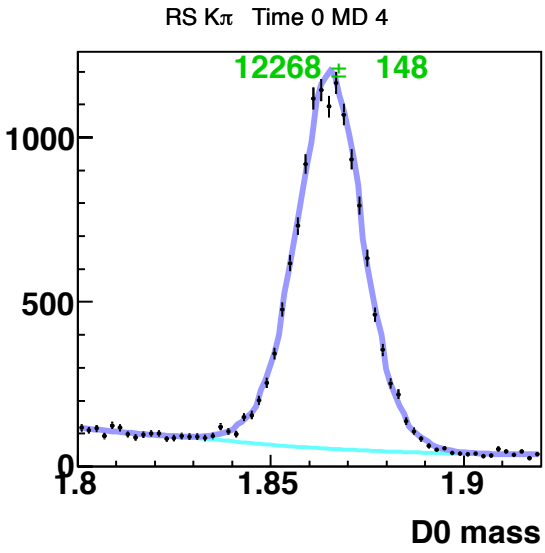

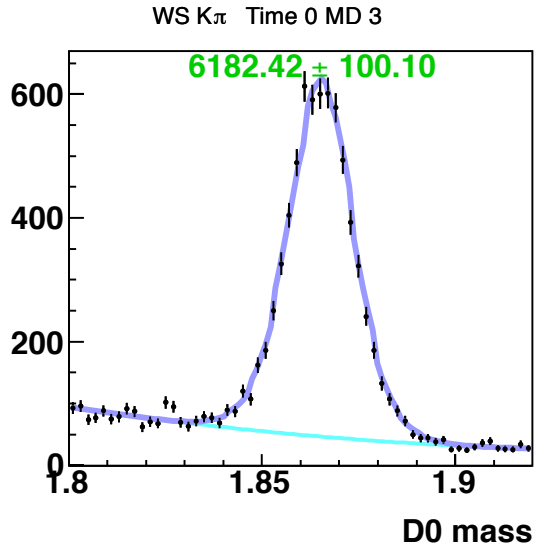

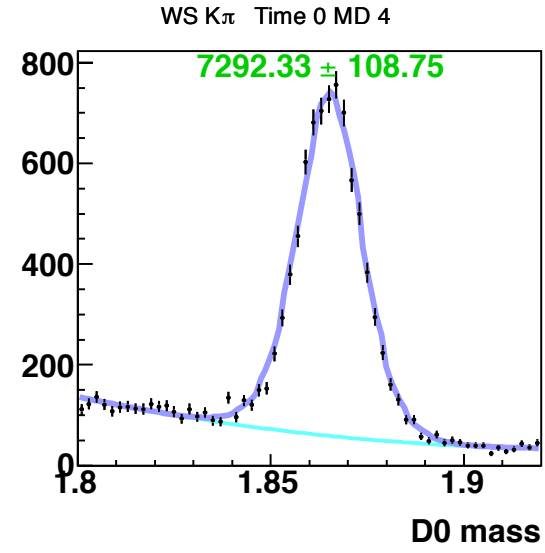

Appendix A: Time-independent $M_{K\pi}$ Distributions

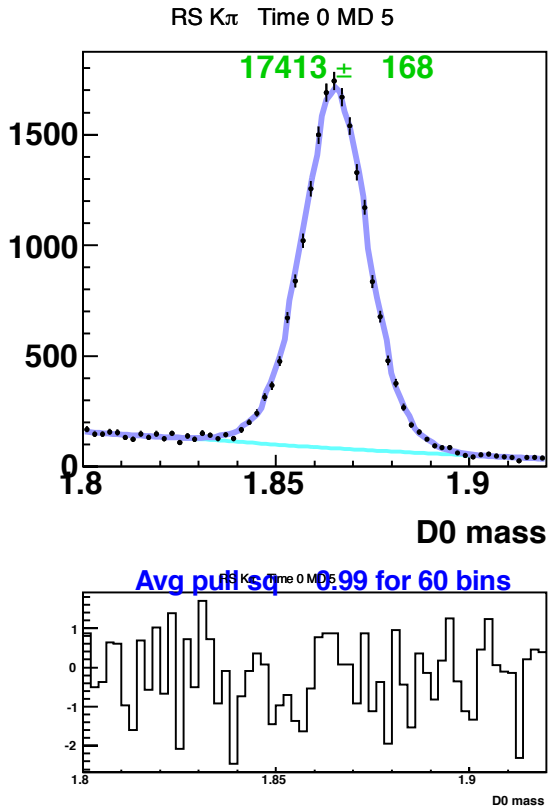

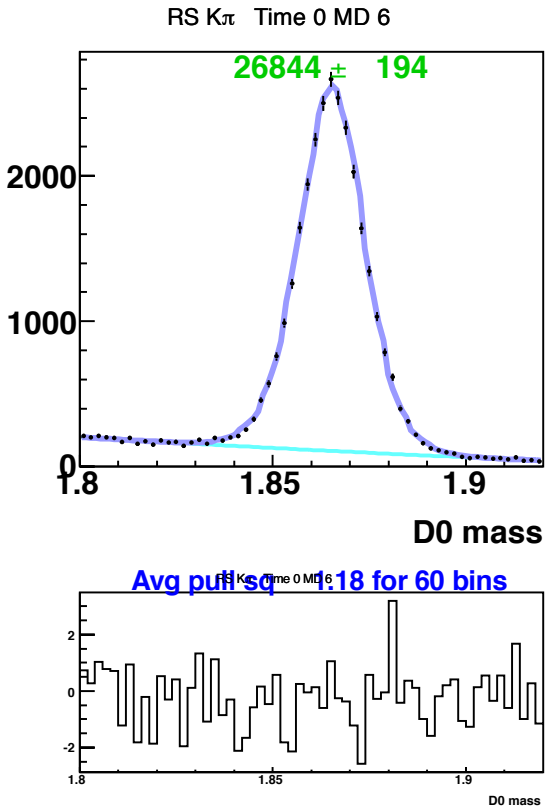

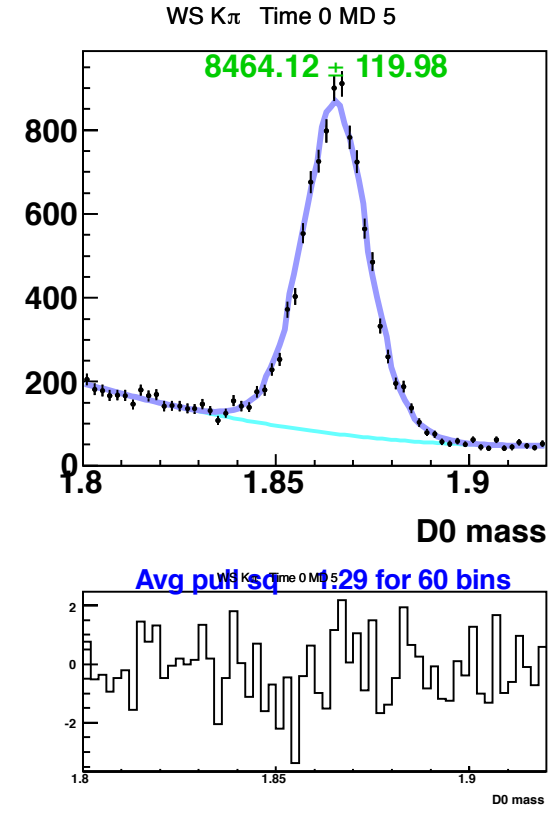

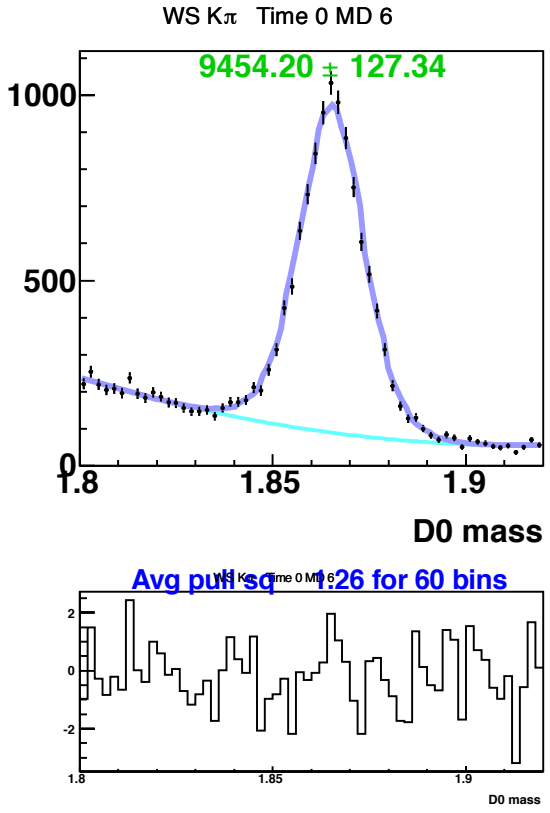

Appendix A: Time-independent $M_{K\pi}$ Distributions

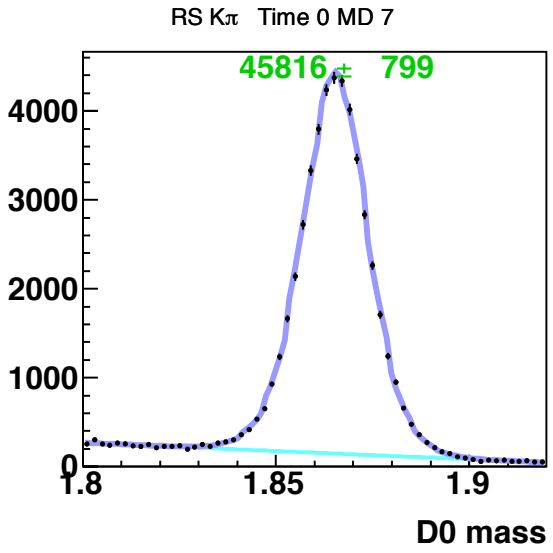

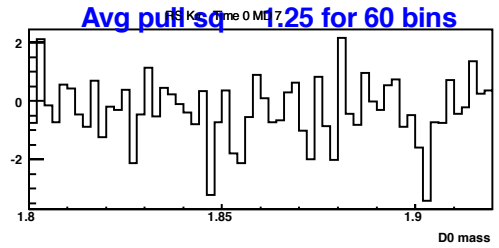

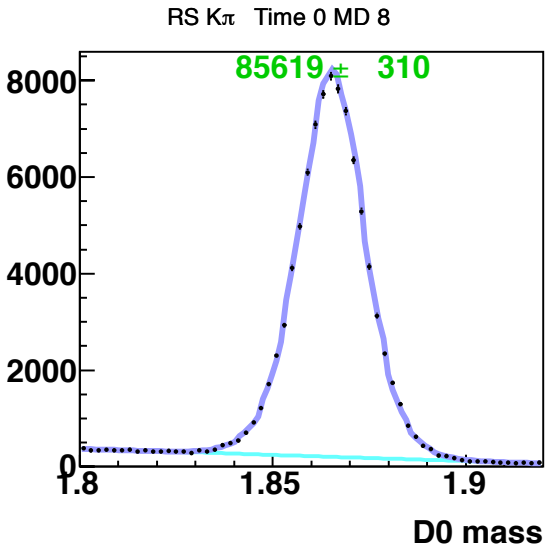

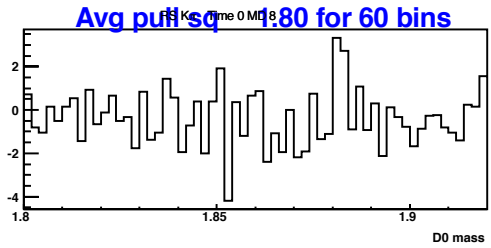

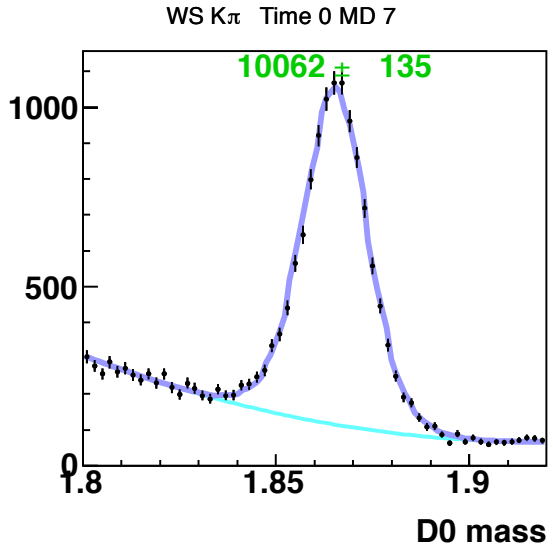

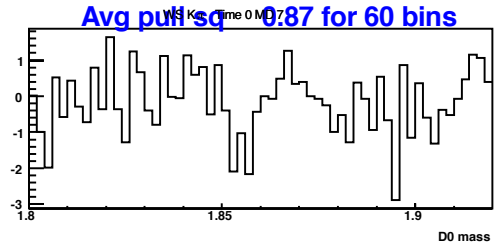

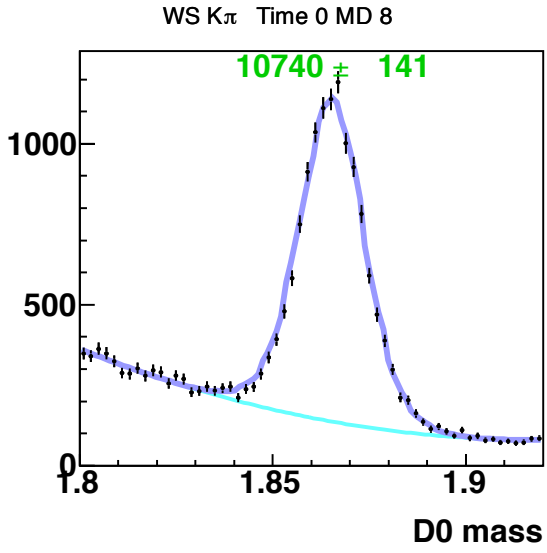

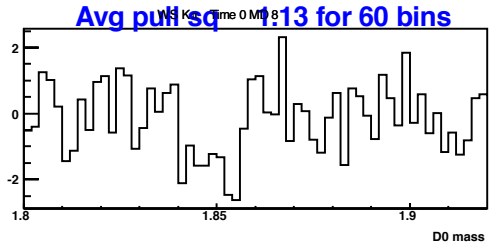

Appendix A: Time-independent $M_{K\pi}$ Distributions

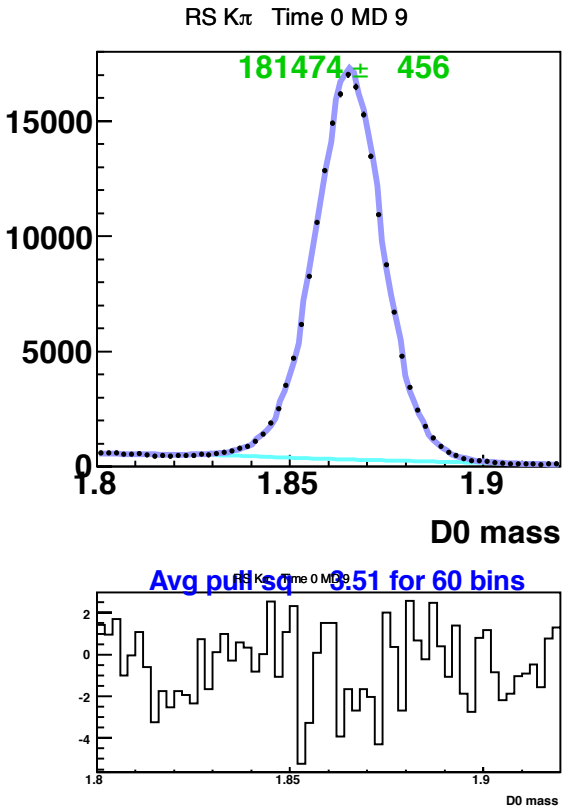

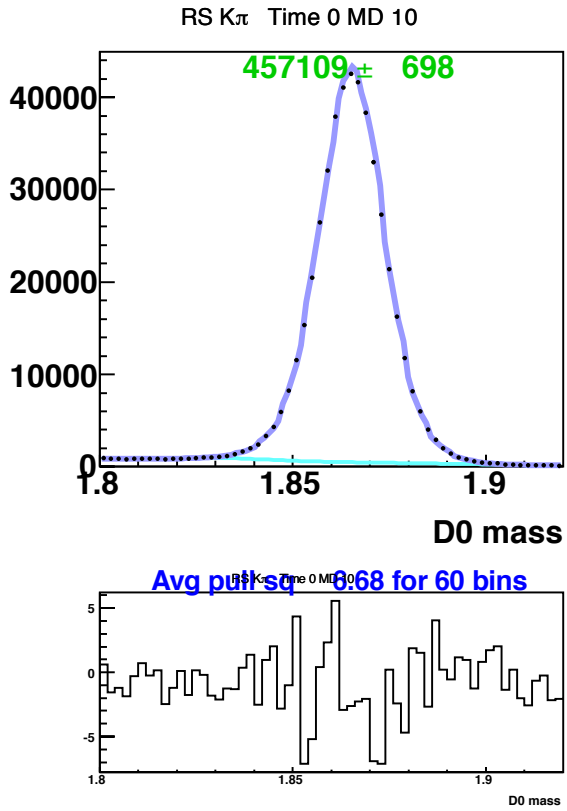

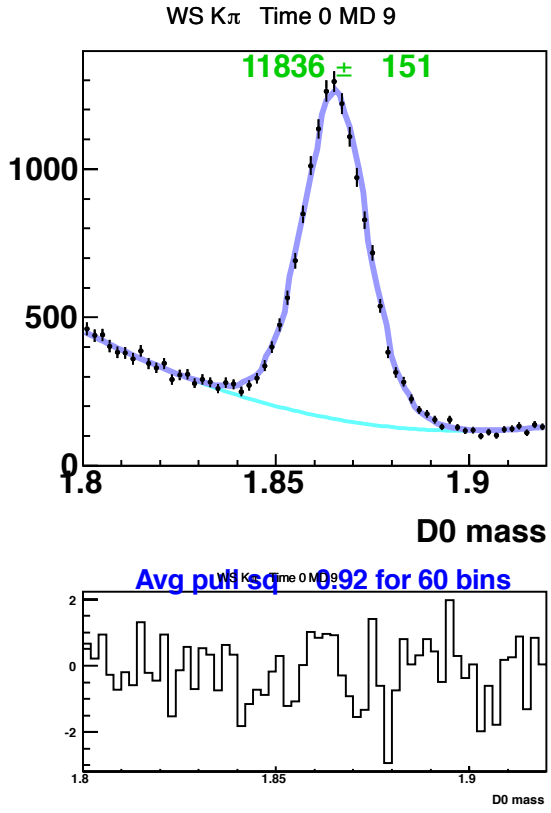

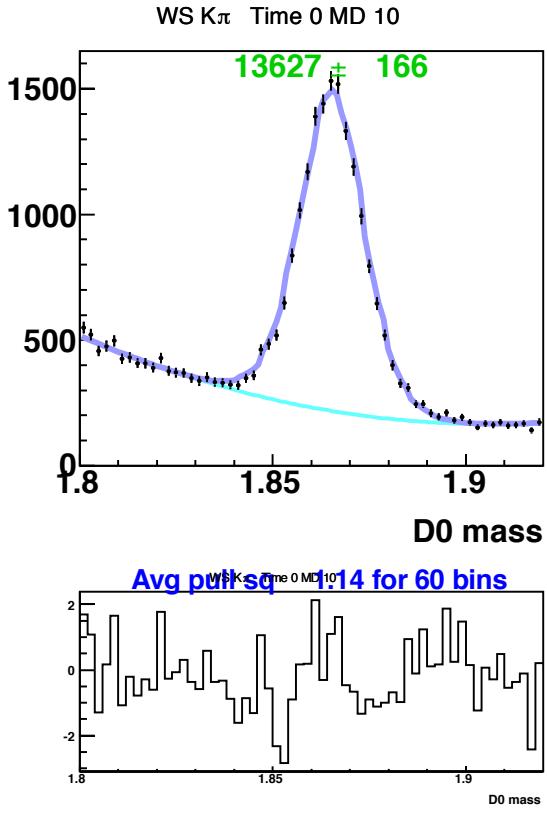

Appendix A: Time-independent $M_{K\pi}$ Distributions

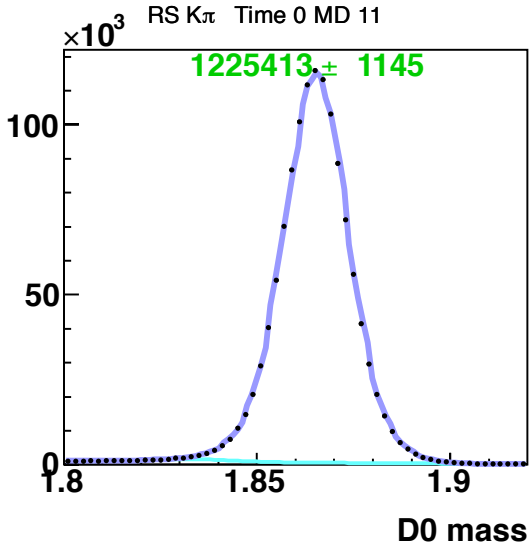

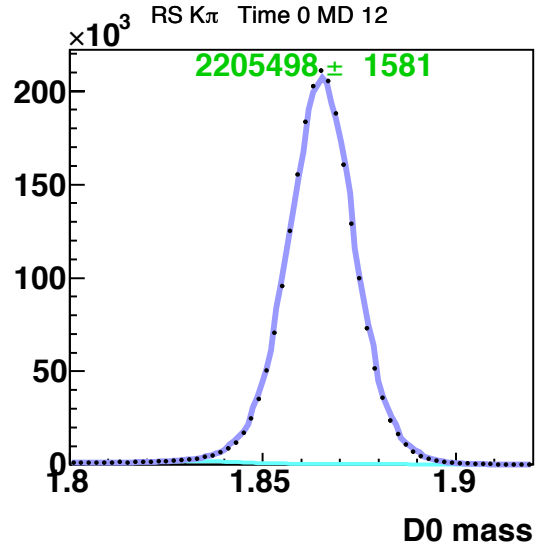

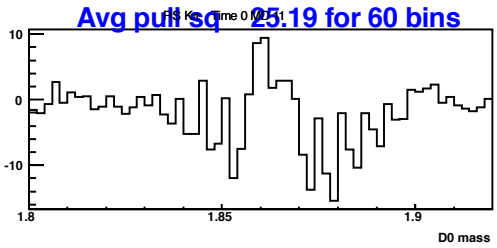

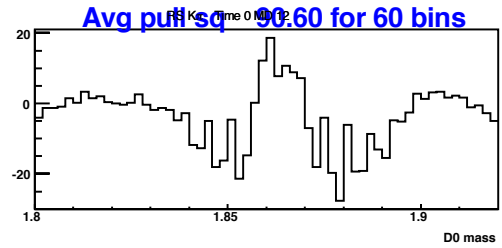

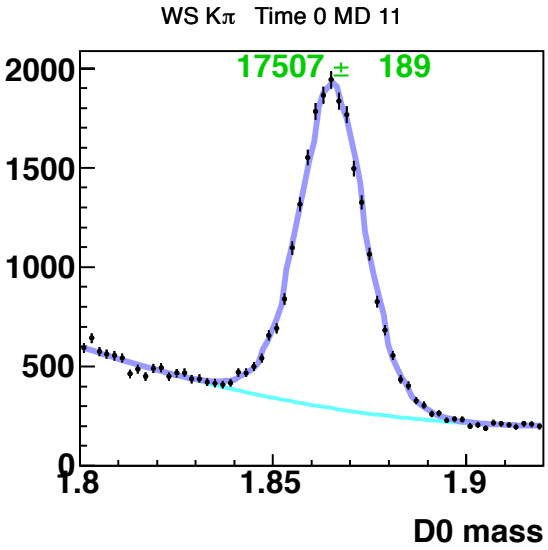

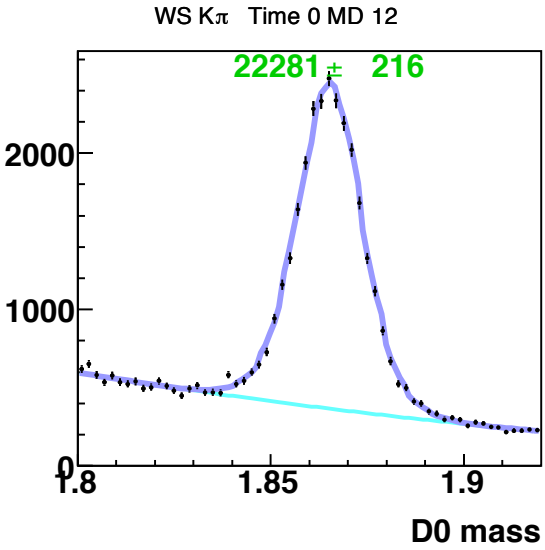

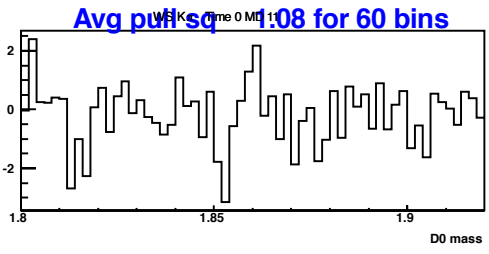

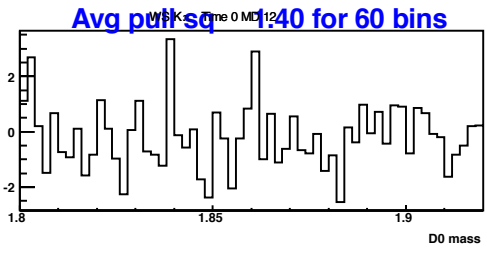

Appendix A: Time-independent $M_{K\pi}$ Distributions

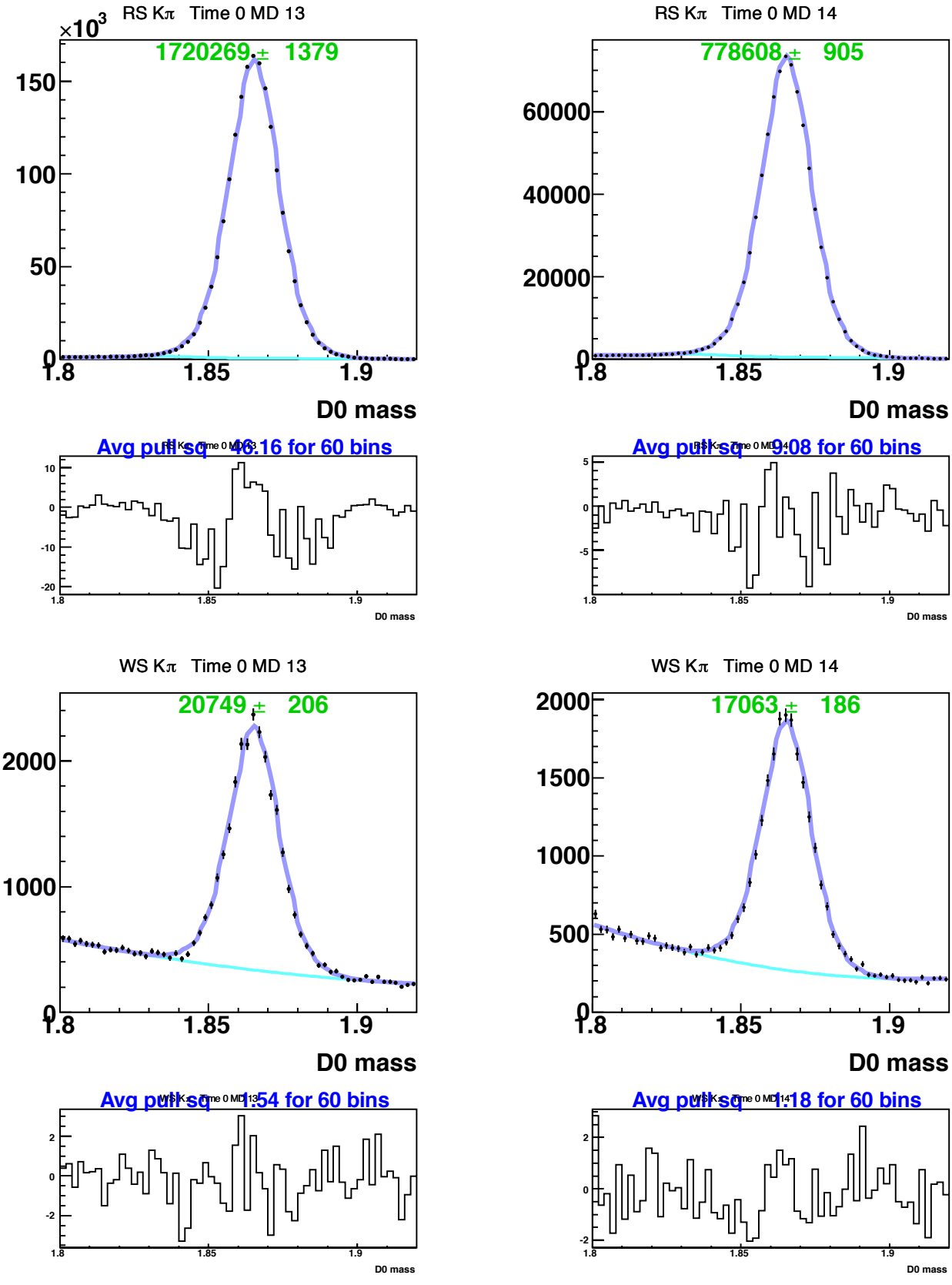

Appendix A: Time-independent $M_{K\pi}$ Distributions

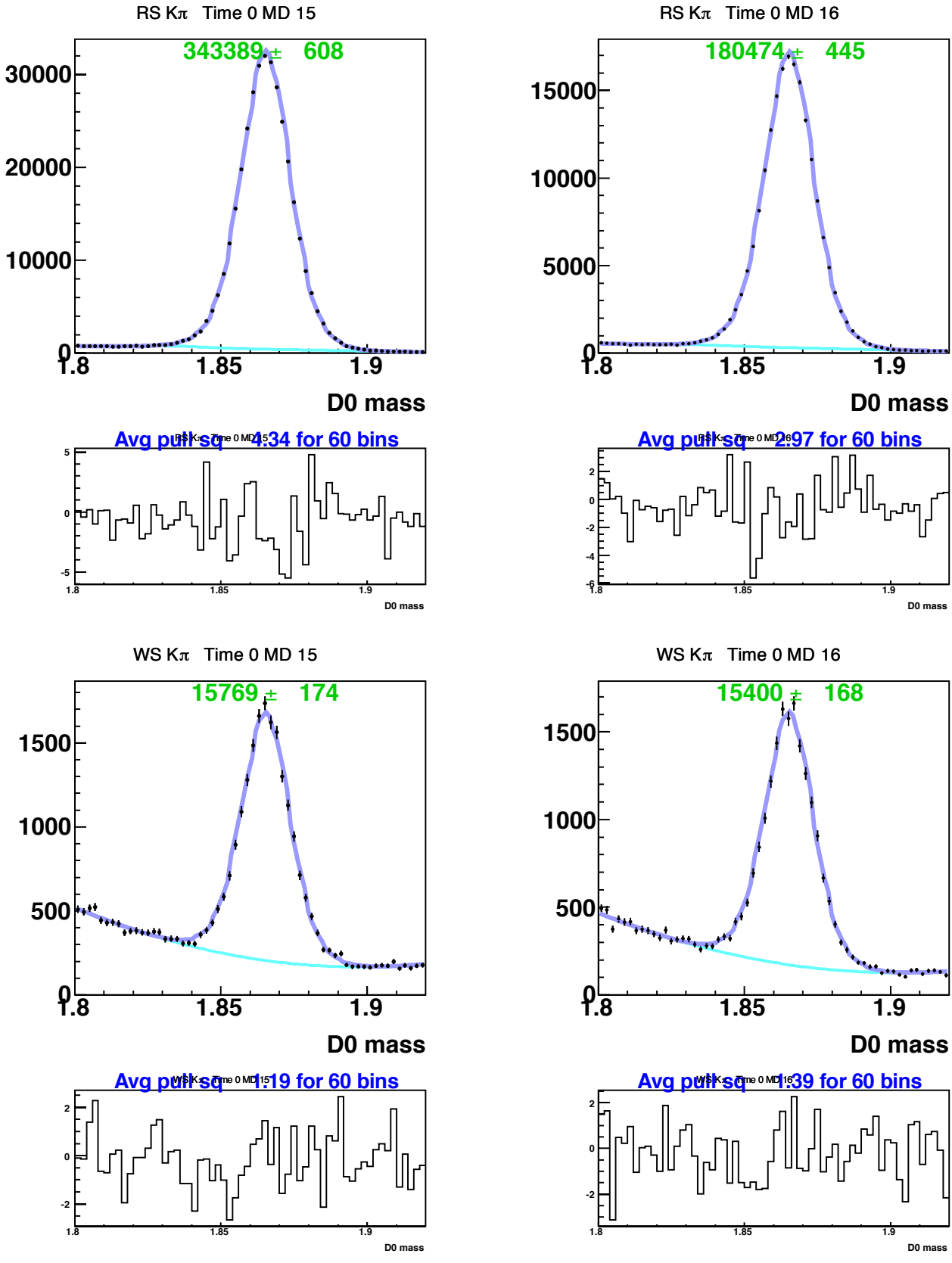

Appendix A: Time-independent $M_{K\pi}$ Distributions

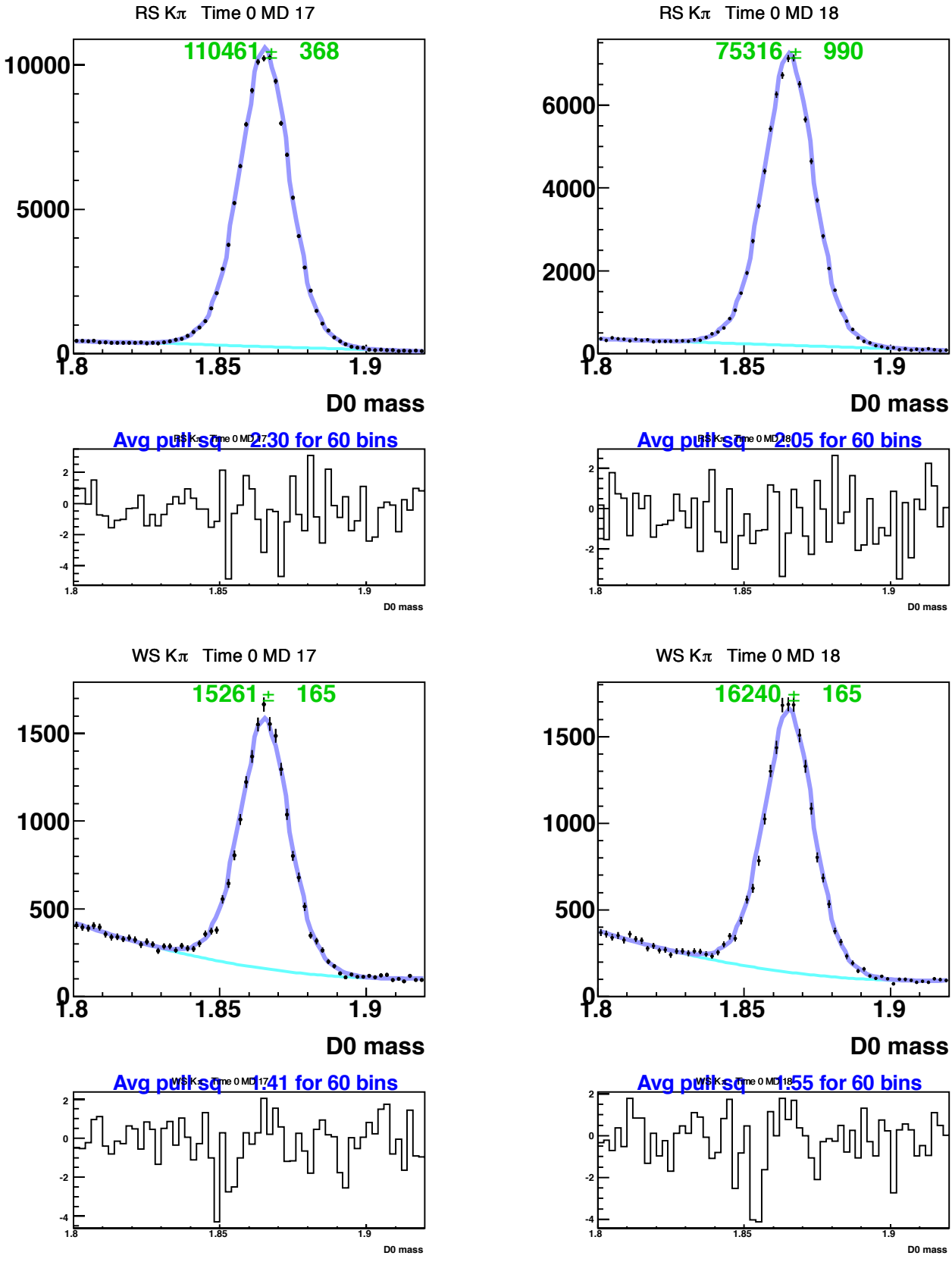

Appendix A: Time-independent $M_{K\pi}$ Distributions

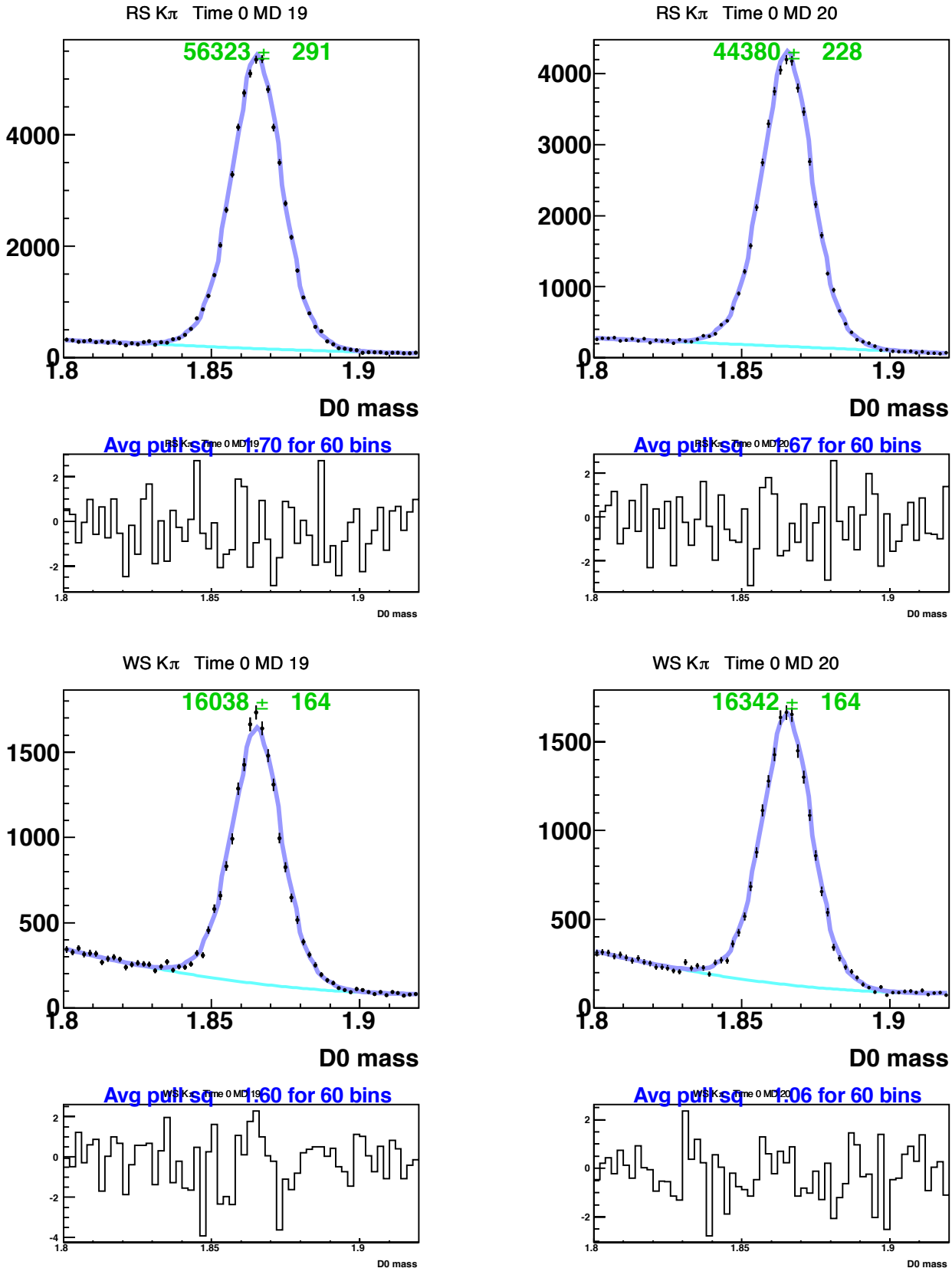

Appendix A: Time-independent $M_{K\pi}$ Distributions

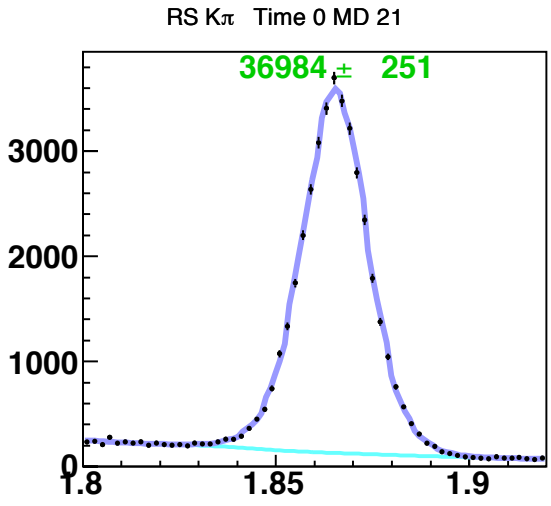

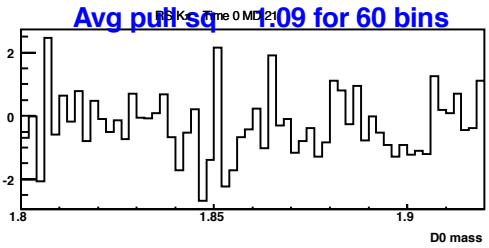

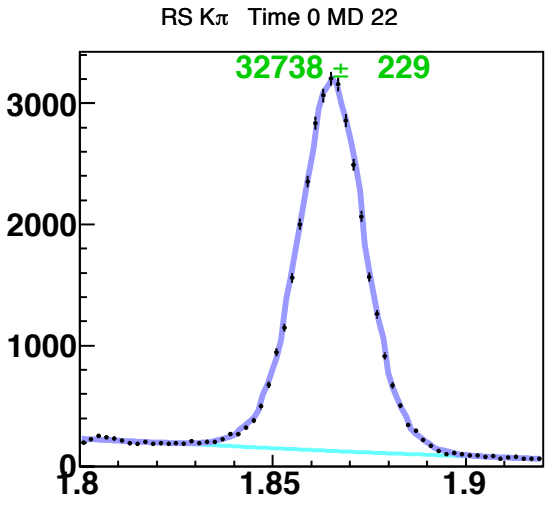

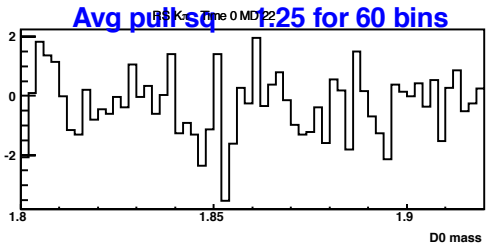

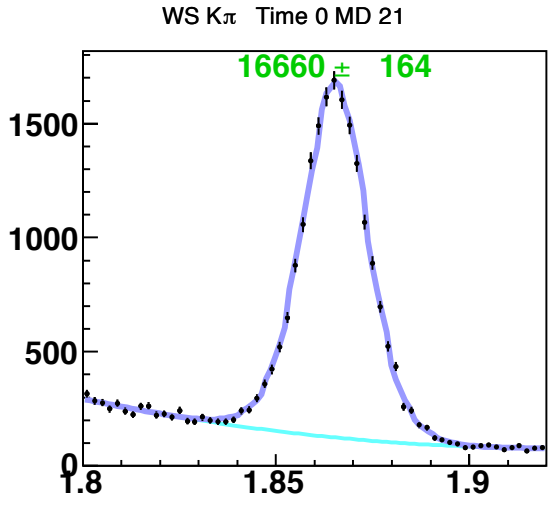

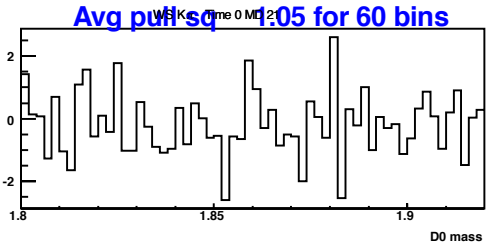

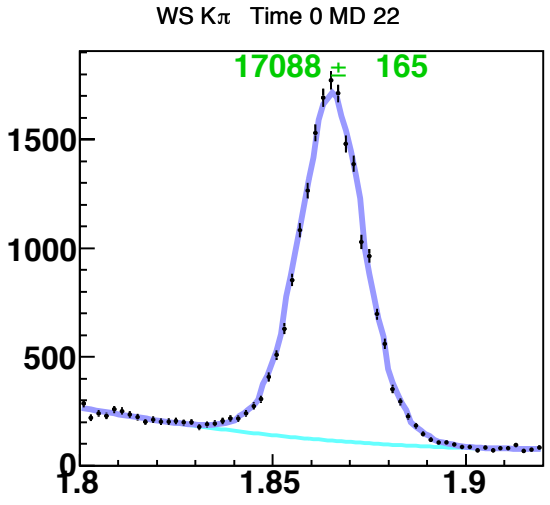

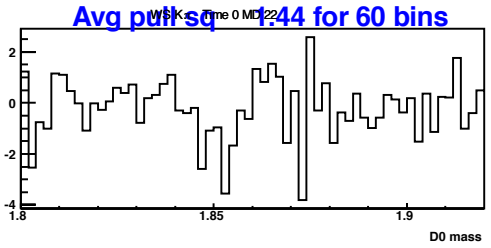

Appendix A: Time-independent $M_{K\pi}$ Distributions

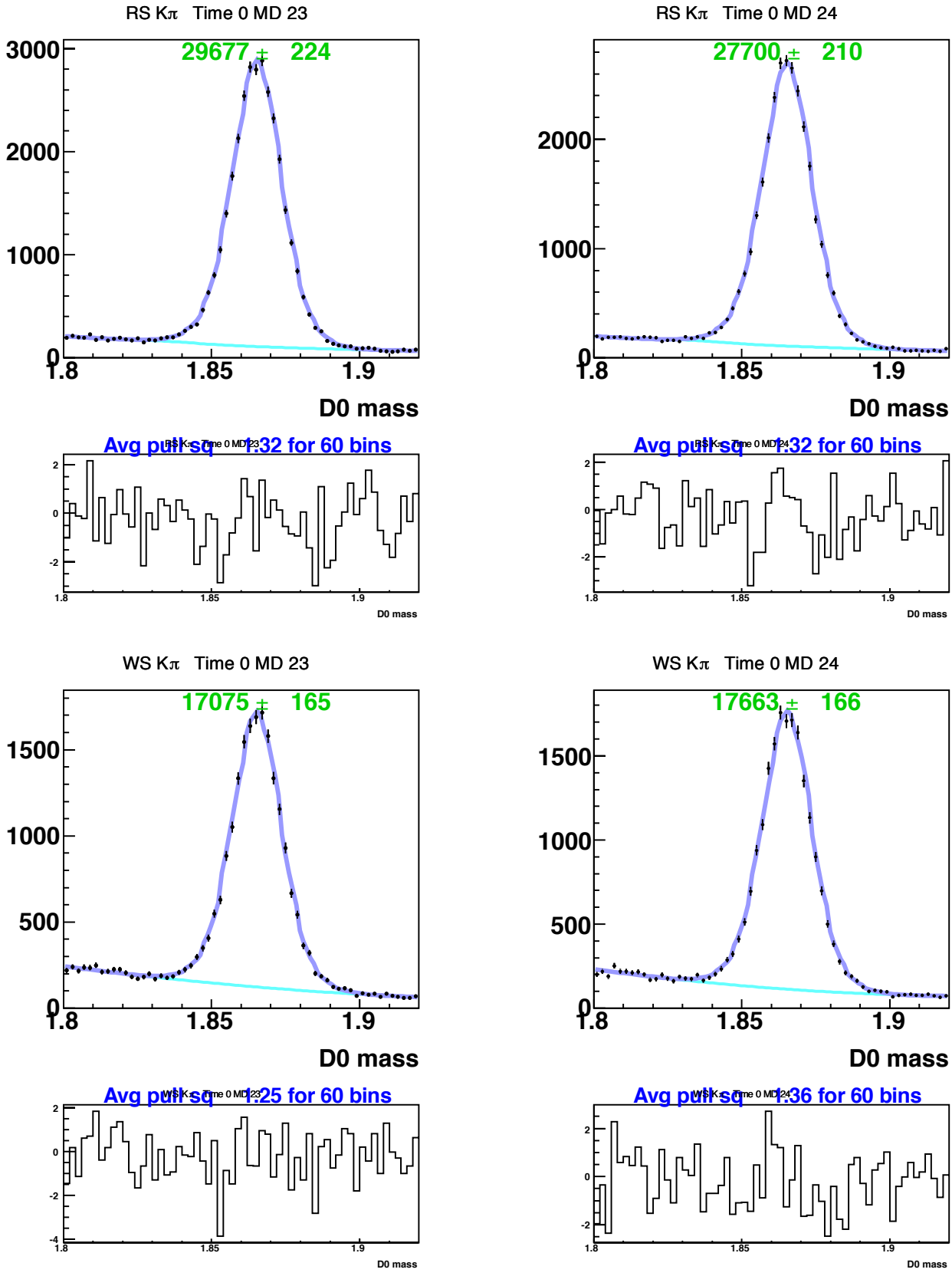

Appendix A: Time-independent $M_{K\pi}$ Distributions

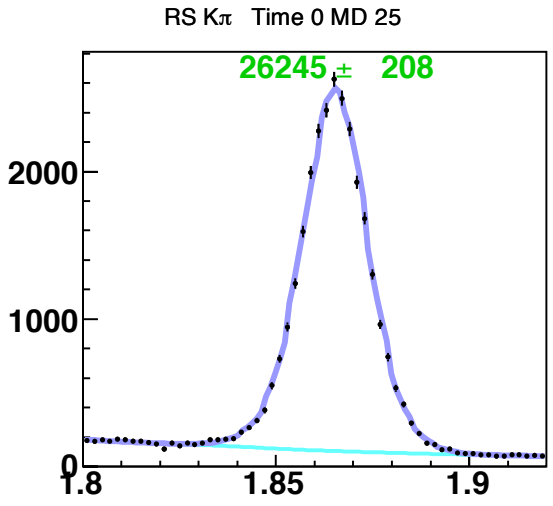

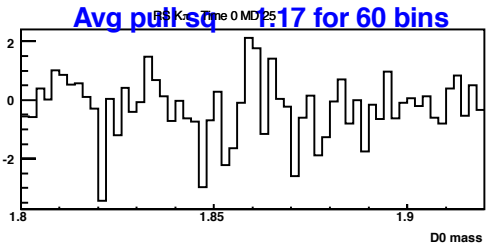

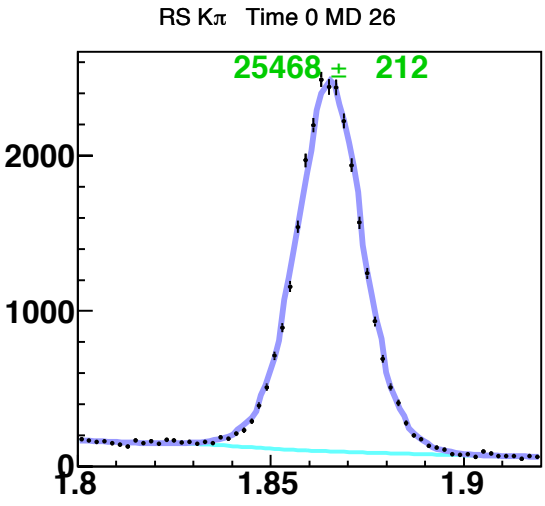

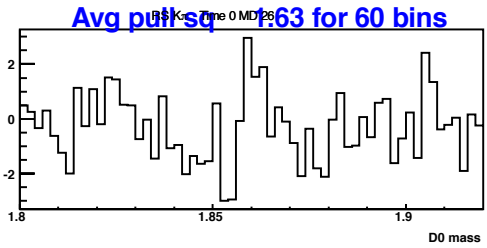

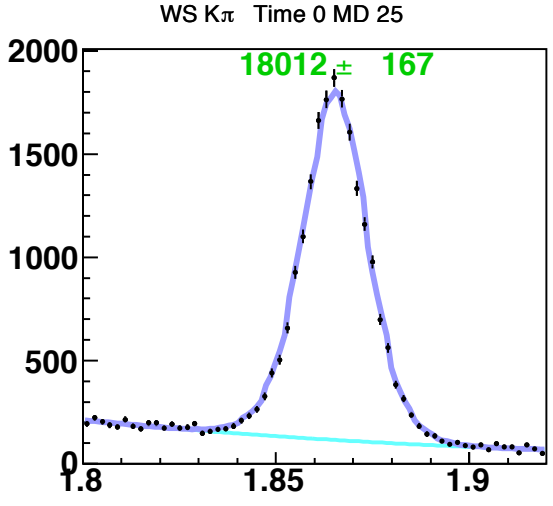

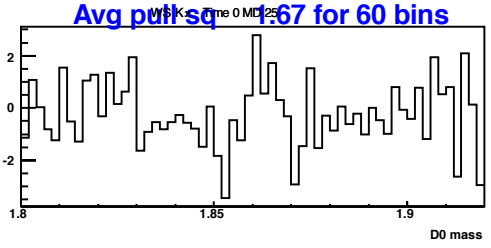

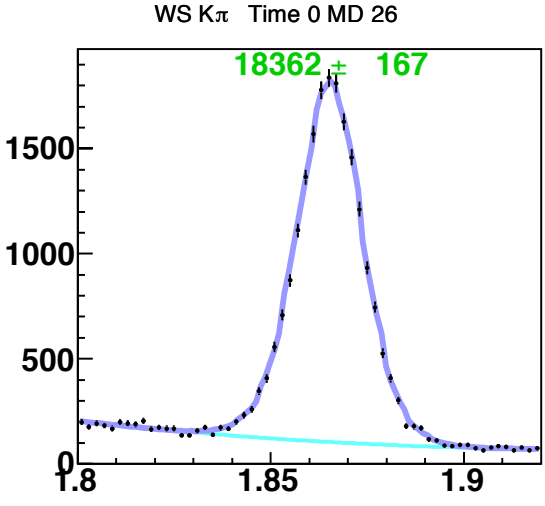

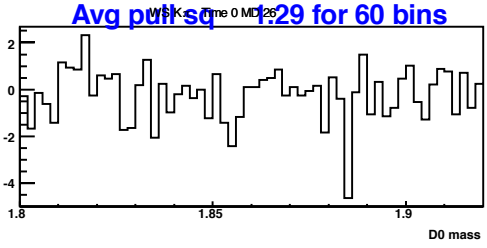

Appendix A: Time-independent $M_{K\pi}$ Distributions

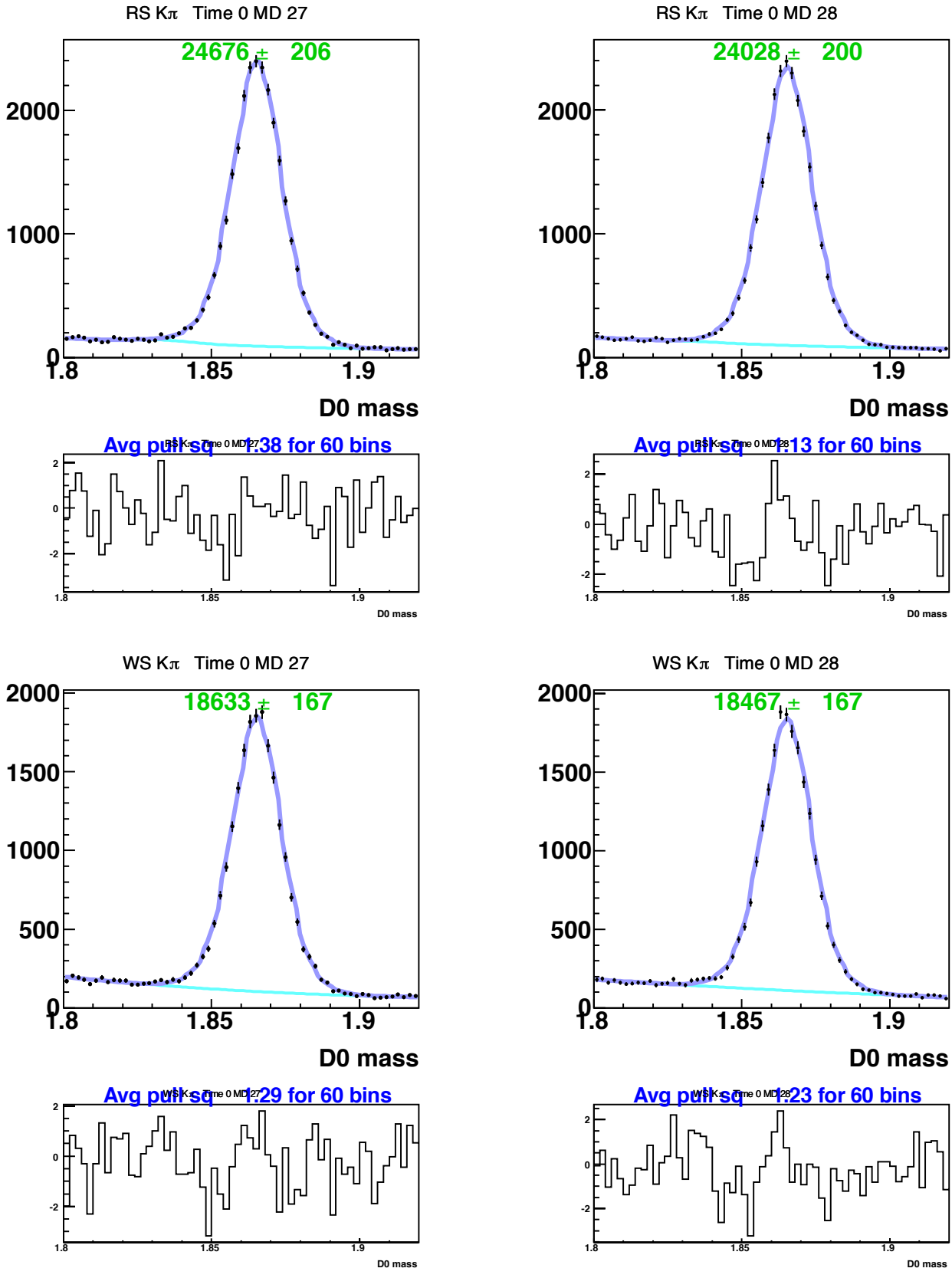

Appendix A: Time-independent $M_{K\pi}$ Distributions

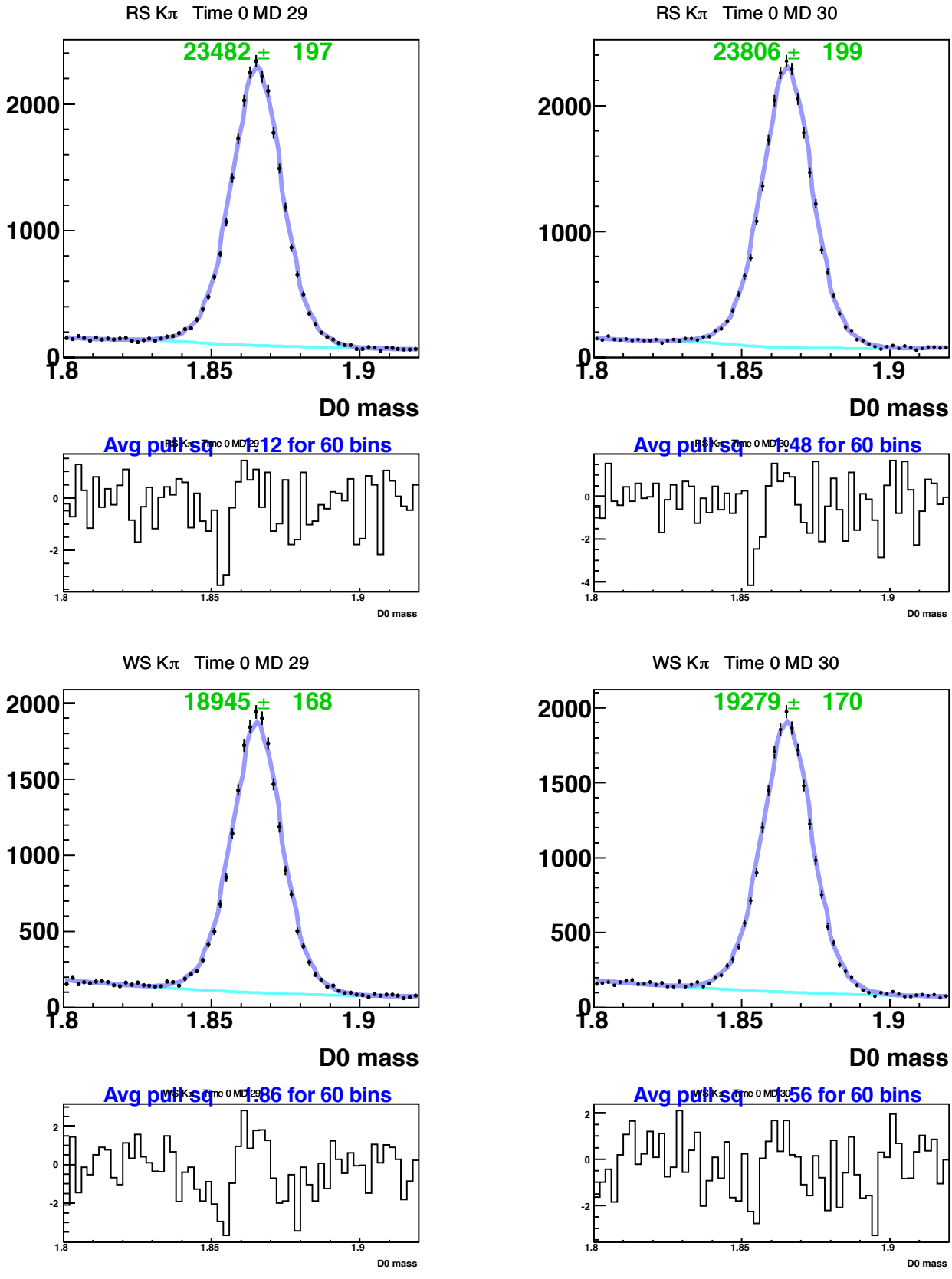

Appendix A: Time-independent $M_{K\pi}$ Distributions

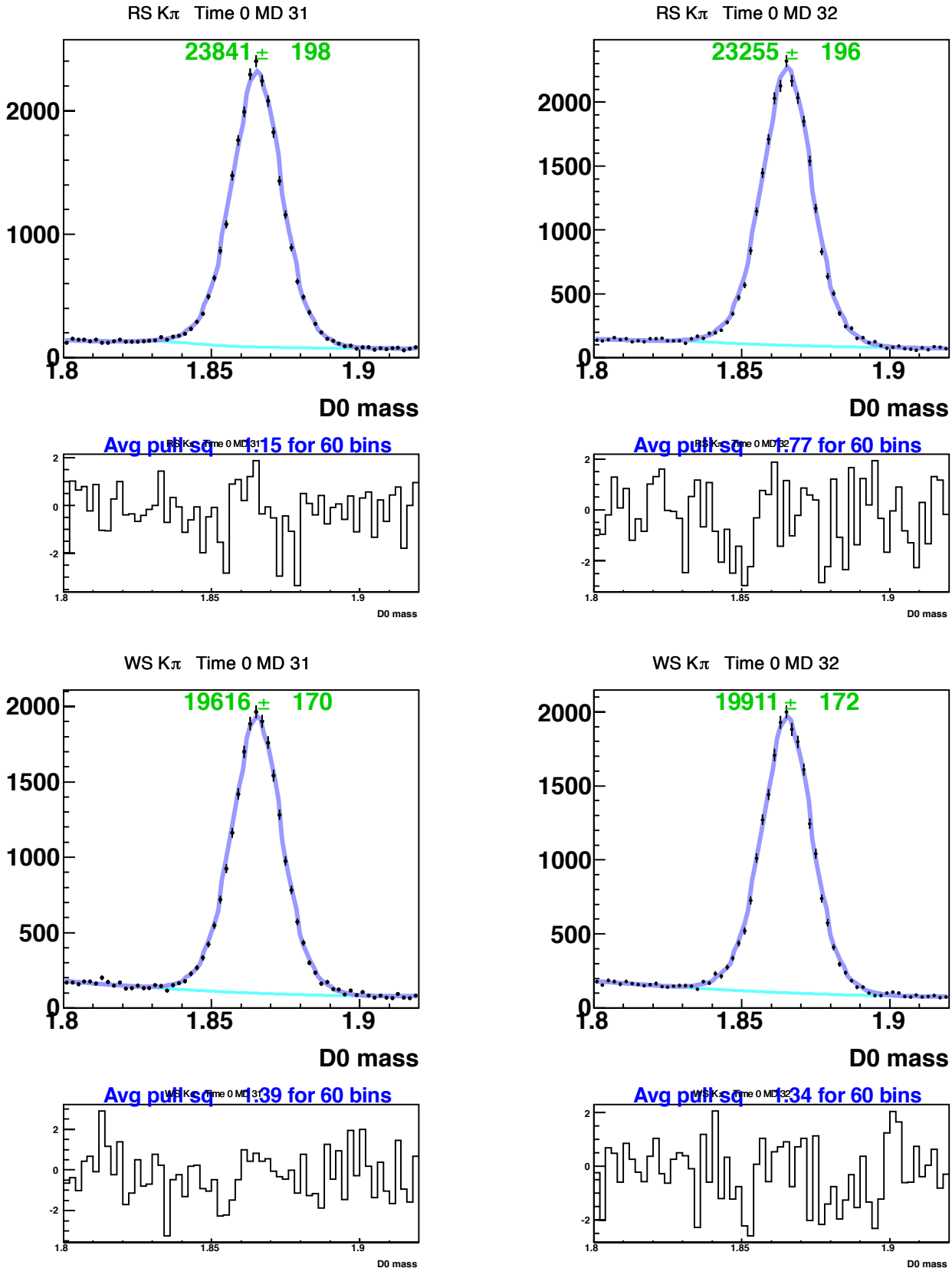

Appendix A: Time-independent $M_{K\pi}$ Distributions

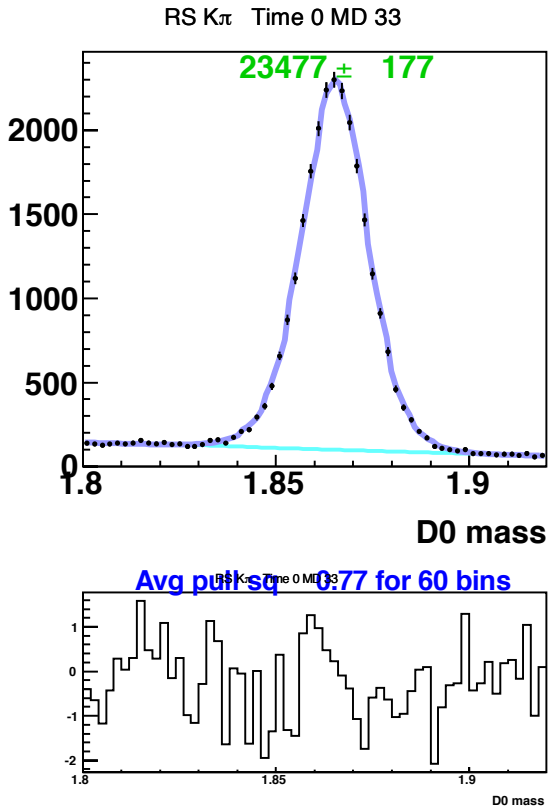

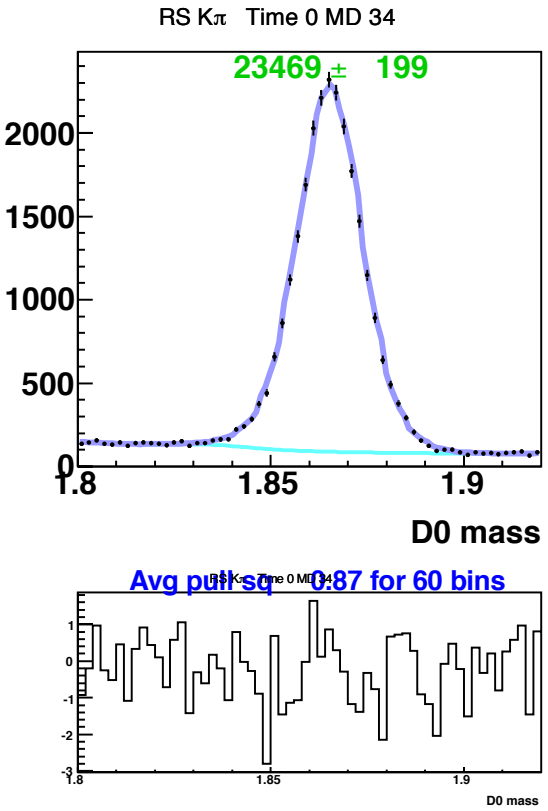

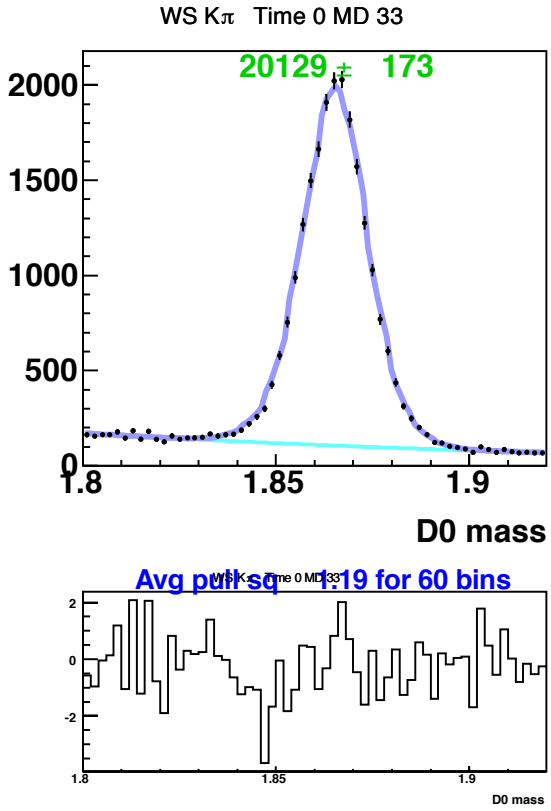

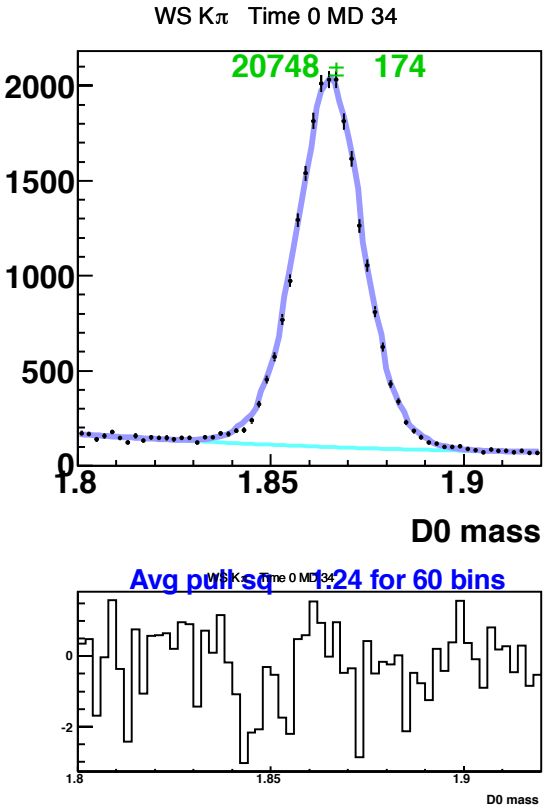

Appendix A: Time-independent $M_{K\pi}$ Distributions

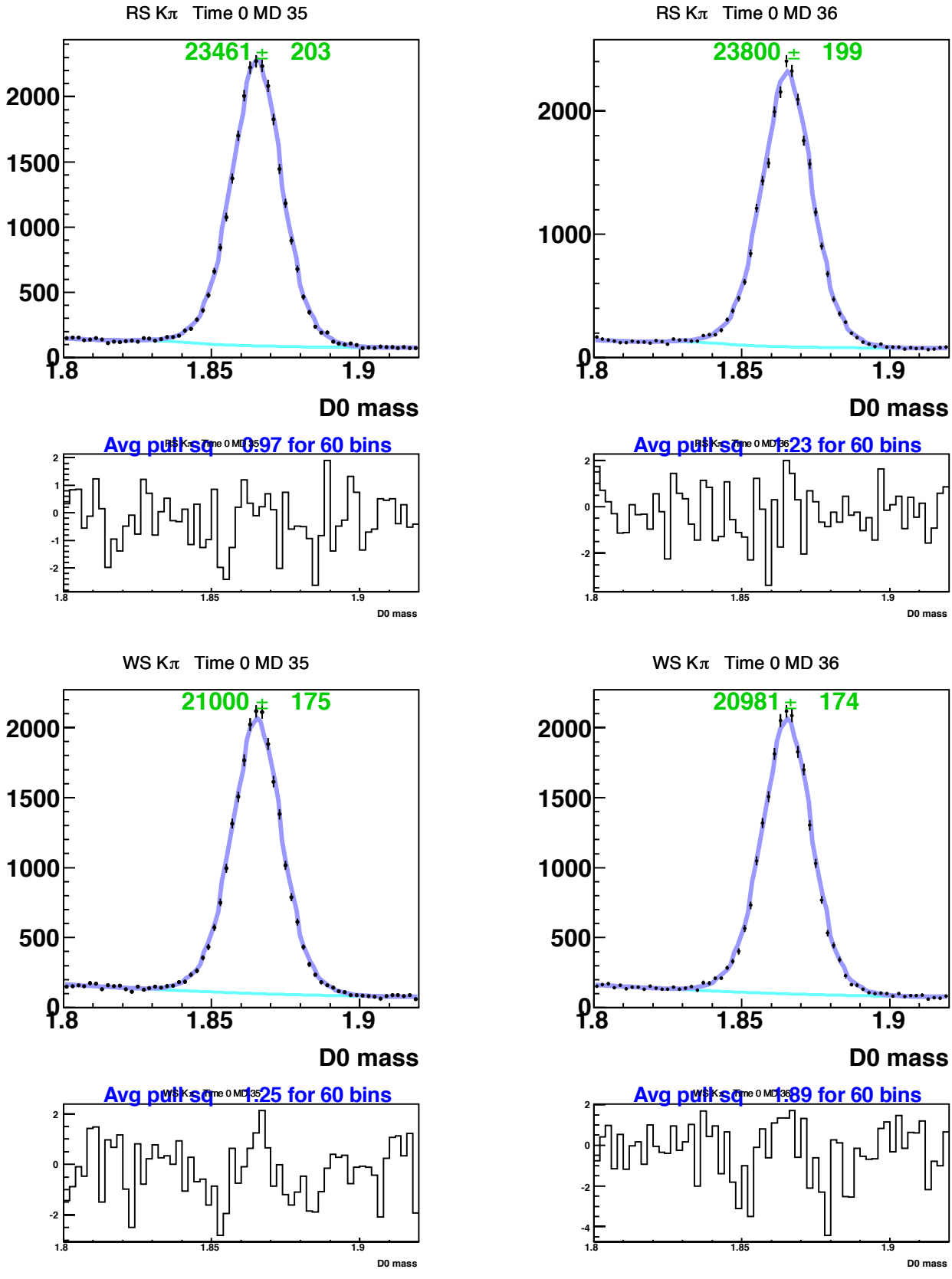

Appendix A: Time-independent $M_{K\pi}$ Distributions

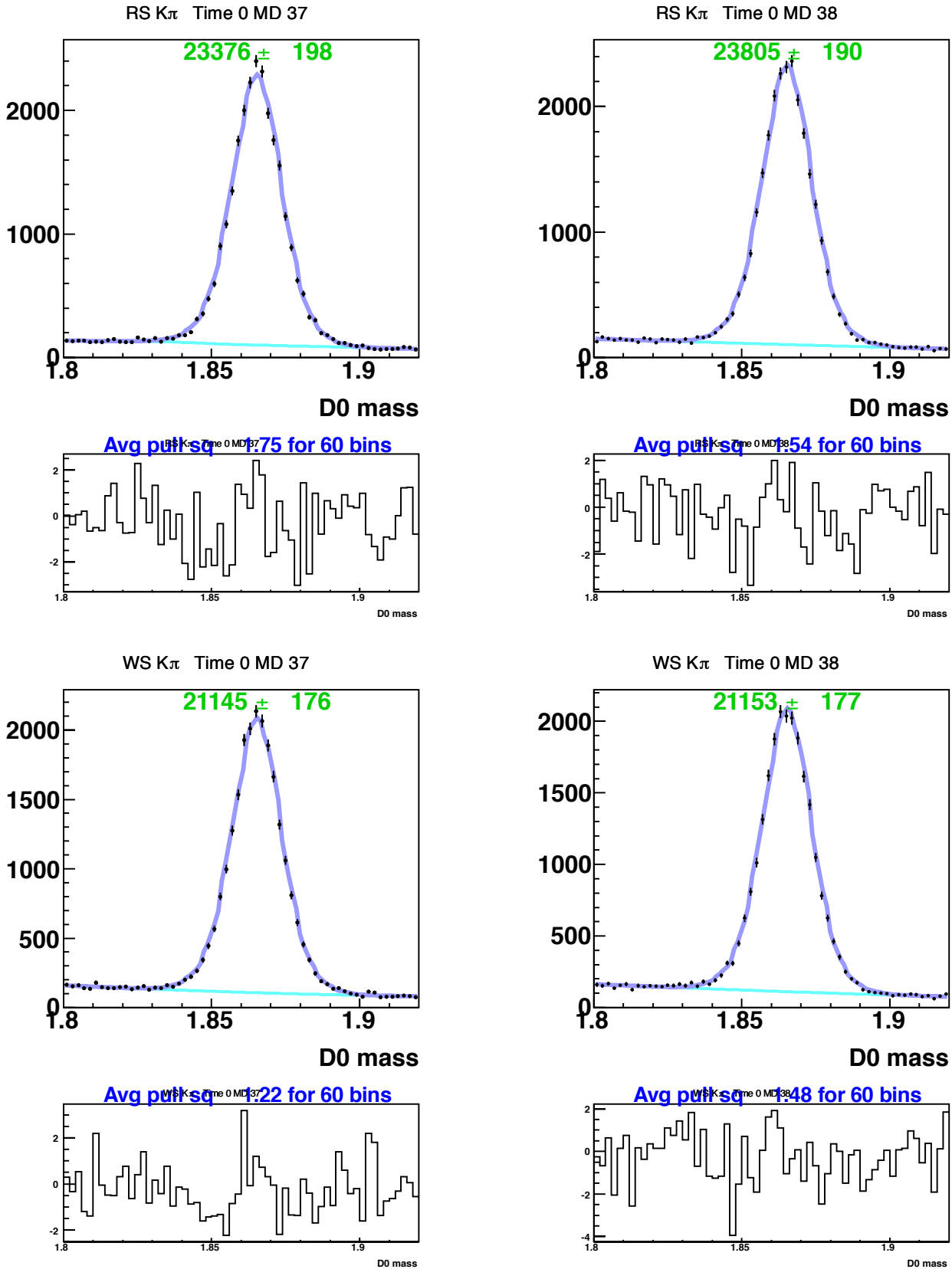

Appendix A: Time-independent $M_{K\pi}$ Distributions

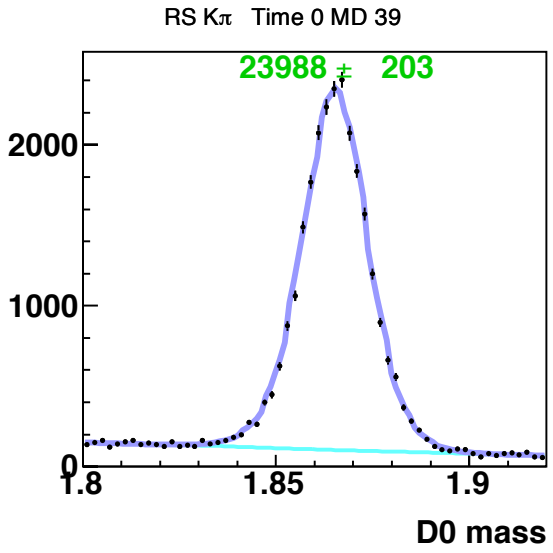

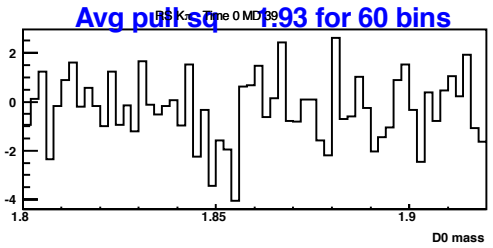

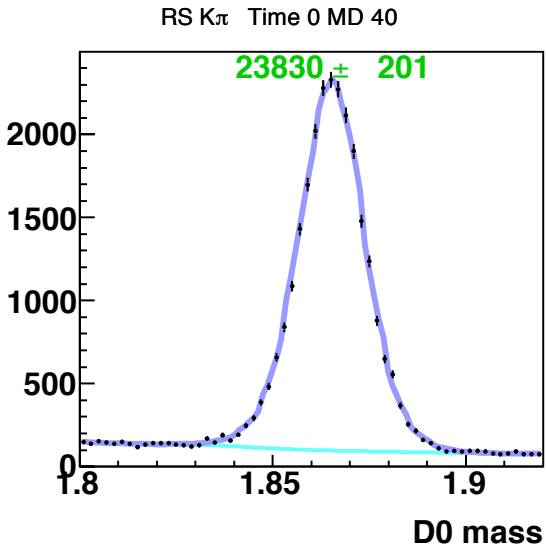

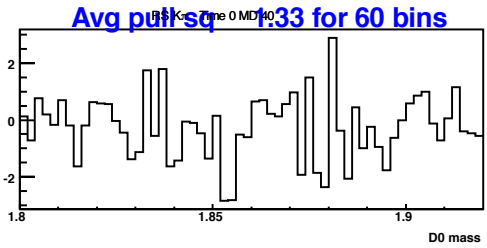

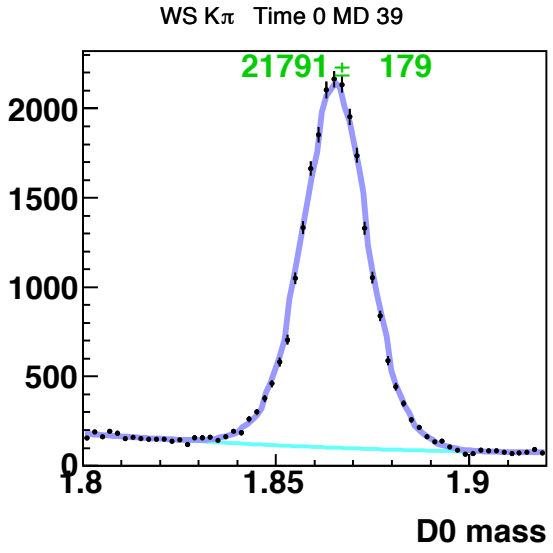

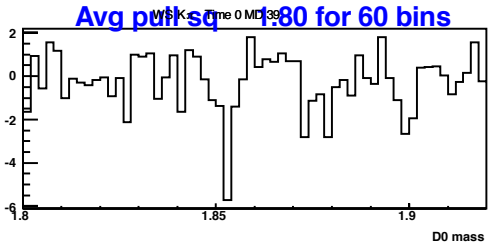

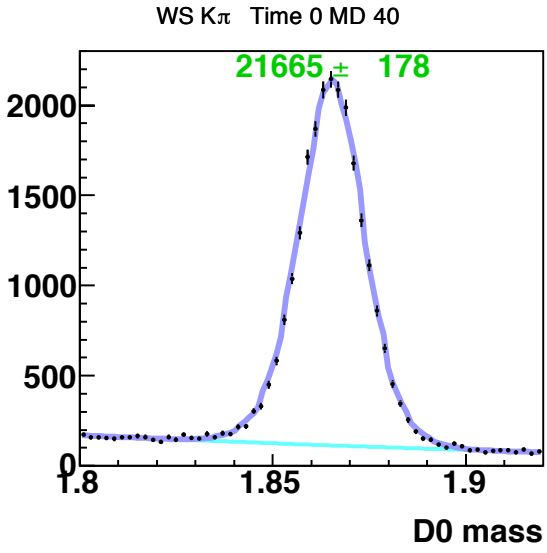

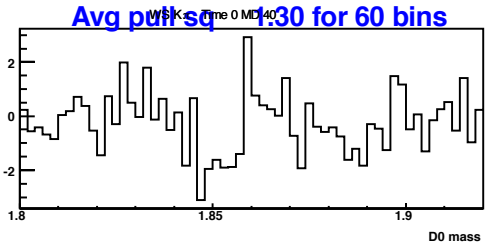

Appendix A: Time-independent $M_{K\pi}$ Distributions

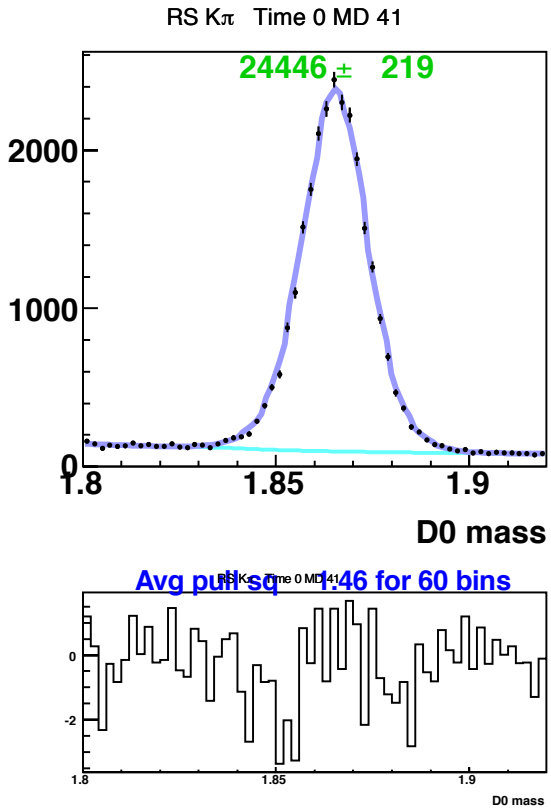

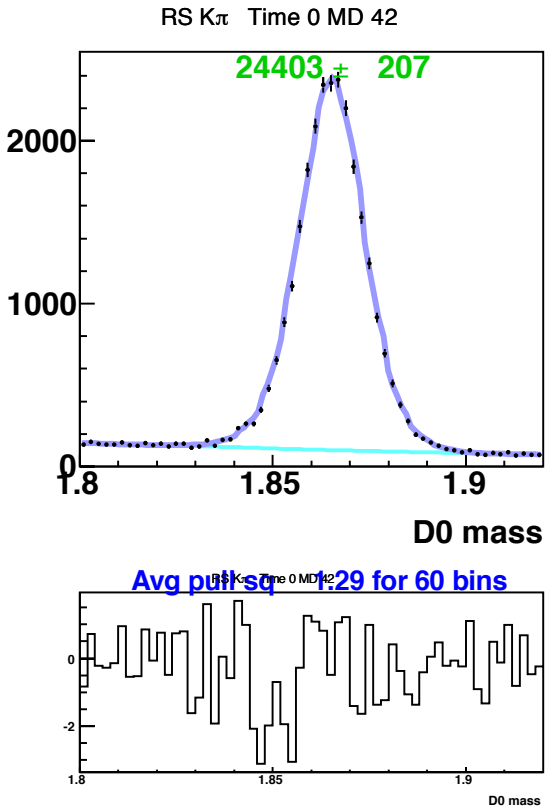

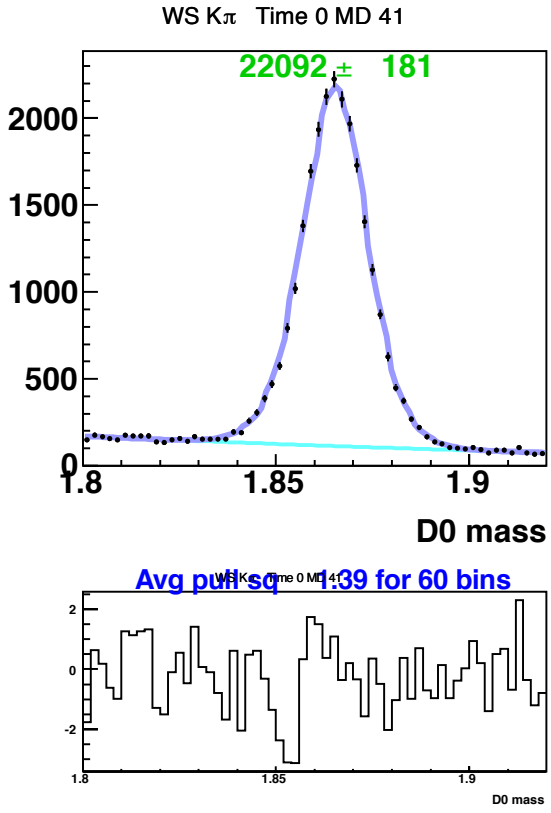

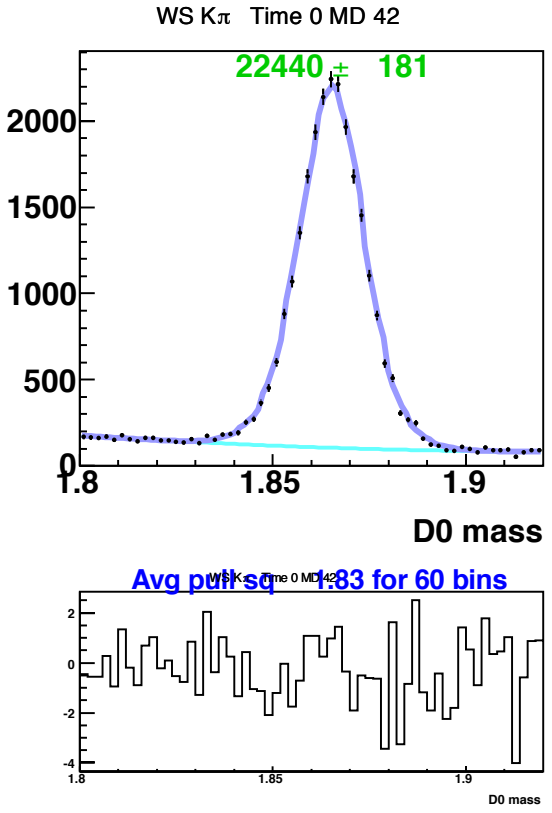

Appendix A: Time-independent $M_{K\pi}$ Distributions

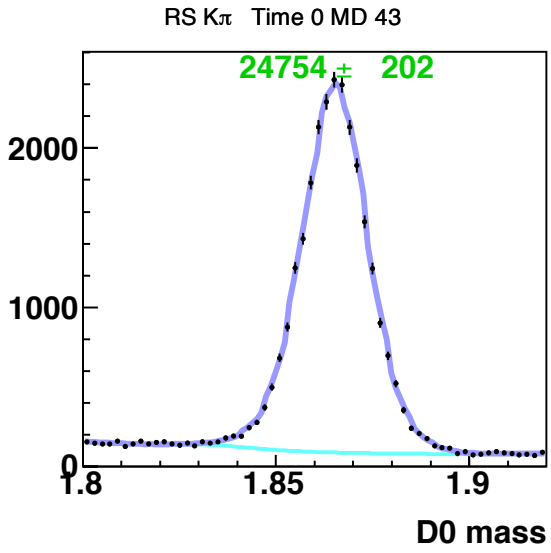

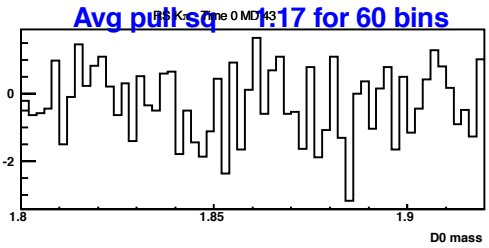

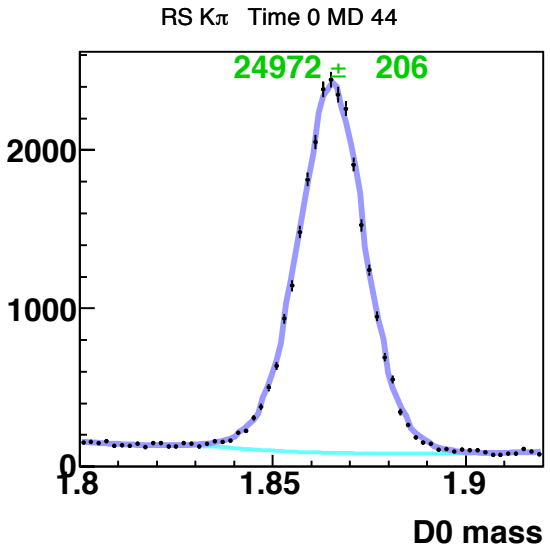

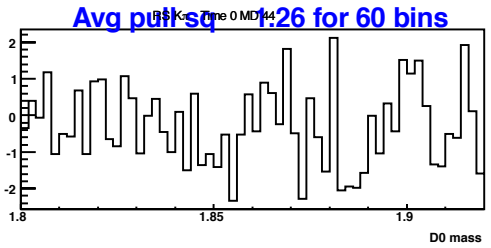

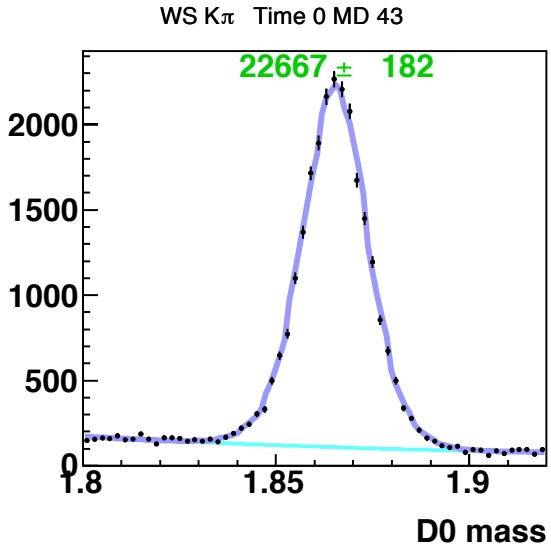

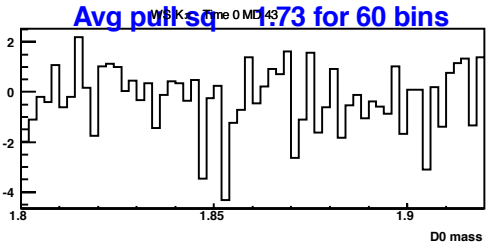

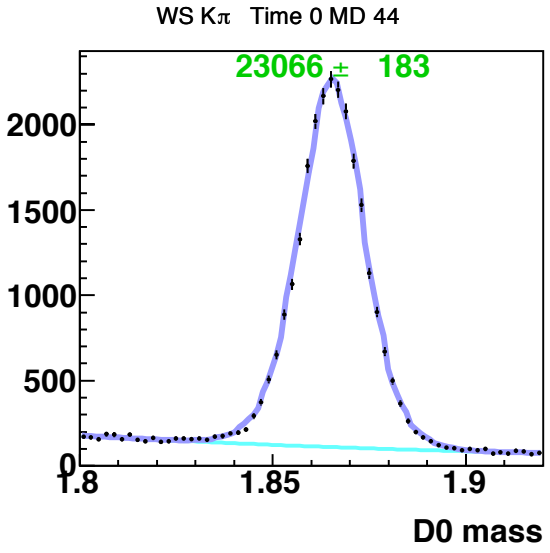

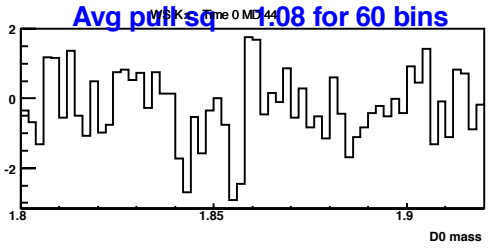

Appendix A: Time-independent $M_{K\pi}$ Distributions

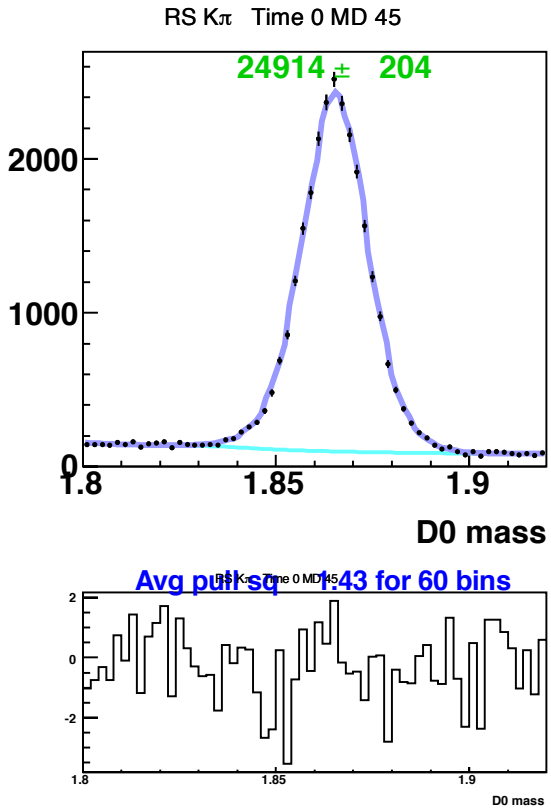

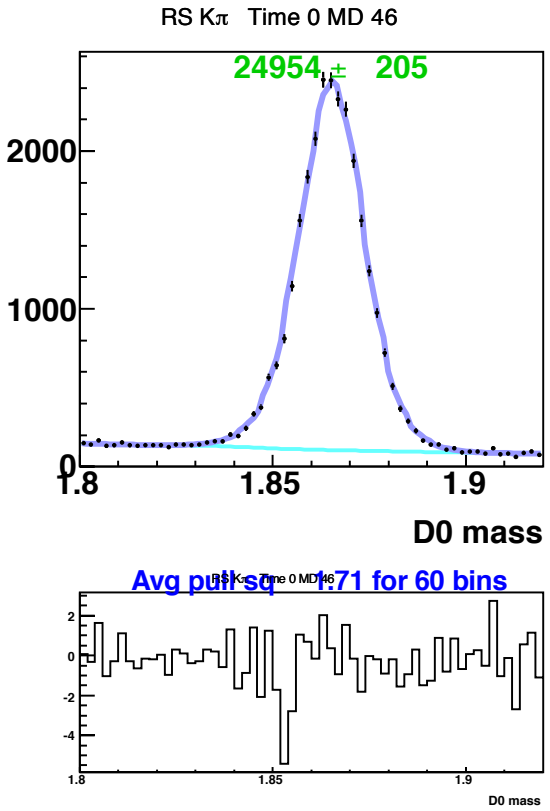

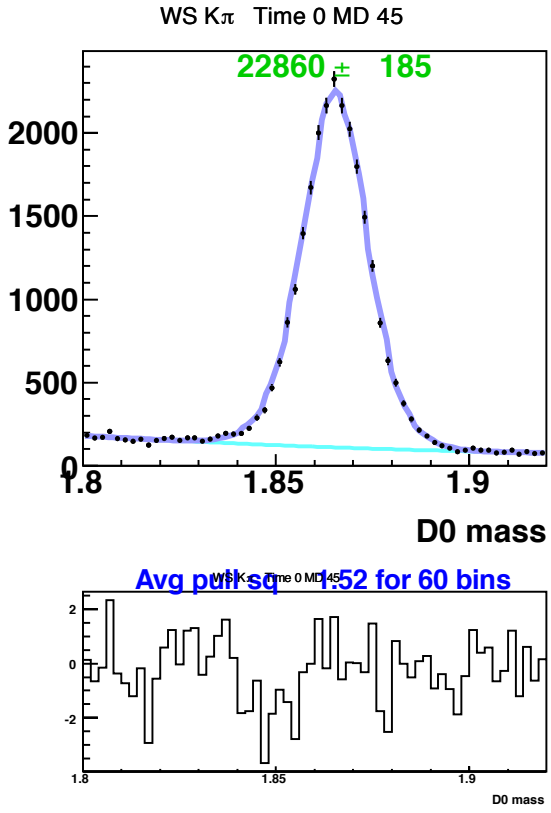

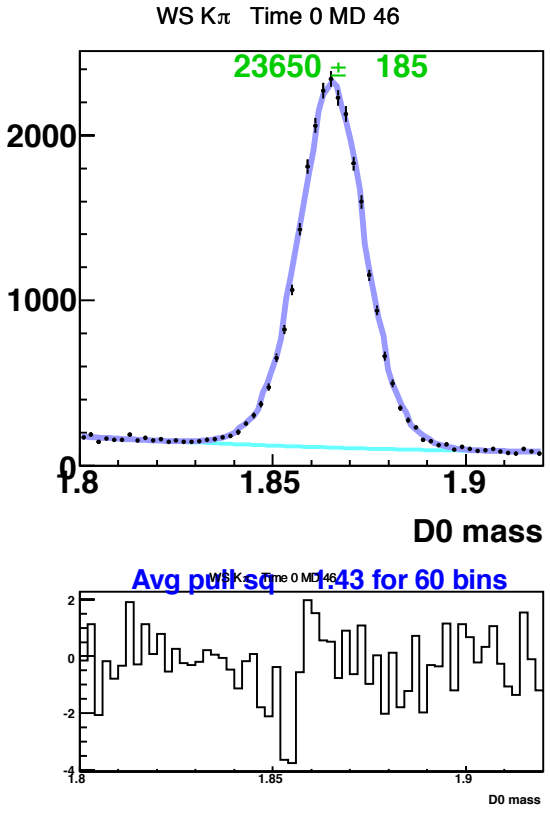

Appendix A: Time-independent $M_{K\pi}$ Distributions

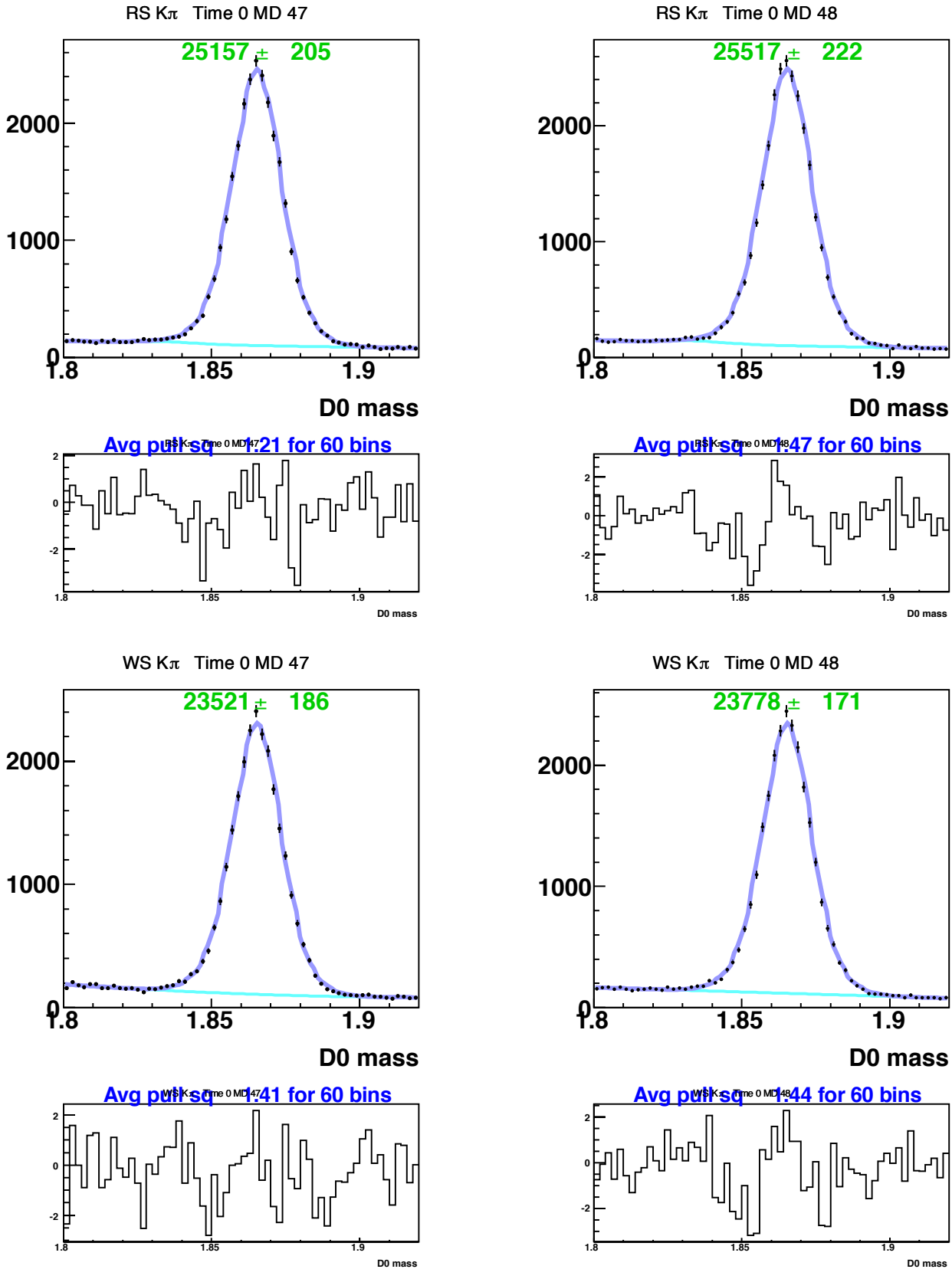

Appendix A: Time-independent $M_{K\pi}$ Distributions

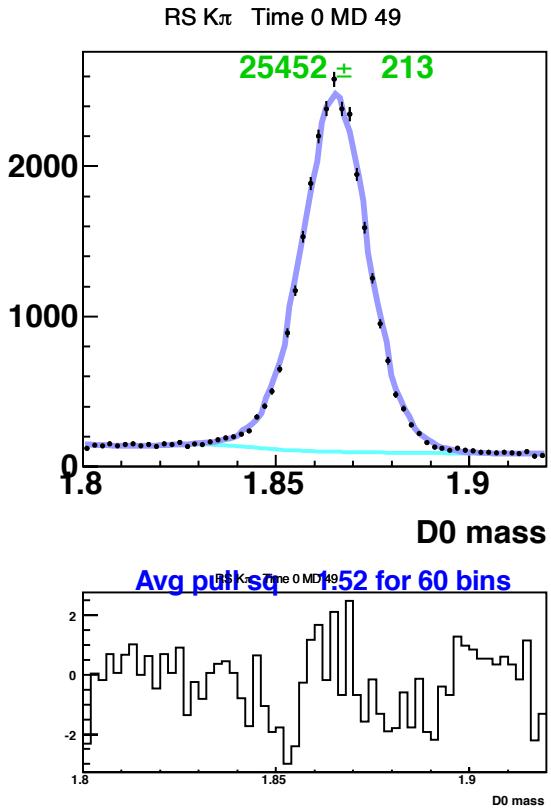

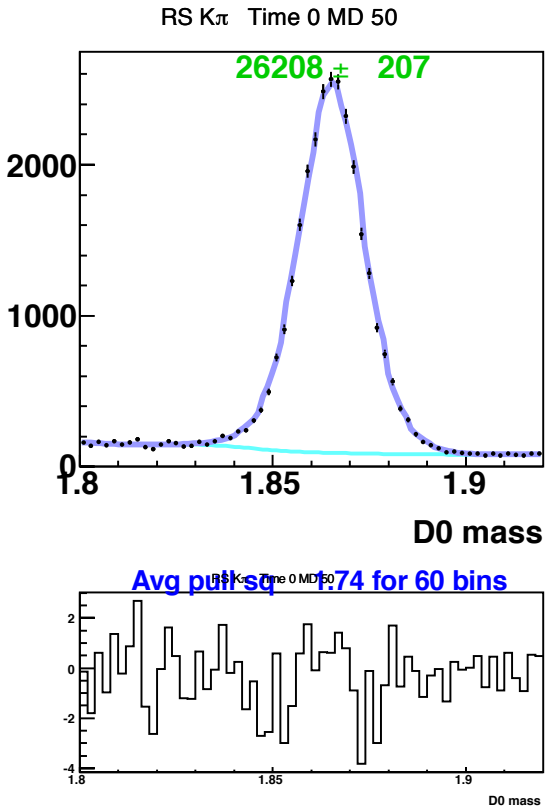

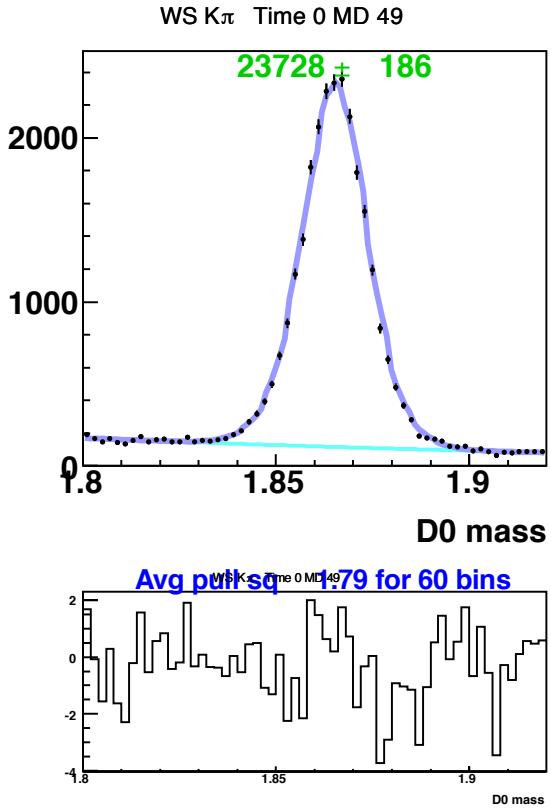

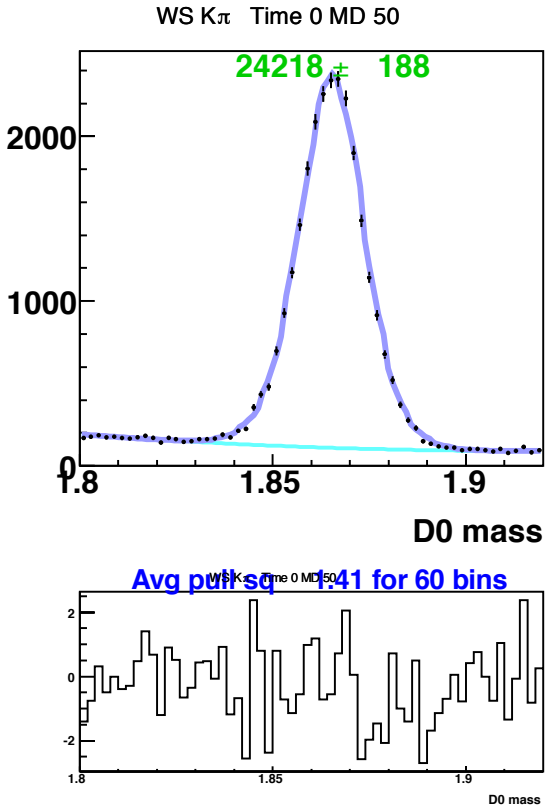

Appendix A: Time-independent $M_{K\pi}$ Distributions

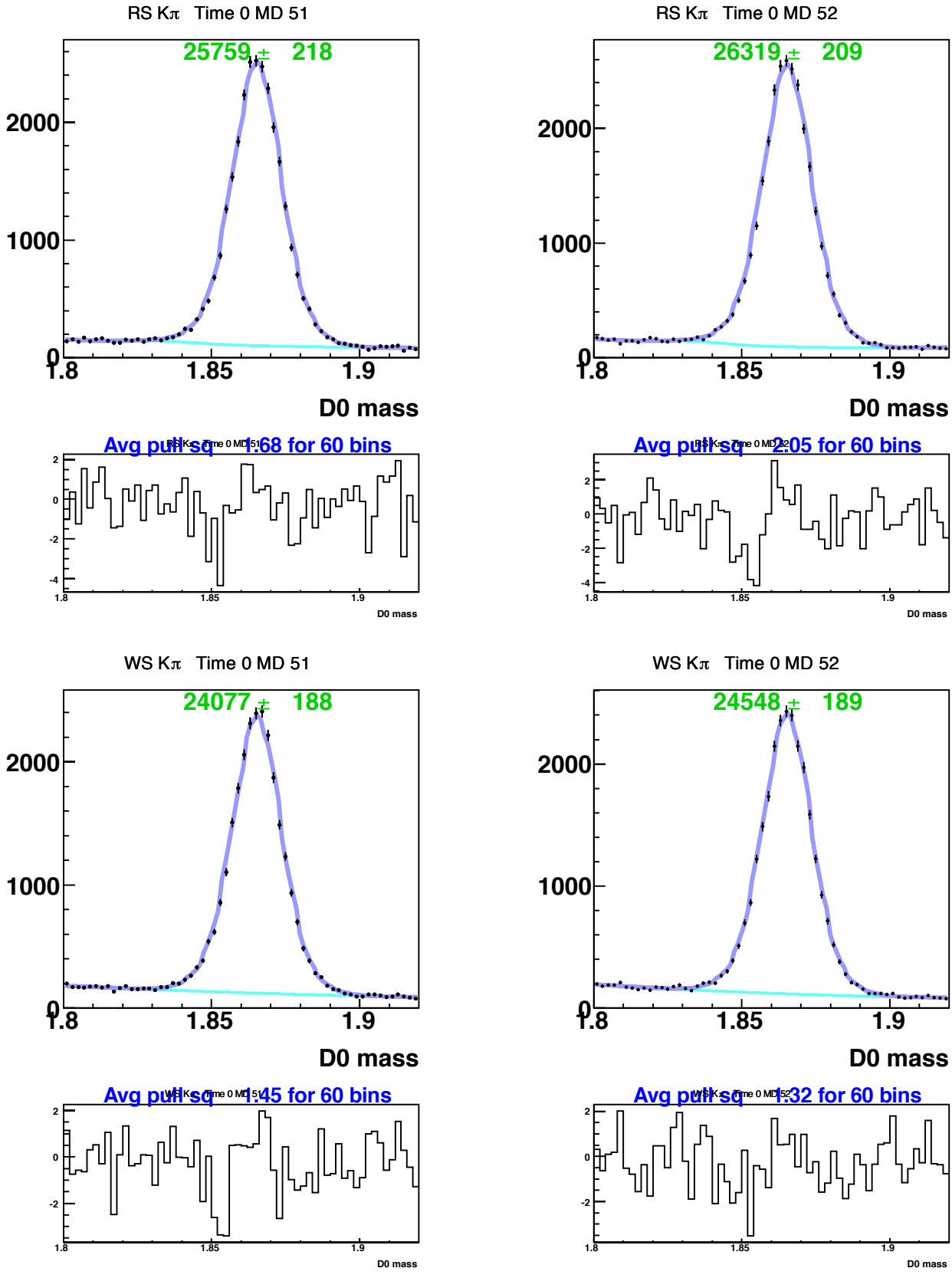

Appendix A: Time-independent $M_{K\pi}$ Distributions

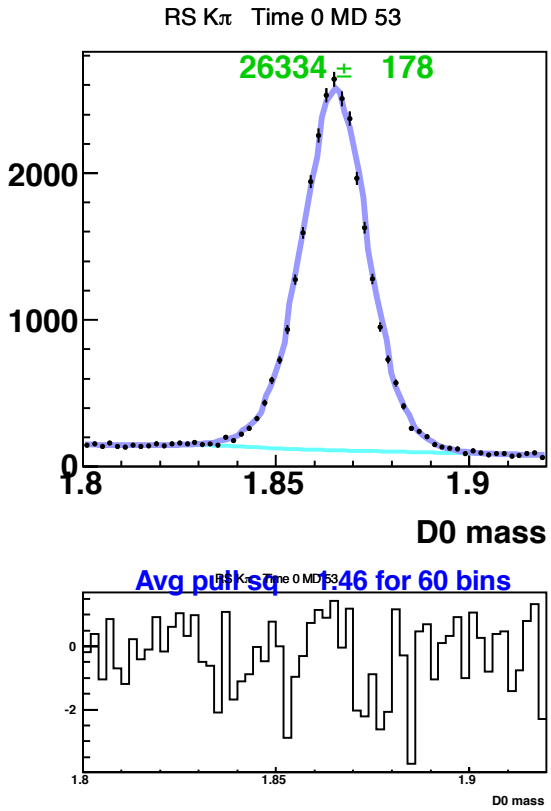

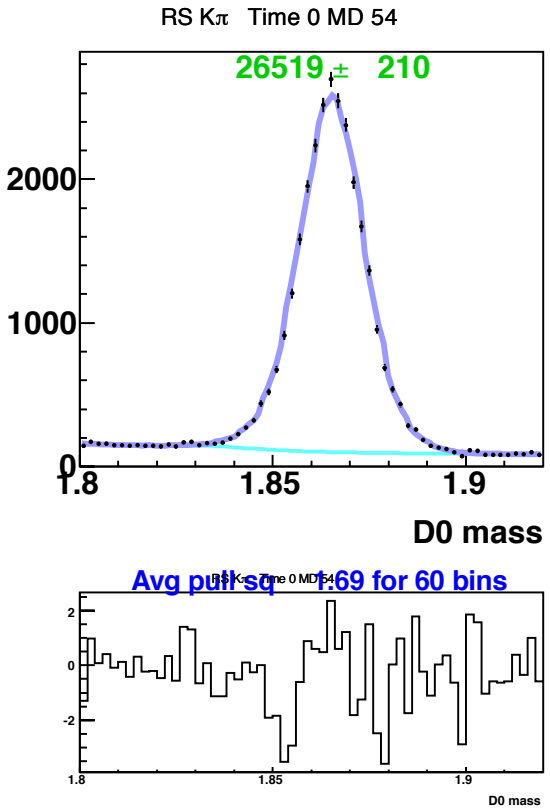

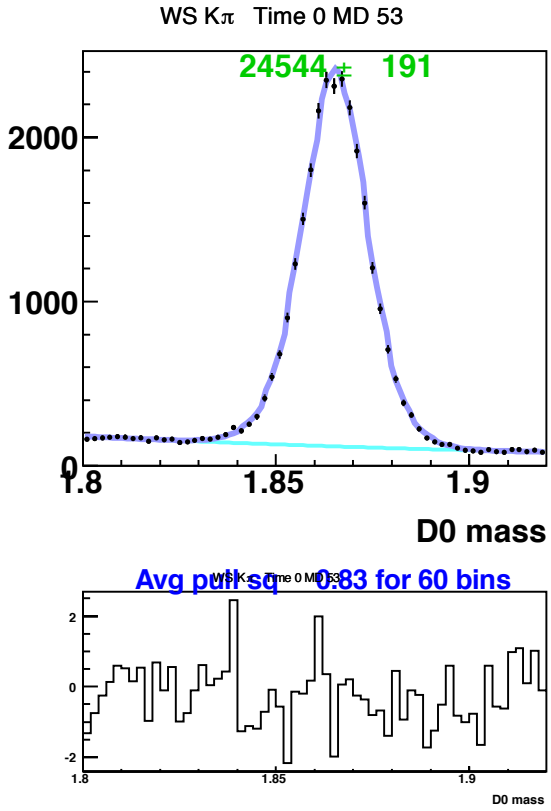

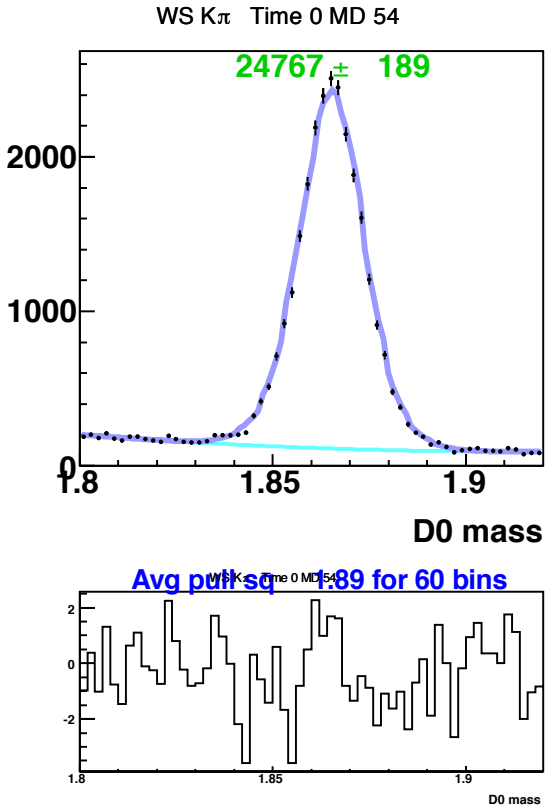

Appendix A: Time-independent $M_{K\pi}$ Distributions

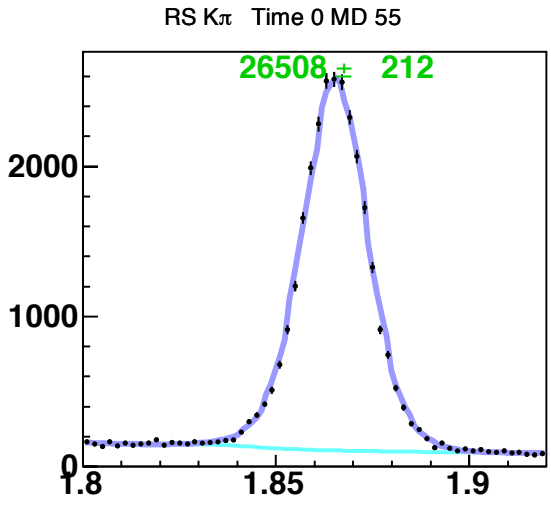

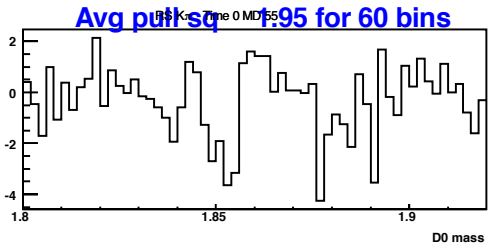

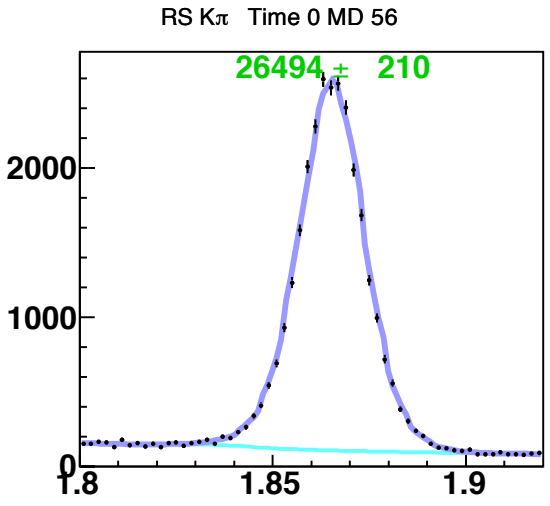

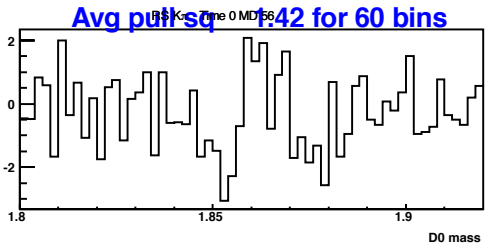

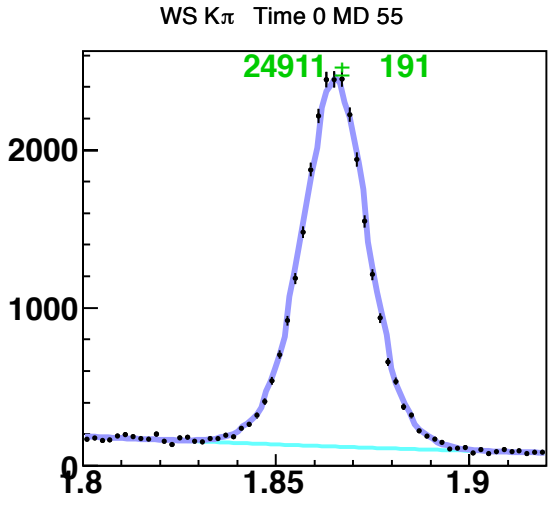

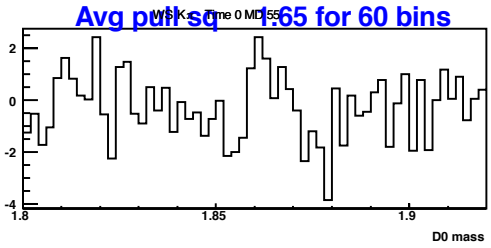

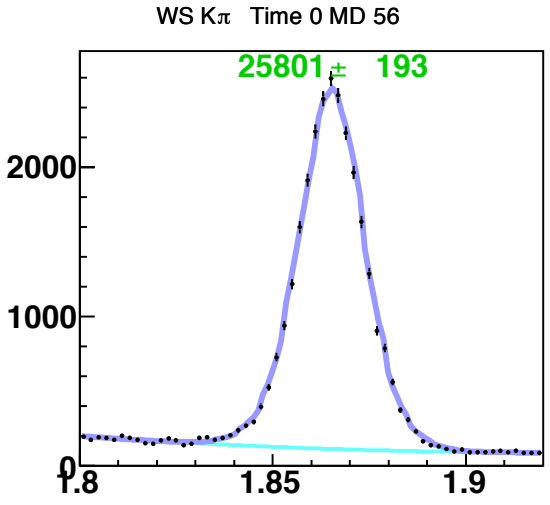

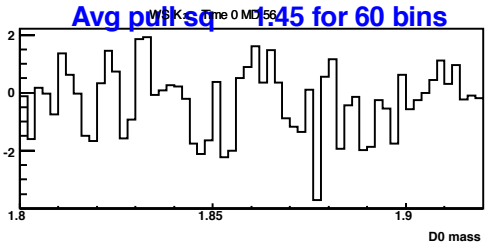

Appendix A: Time-independent $M_{K\pi}$ Distributions

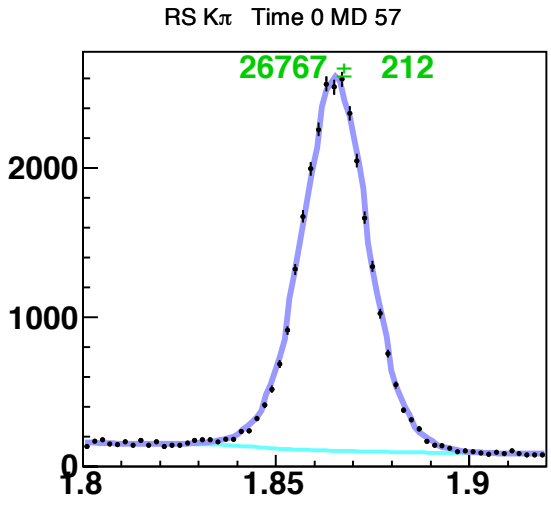

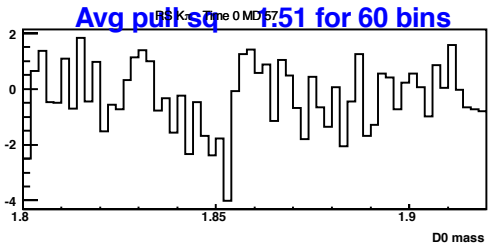

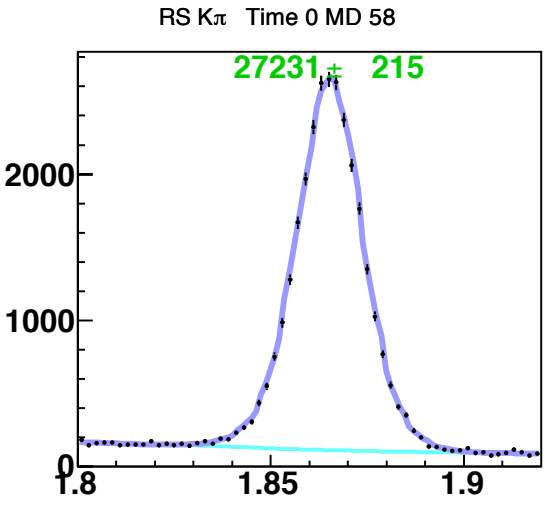

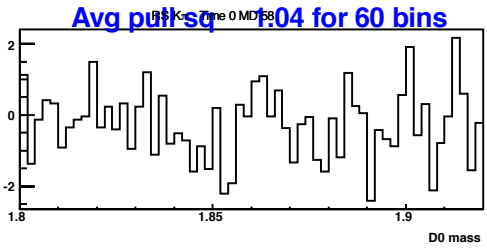

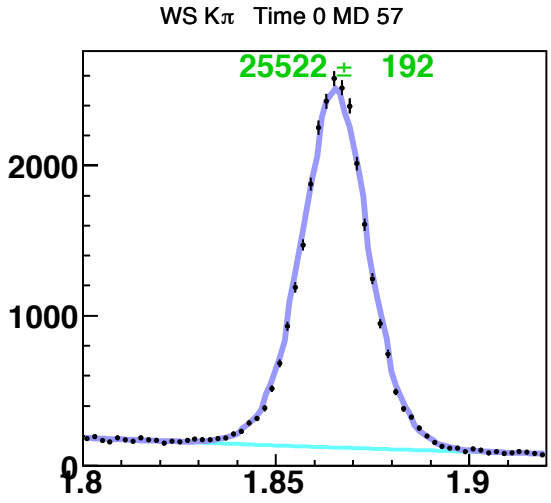

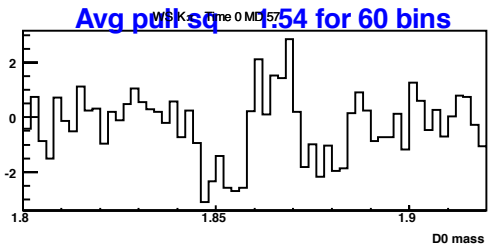

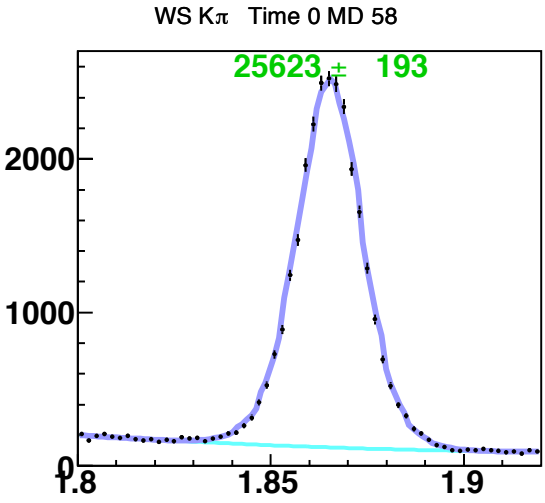

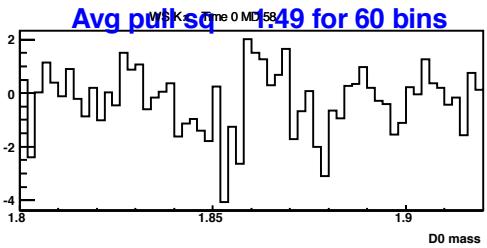

Appendix A: Time-independent $M_{K\pi}$ Distributions

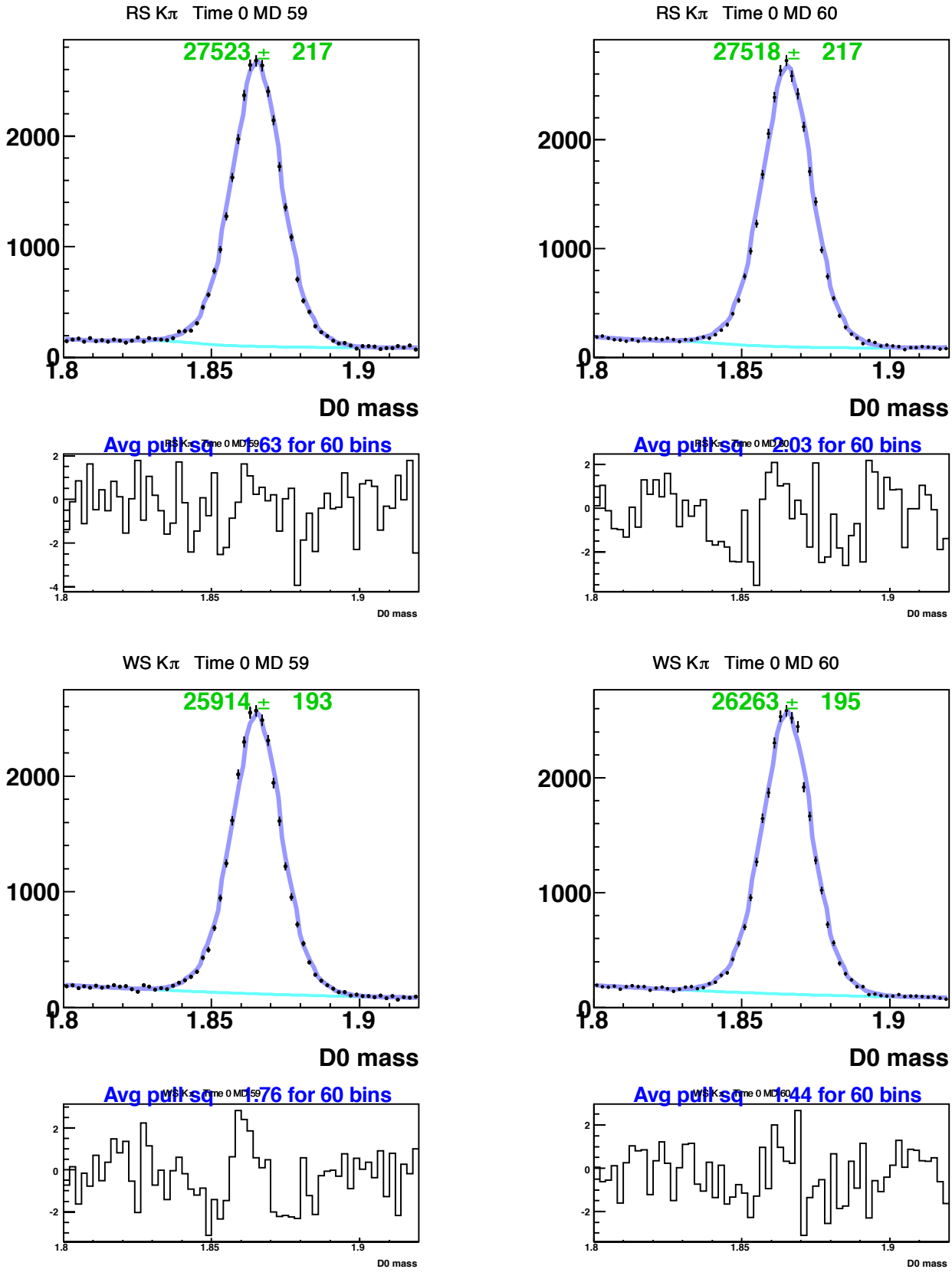

Appendices

B Mass Difference Fits

The following pages show the fits for the mass difference plots for events $|d_0| \leq 60$ microns. For each plot, the x-axis is the mass difference in MeV. The y-axis is the number of D^0s per 0.5 MeV wide bin. The title shows the decay time range, in terms of the D^0 lifetime. The black points (with error bars) are the D^0 yields and uncertainties from the fits to the $K\pi$ mass plots. The green line is the fit. The blue number is the signal with uncertainty. Below the distribution is the pulls for the data compared to the fit, along with the fit χ^2. The top row on each page is for Right-Sign events, the bottom row is for Wrong-Sign events. There are 20 time bins.

The fit uses the ROOT "chi-square" and integral options. Each fit only has two free parameters: the (signal) amplitude for D^*s, and the (background) amplitude for D^0 + fake tagging pion. The signal and background shapes are fixed beforehand from a fit to the time-summed data.

Appendix B: Δm Yield Fits $d_0 < 60\mu$m

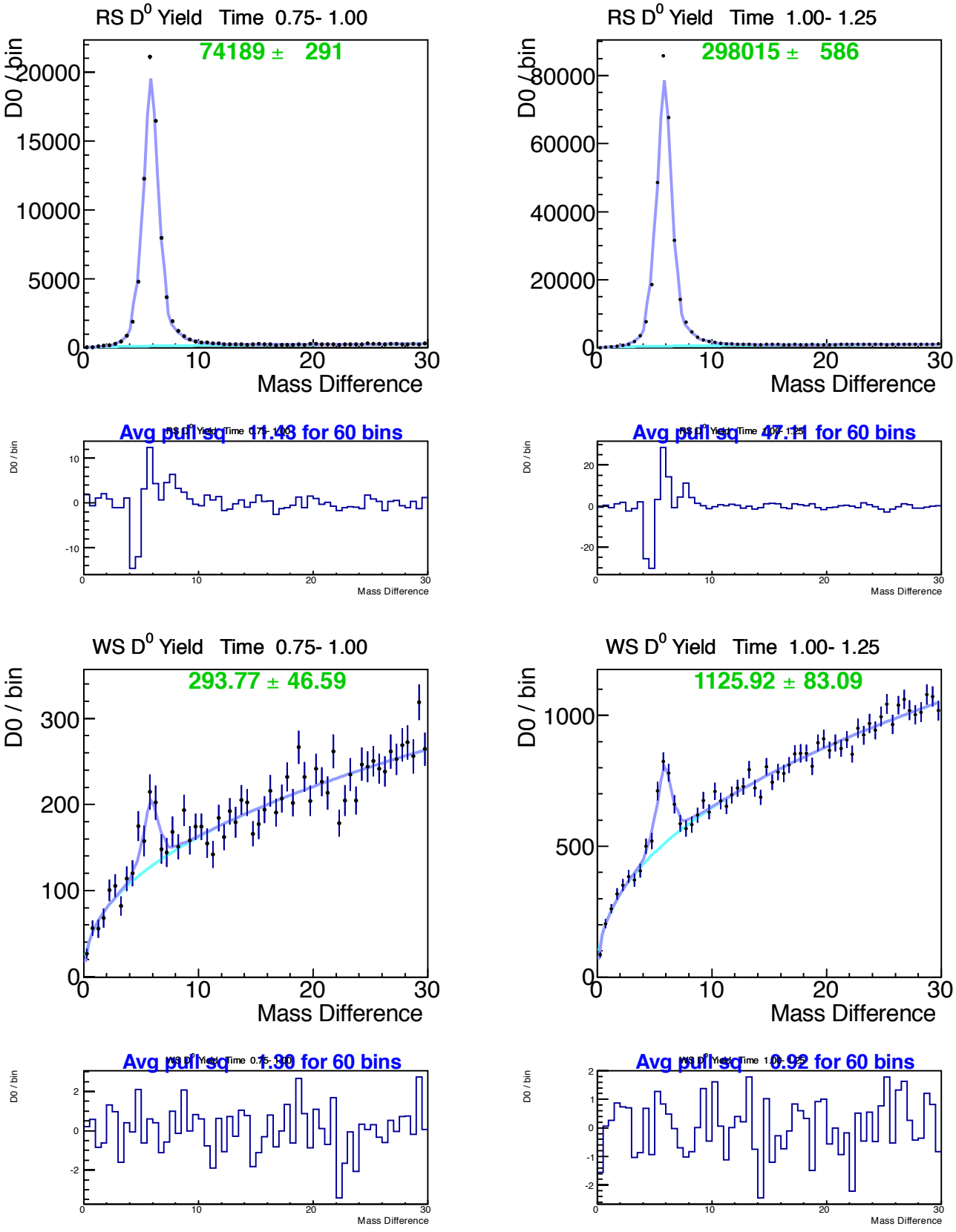

Appendix B: Δm Yield Fits $d_0 < 60\mu$m

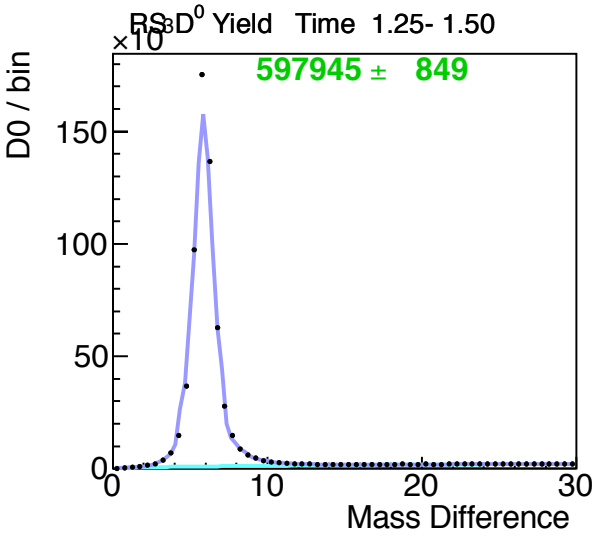

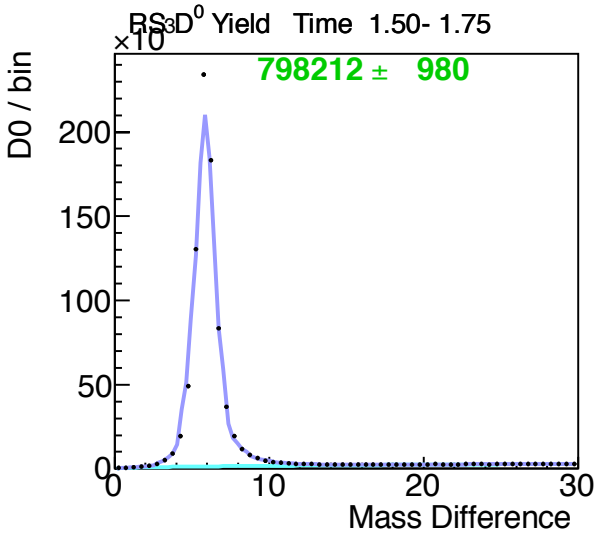

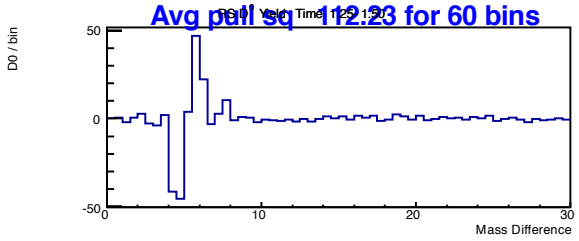

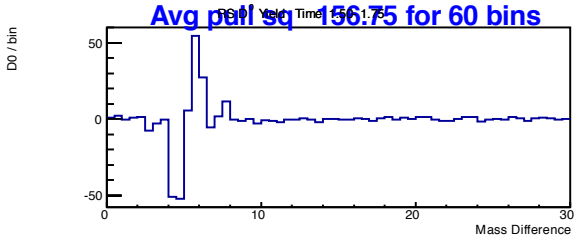

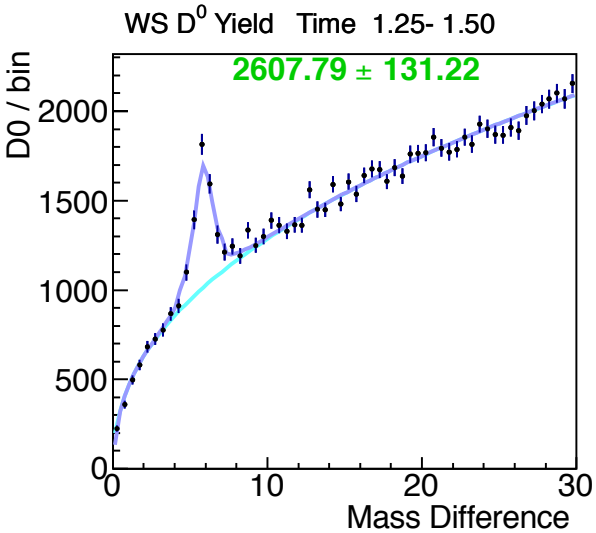

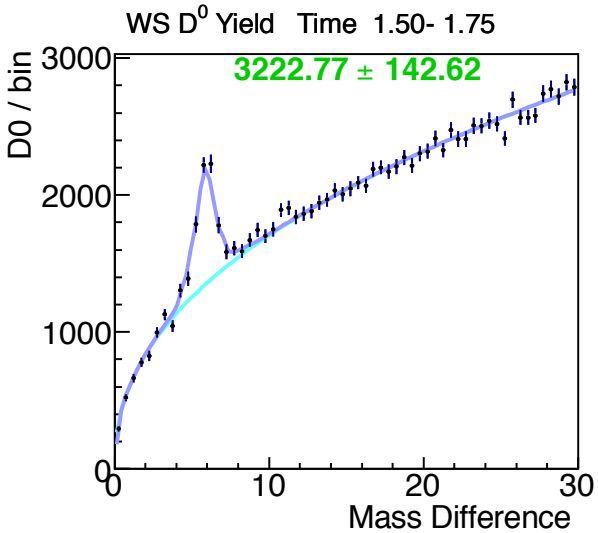

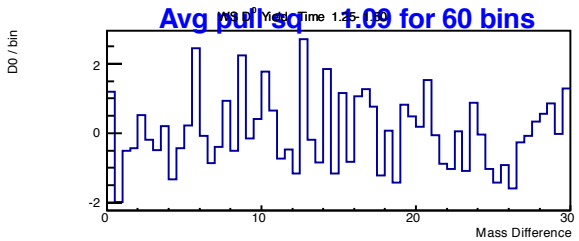

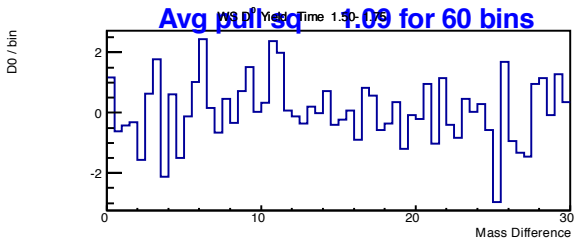

Appendix B: Δm Yield Fits $d_0 < 60\mu$m

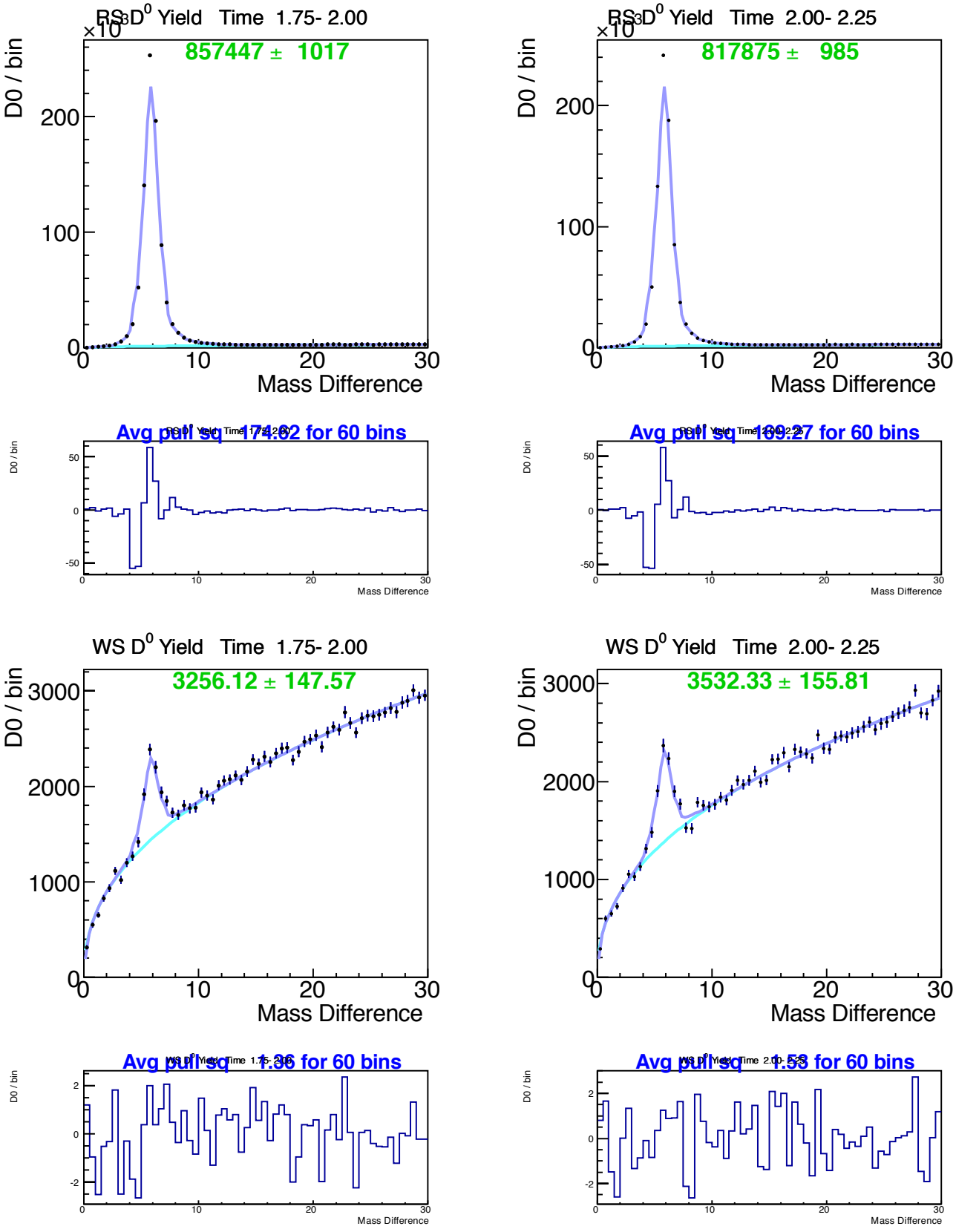

Appendix B: Δm Yield Fits $d_0 < 60\mu$m

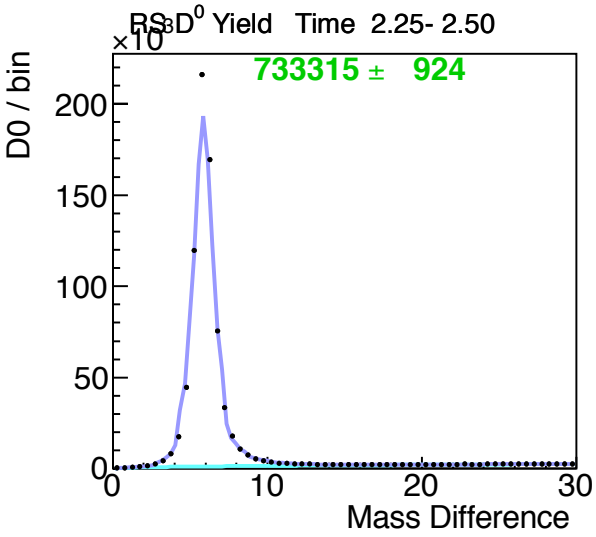

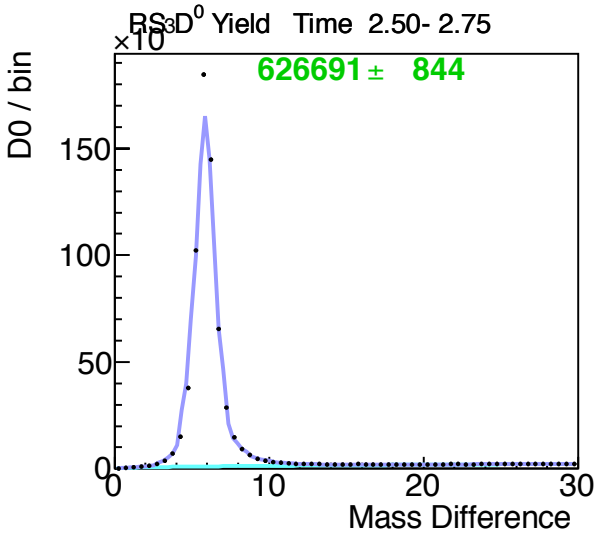

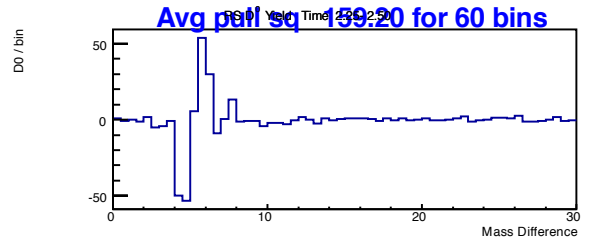

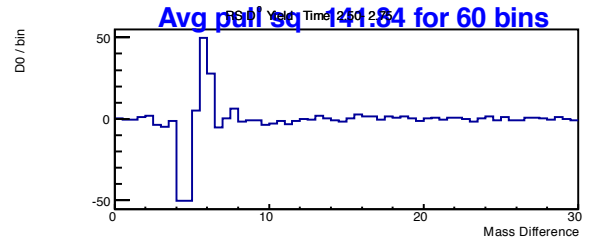

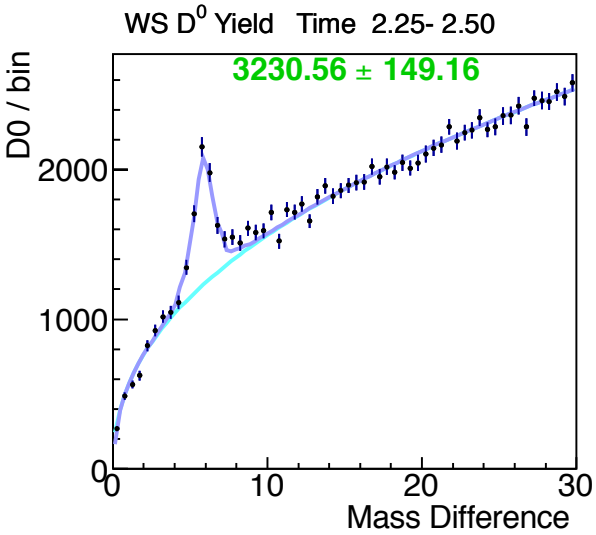

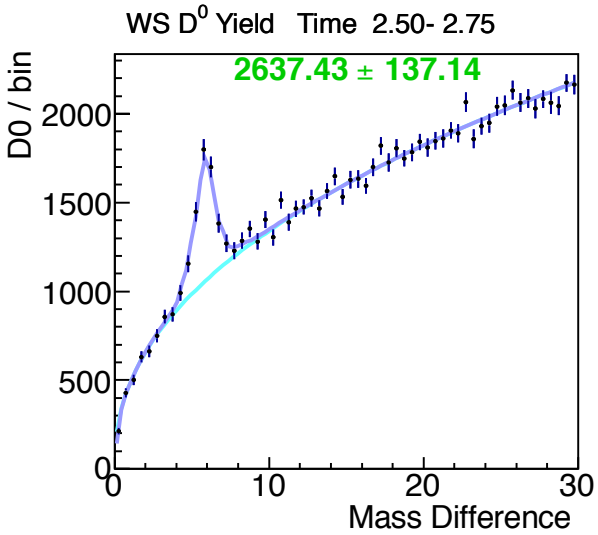

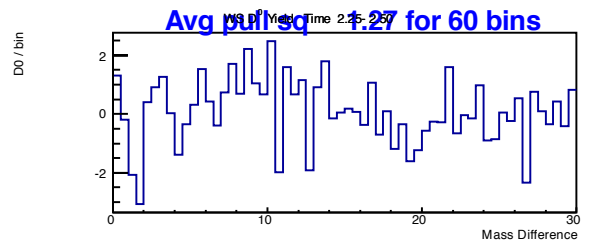

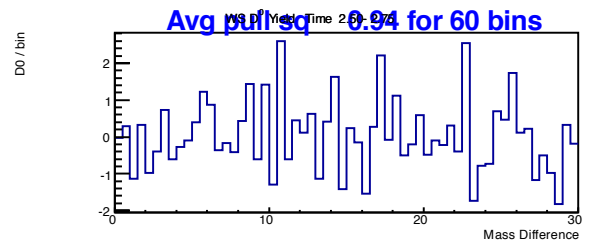

Appendix B: Δm Yield Fits $d_0 < 60\mu$m

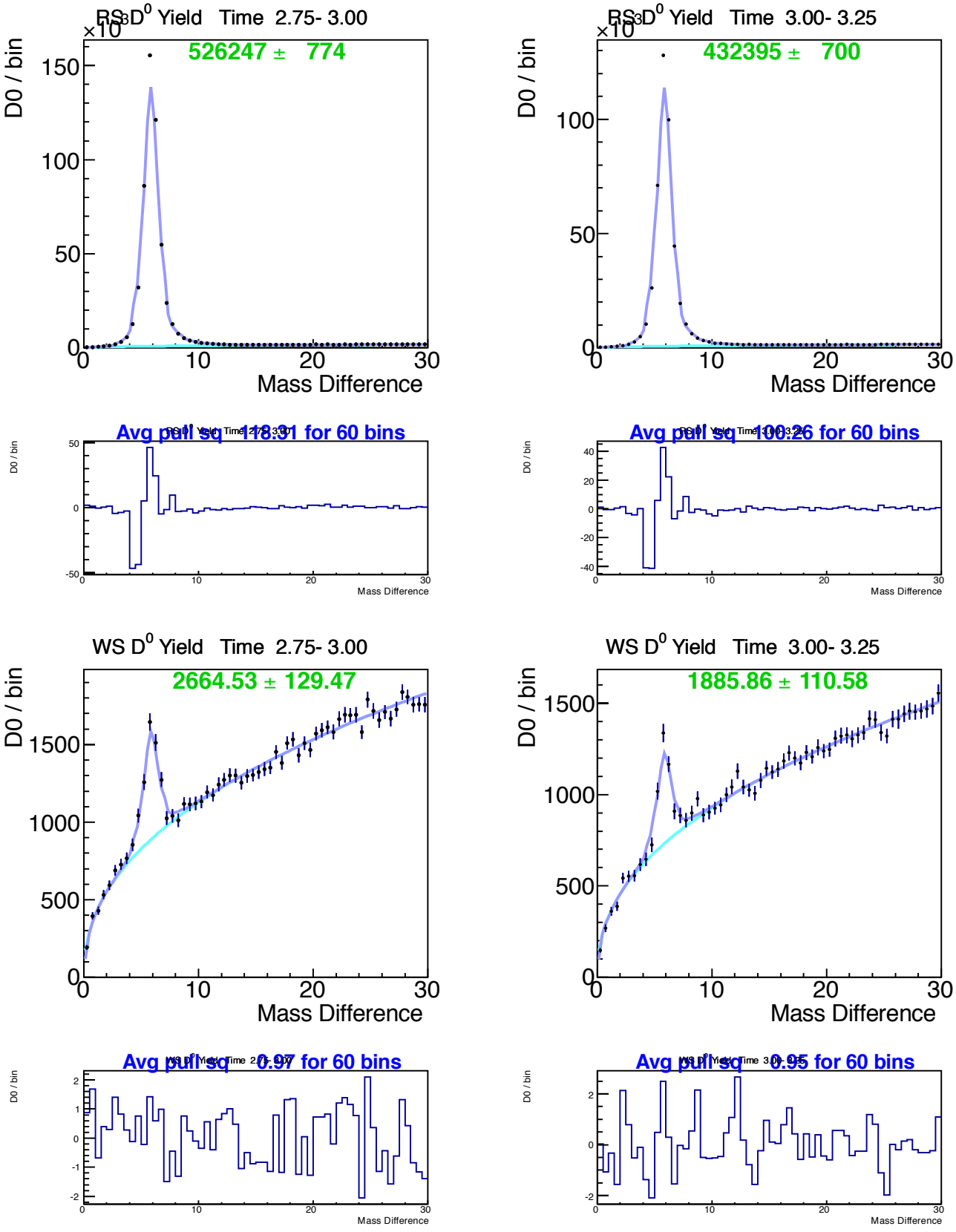

Appendix B: Δm Yield Fits $d_0 < 60\mu$m

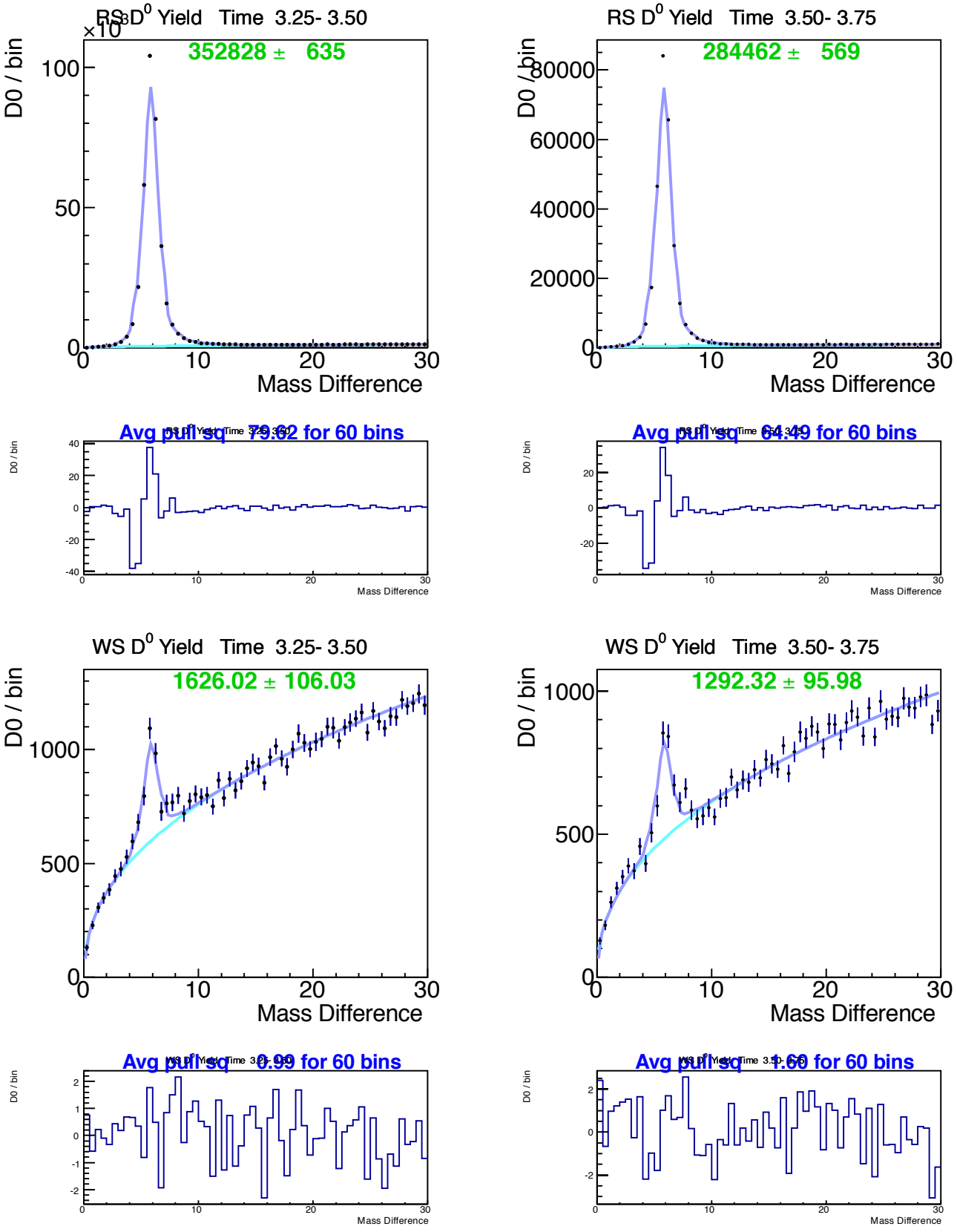

Appendix B: Δm Yield Fits $d_0 < 60\mu$m

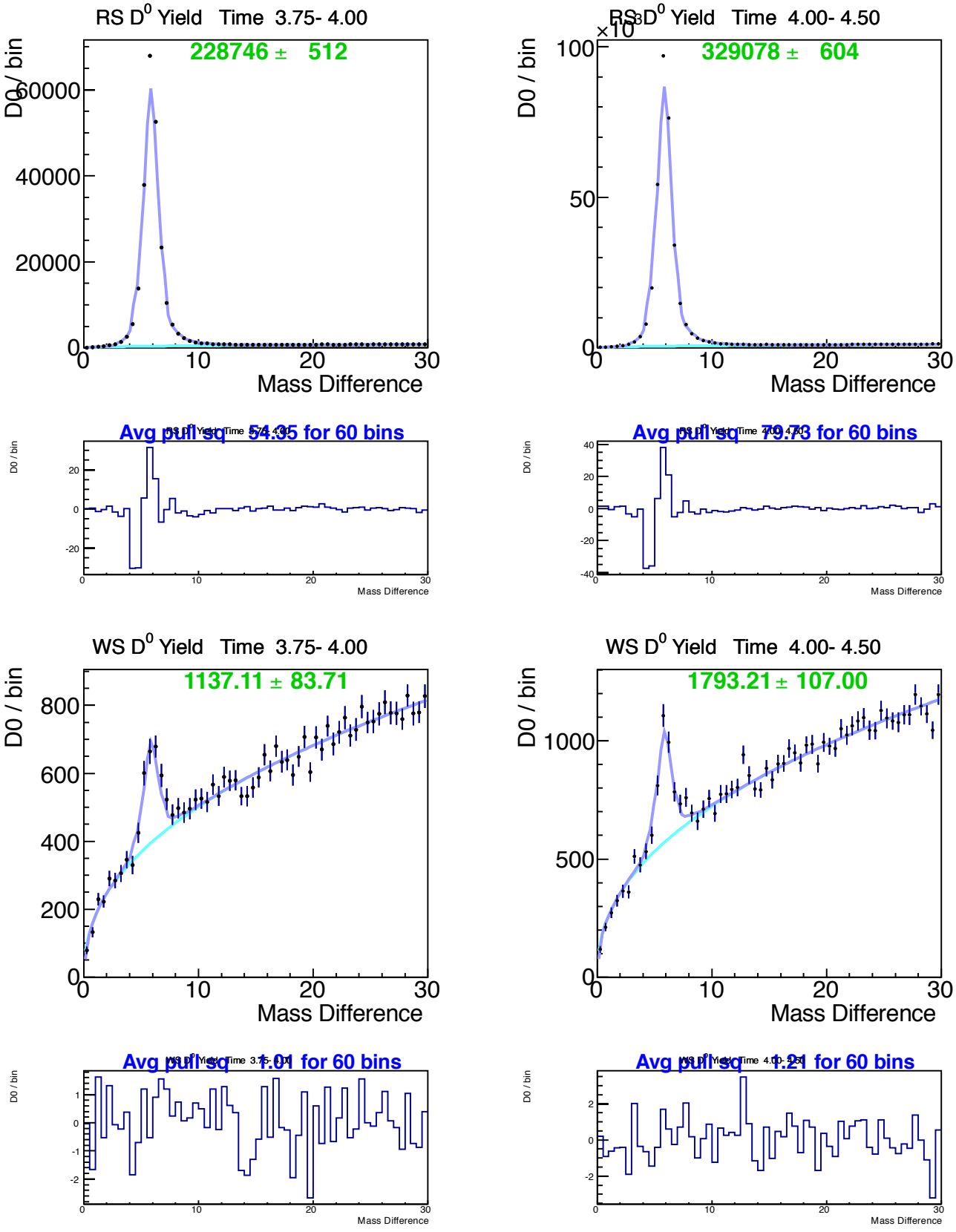

Appendix B: Δm Yield Fits $d_0 < 60\mu$m

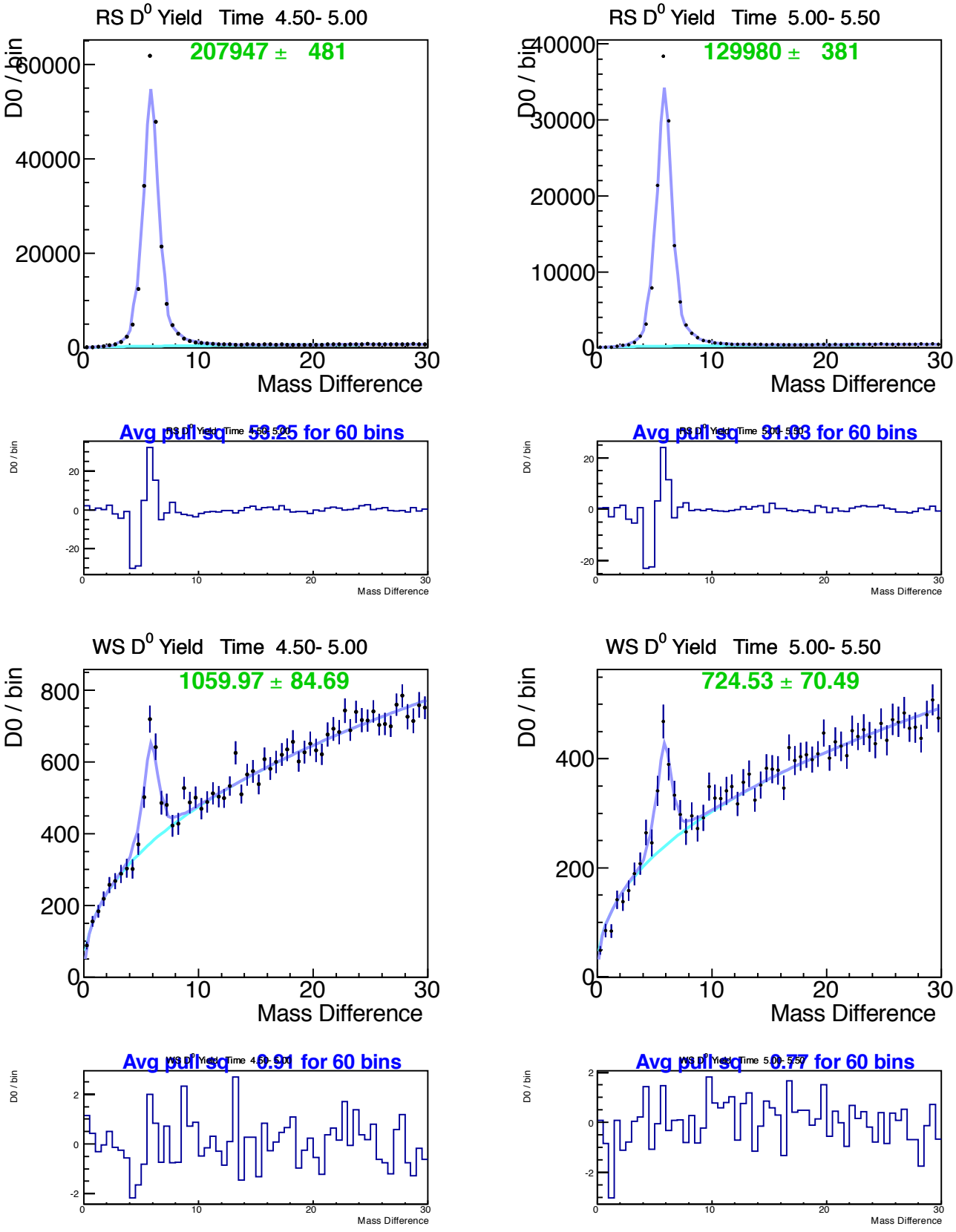

Appendix B: Δm Yield Fits $d_0 < 60\mu$m

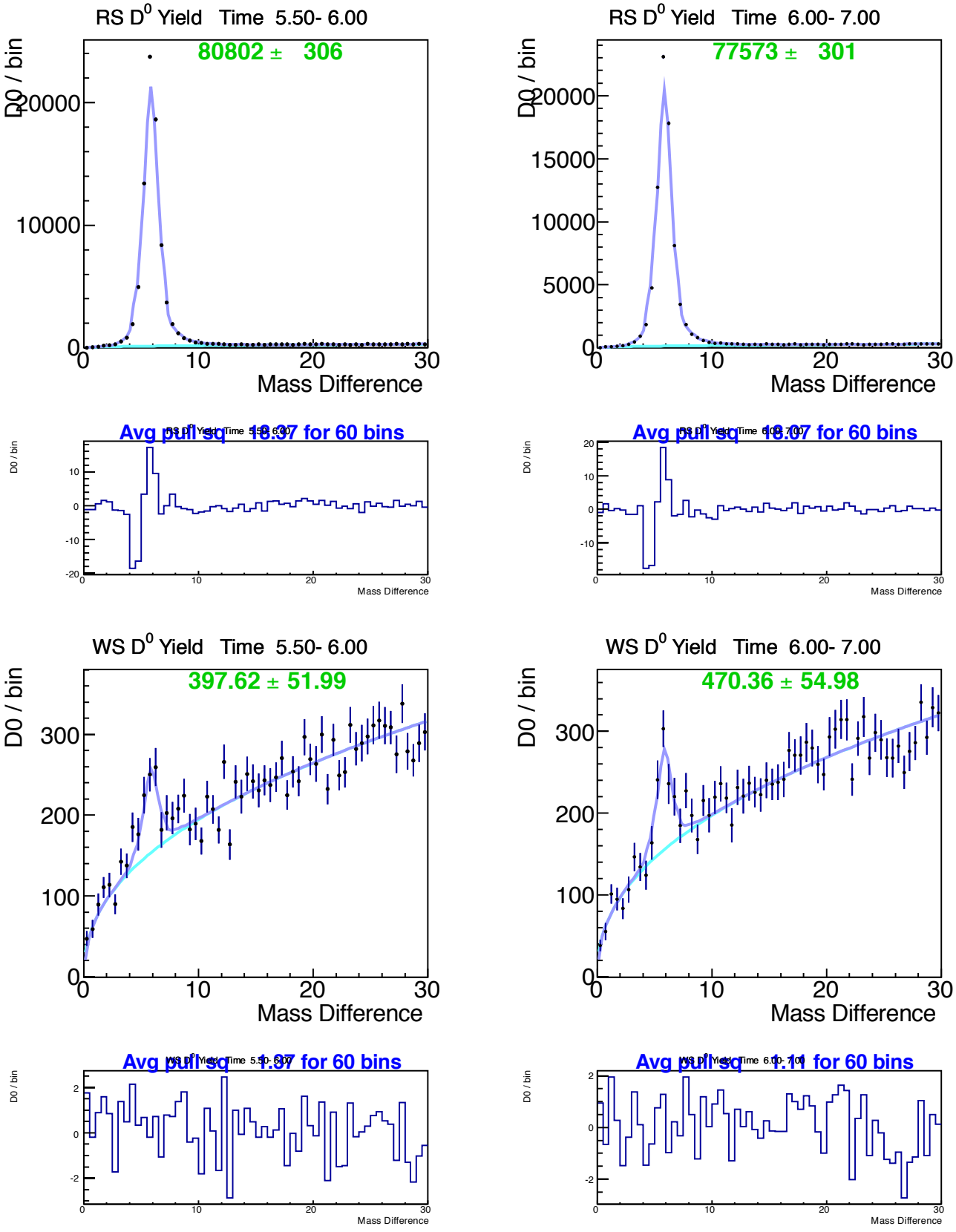

Appendix B: Δm Yield Fits $d_0 < 60\mu$m

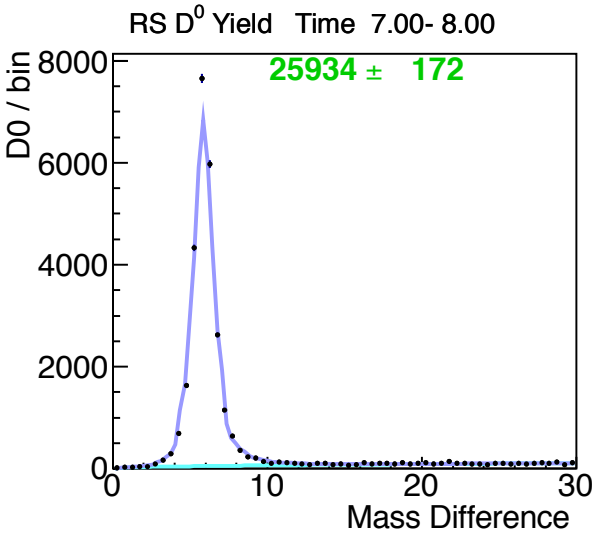

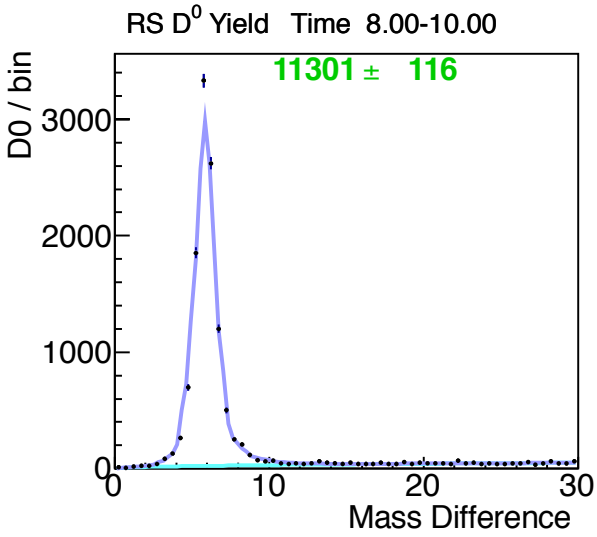

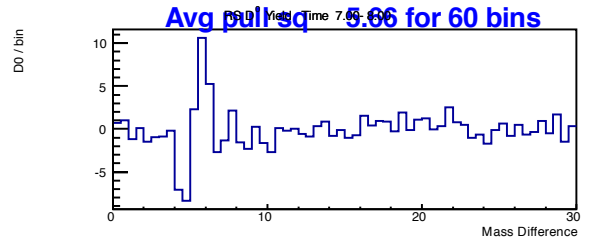

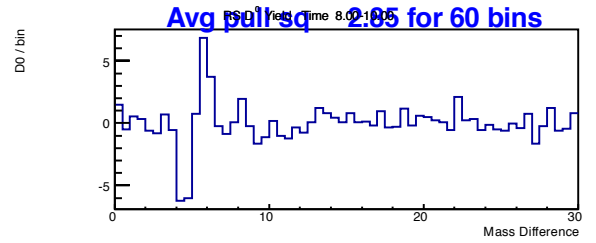

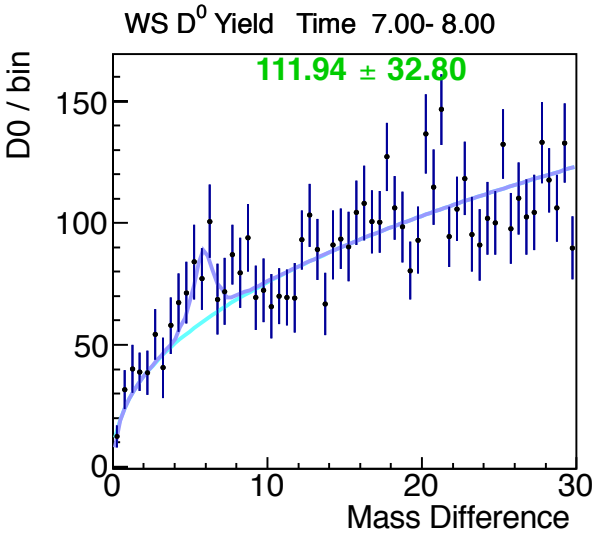

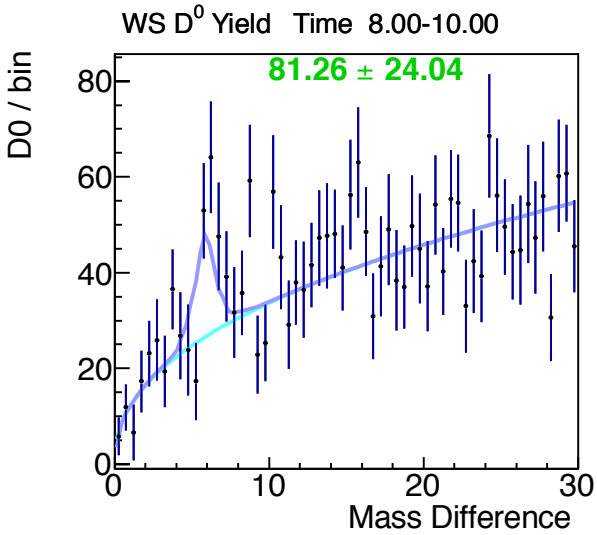

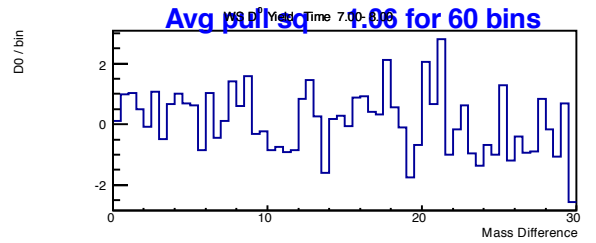

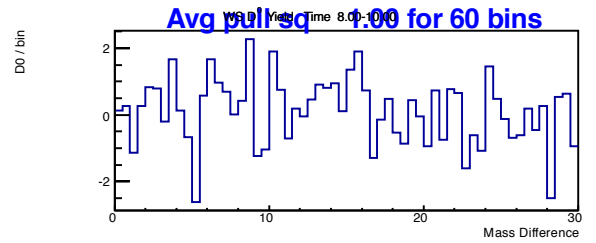

C Mass Difference Fits For Events Outside the IP Cut

This appendix is similar to Appendix B, except that the D^* yields are for events with $|d_0| > 60$ microns. This region will have a higher concentration of D^* not produced at the primary vertex, and is used to calculate the amount of prompt D^*s (at all IP values).

Appendix C: Δm Yield Fits $d_0 > 60\mu$m

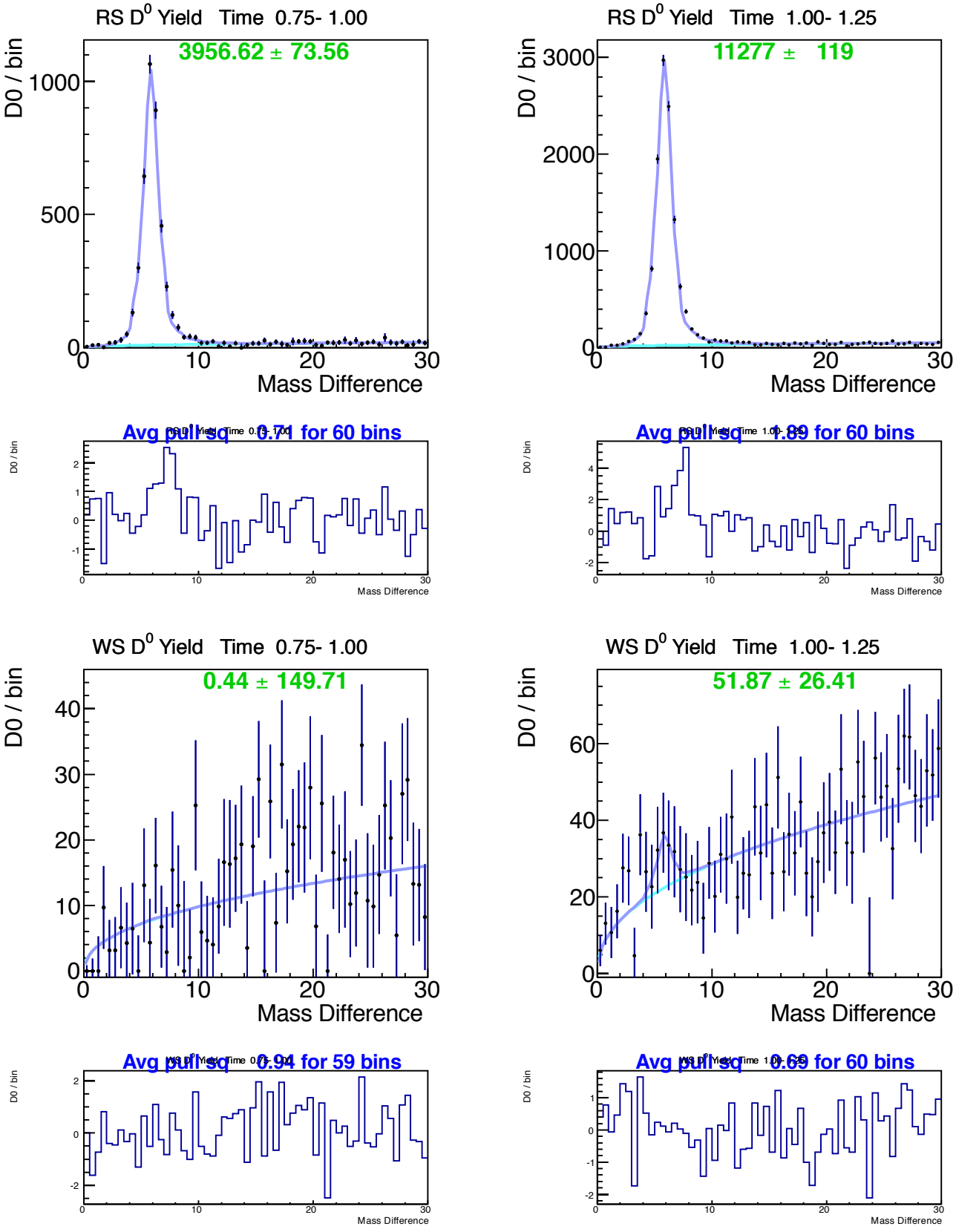

Appendix C: Δm Yield Fits $d_0 > 60\mu$m

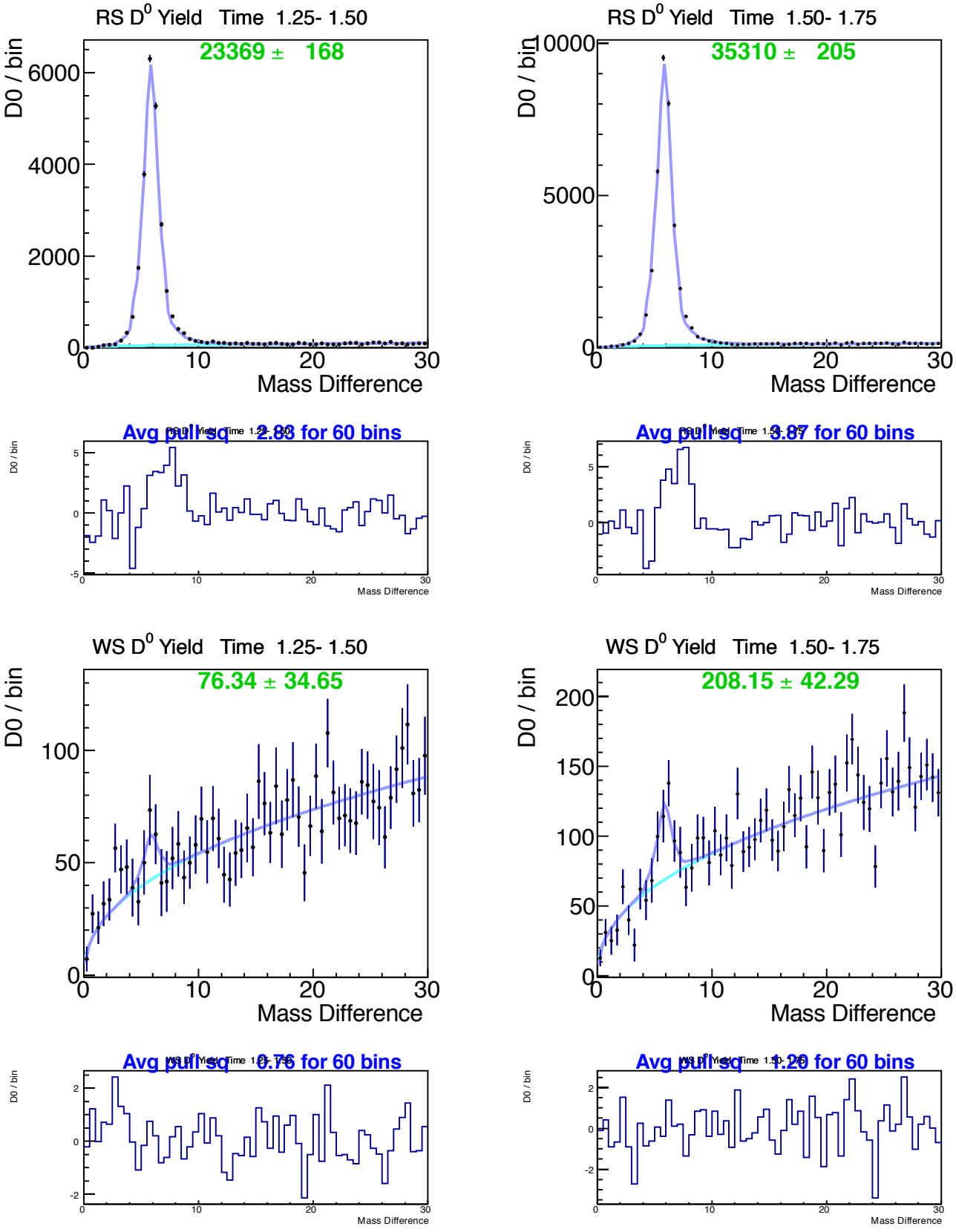

Appendix C: Δm Yield Fits $d_0 > 60\mu$m

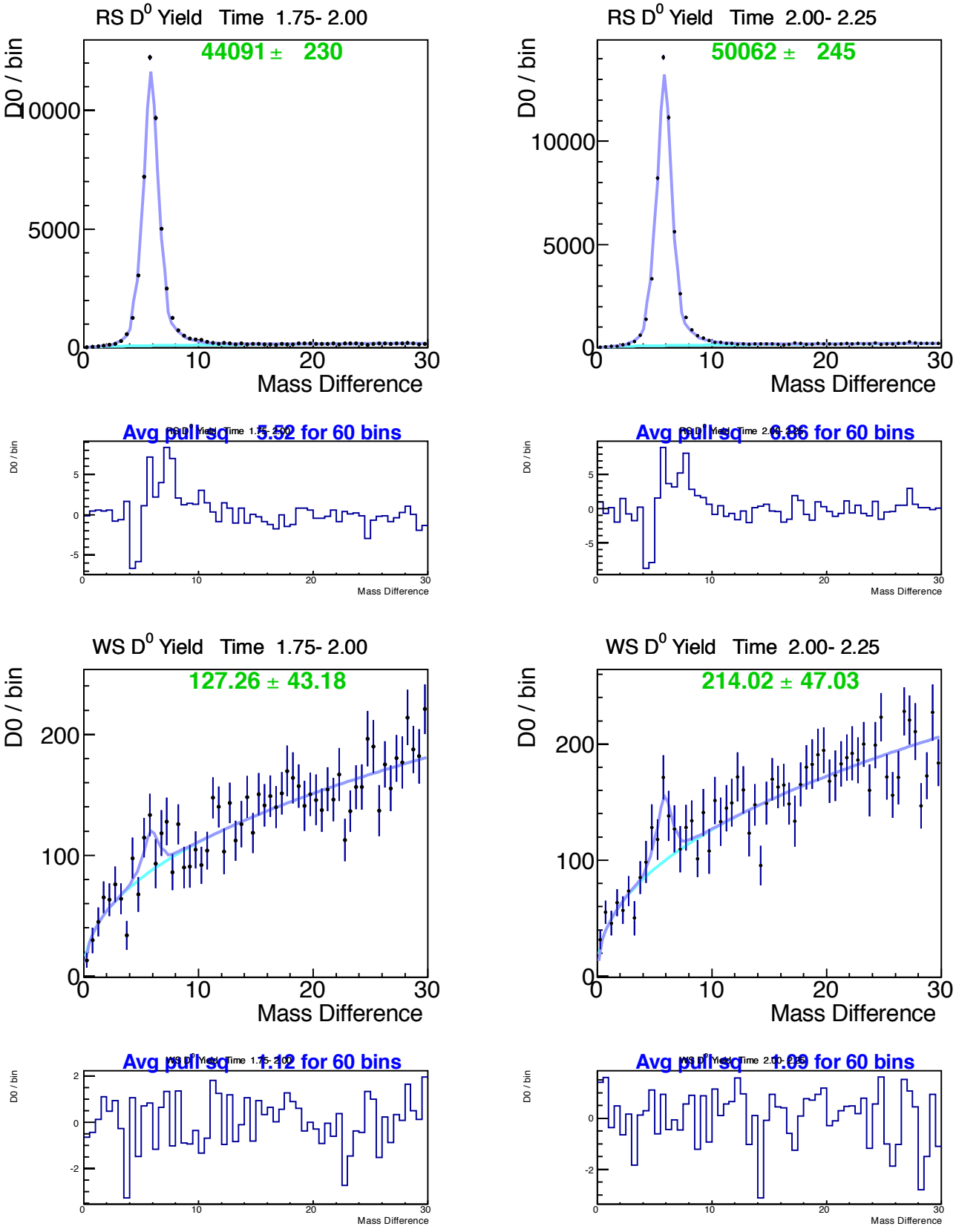

Appendix C: Δm Yield Fits $d_0 > 60\mu$m

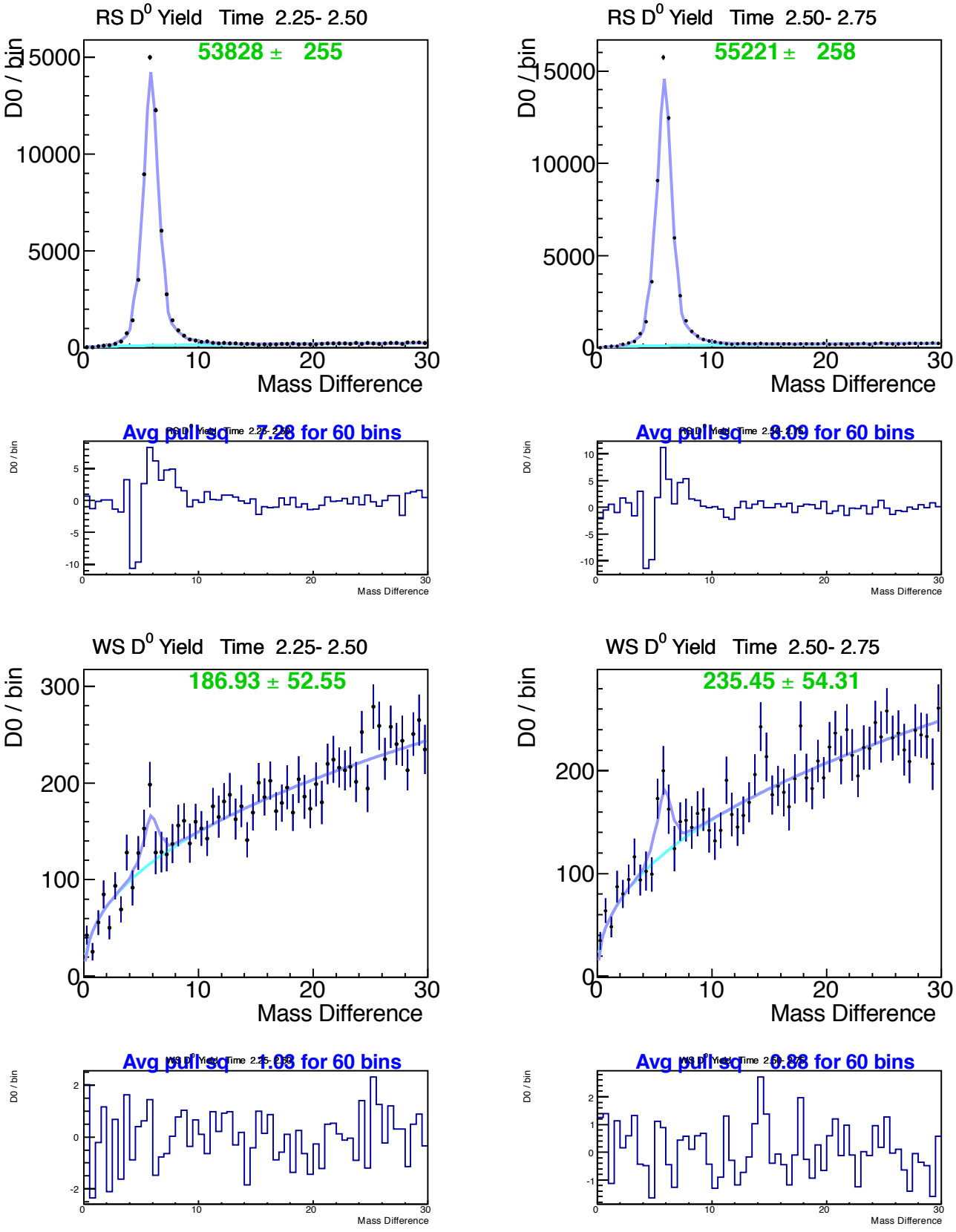

Appendix C: Δm Yield Fits $d_0 > 60\mu$m

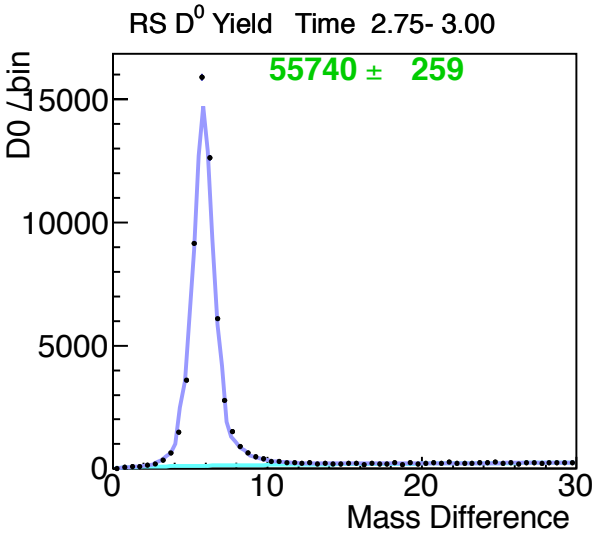

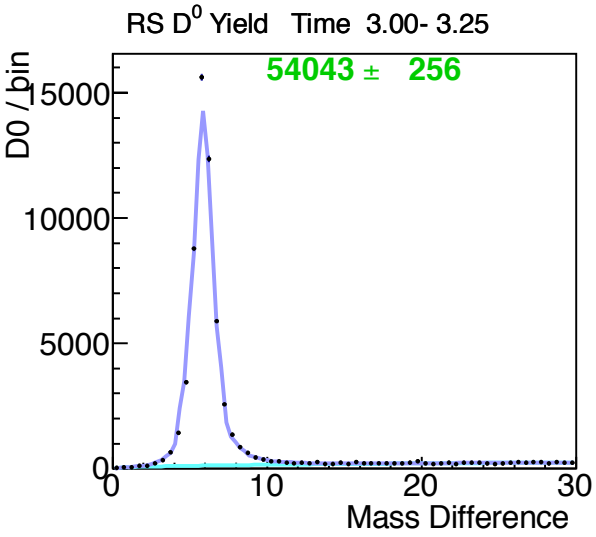

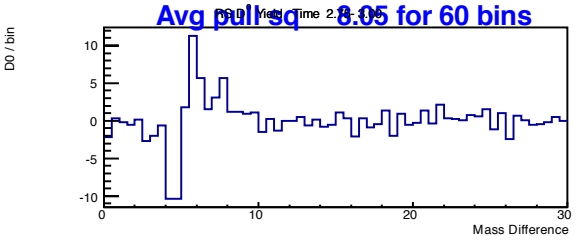

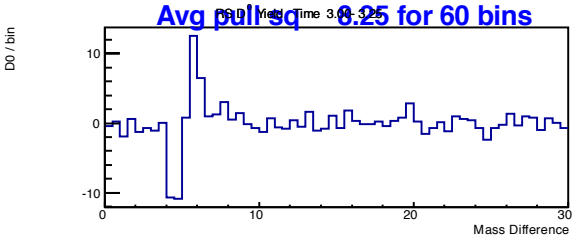

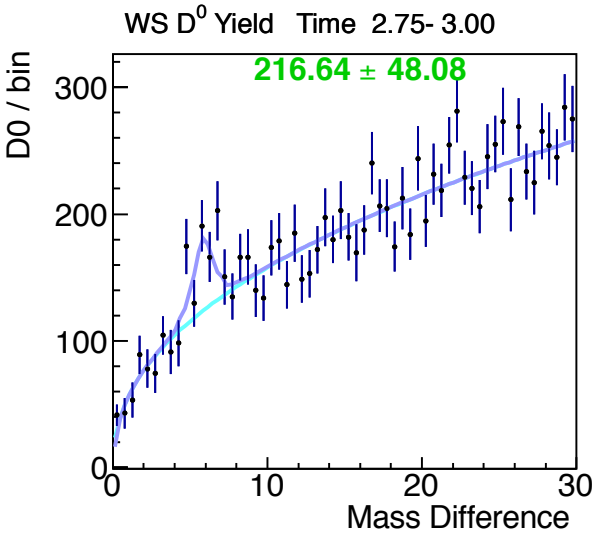

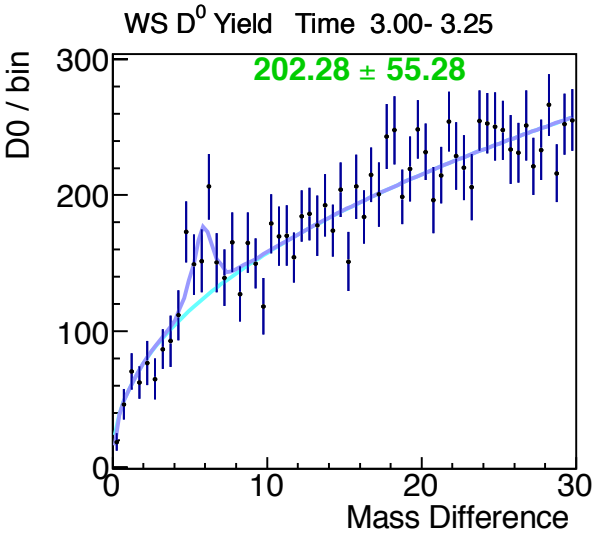

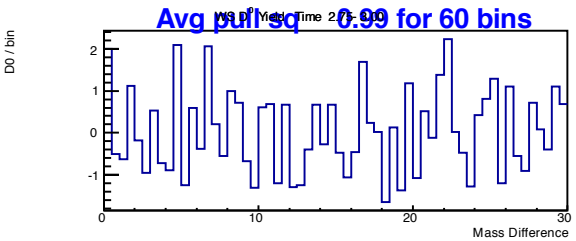

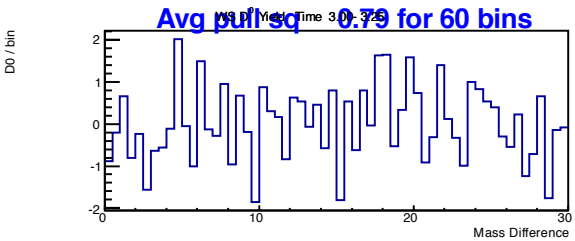

Appendix C: Δm Yield Fits $d_0 > 60\mu$m

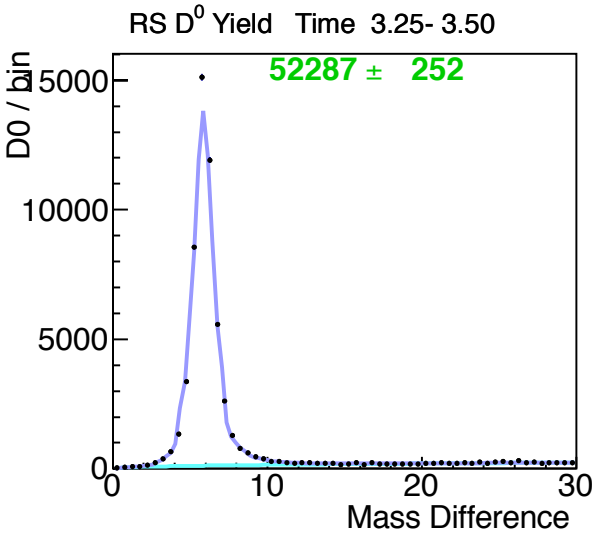

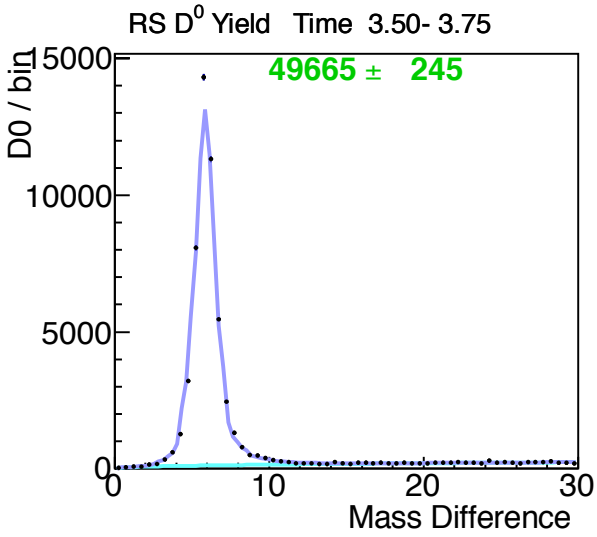

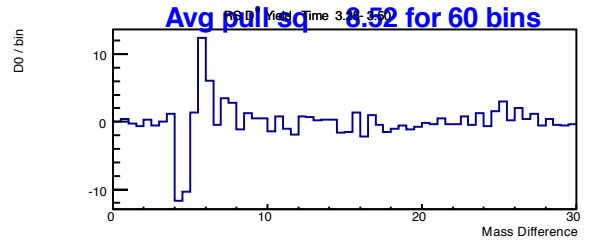

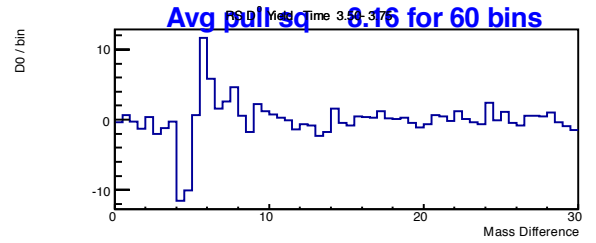

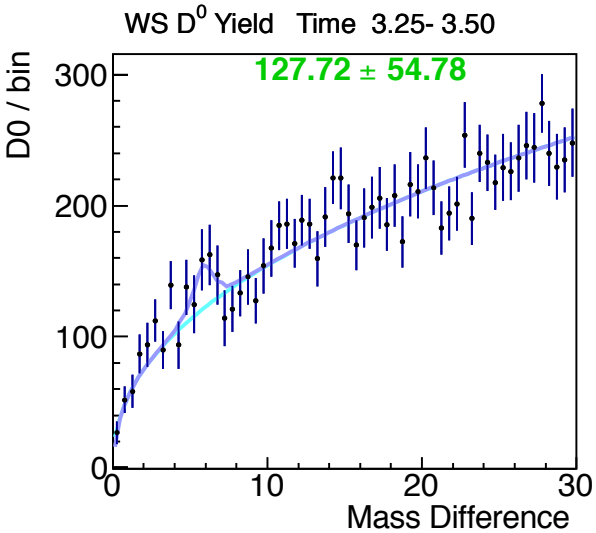

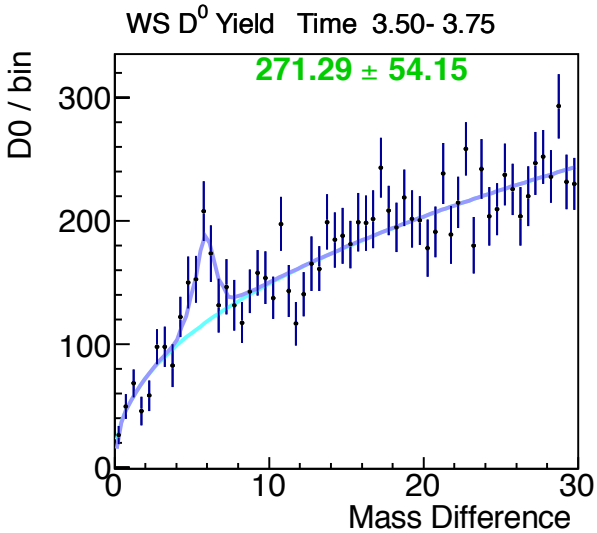

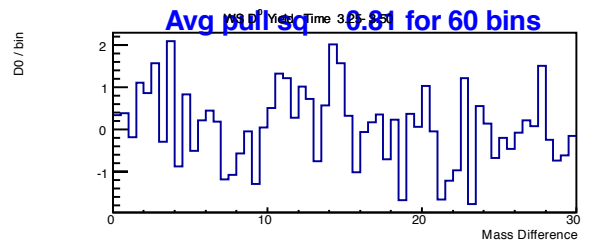

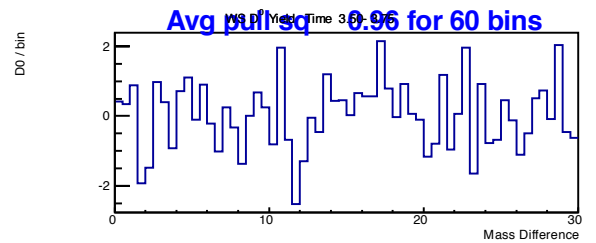

Appendix C: Δm Yield Fits $d_0 > 60\mu$m

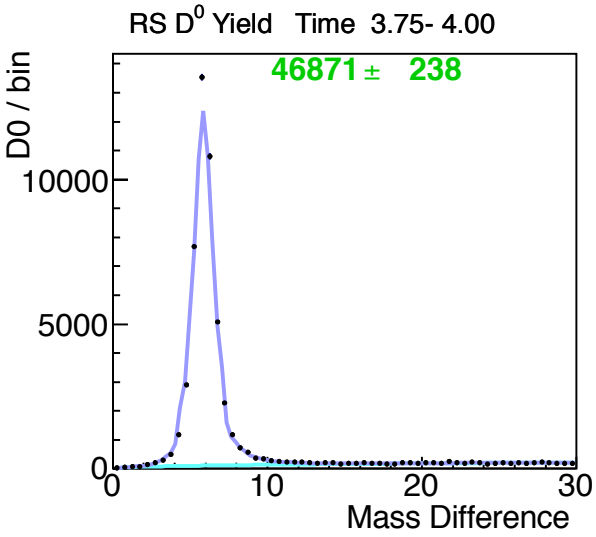

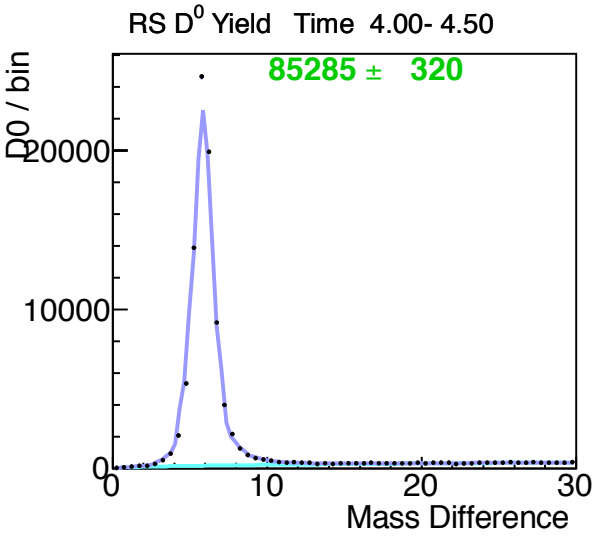

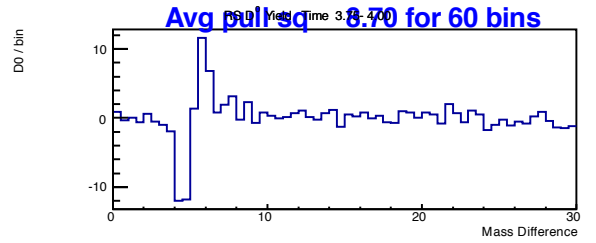

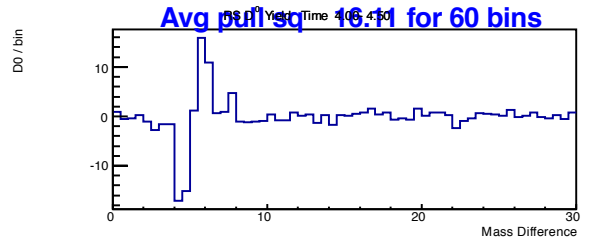

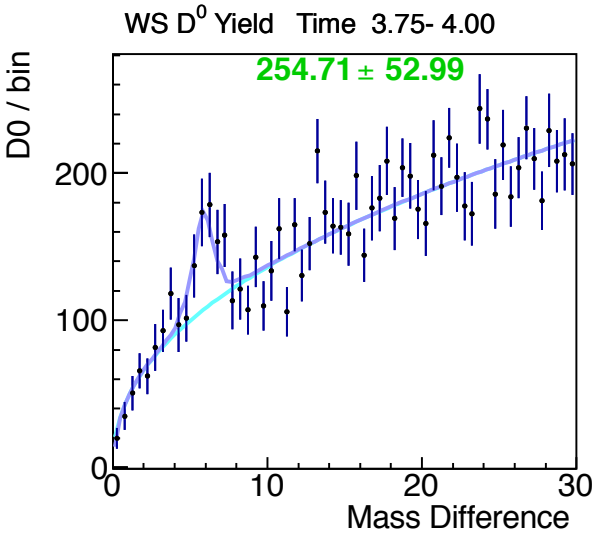

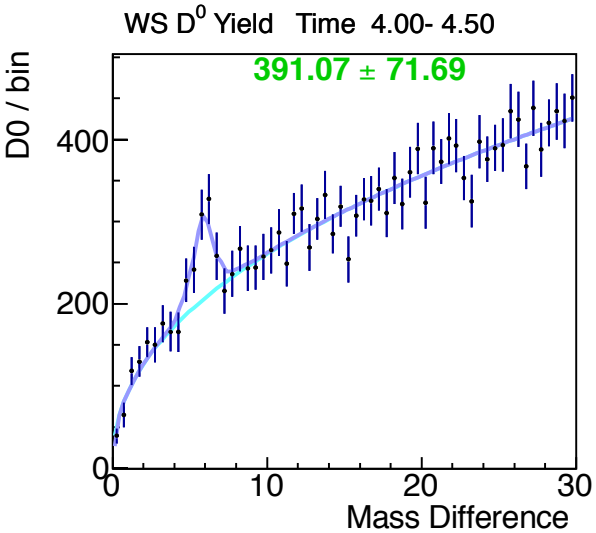

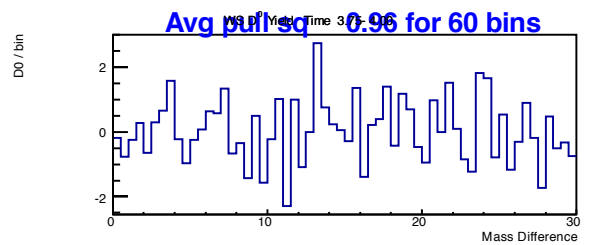

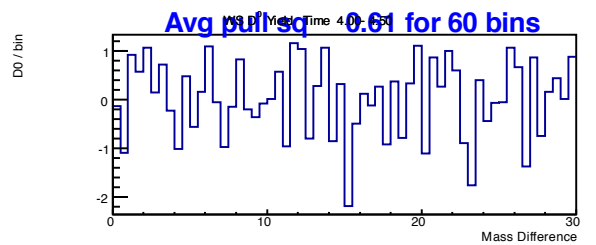

Appendix C: Δm Yield Fits $d_0 > 60\mu$m

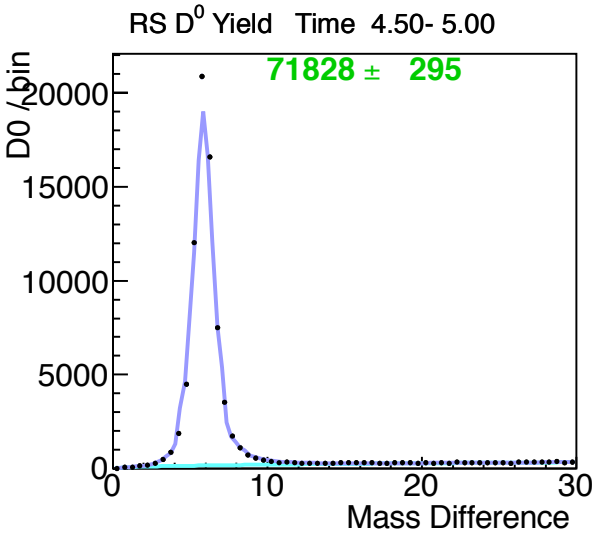

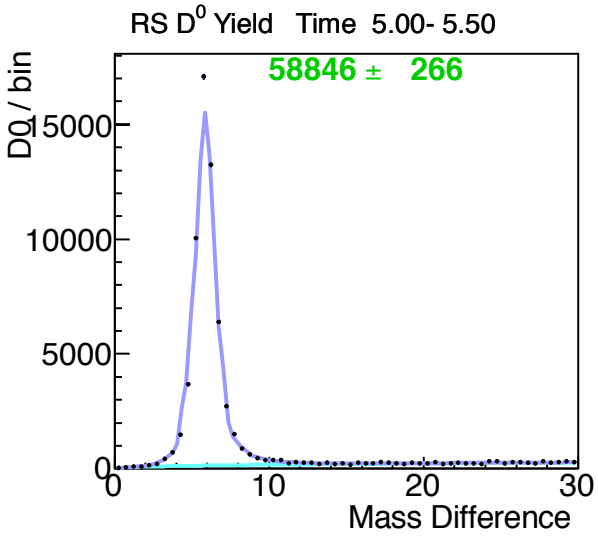

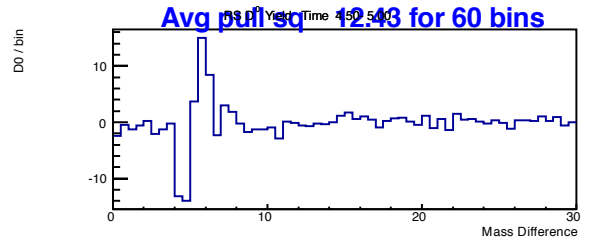

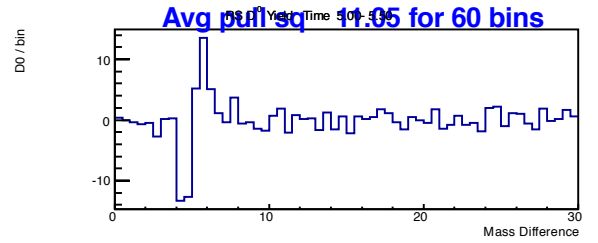

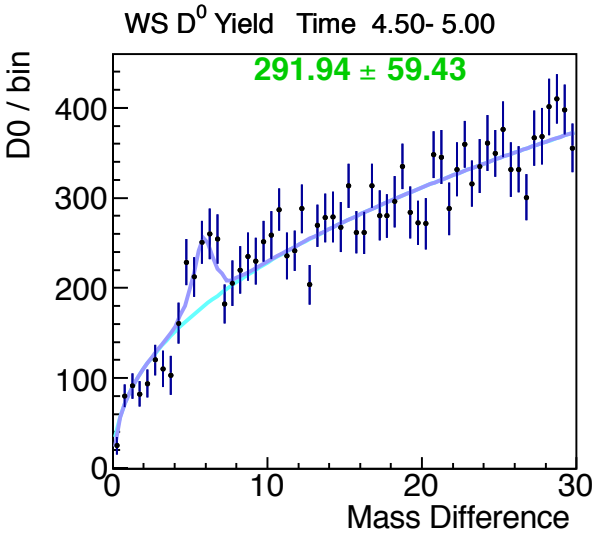

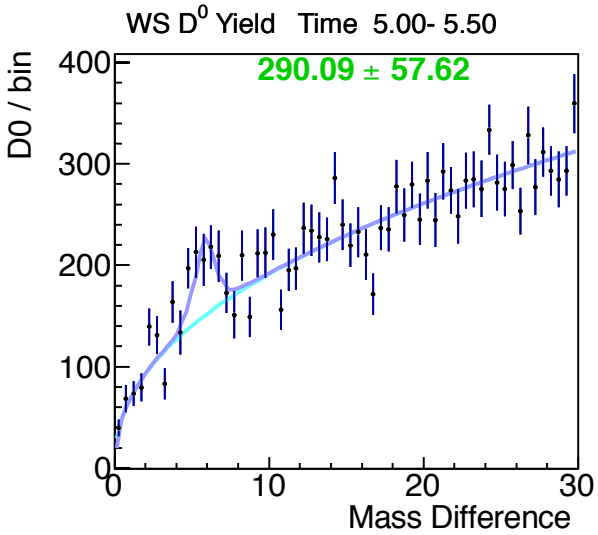

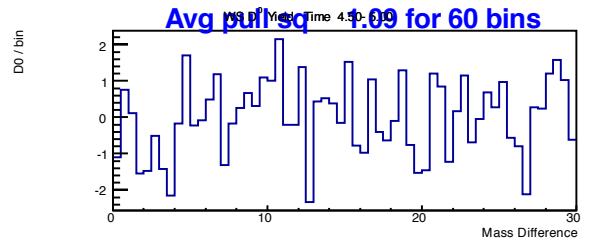

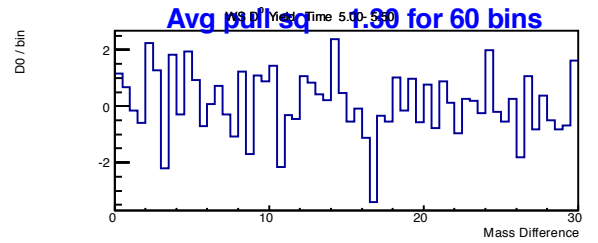

Appendix C: Δm Yield Fits $d_0 > 60\mu$m

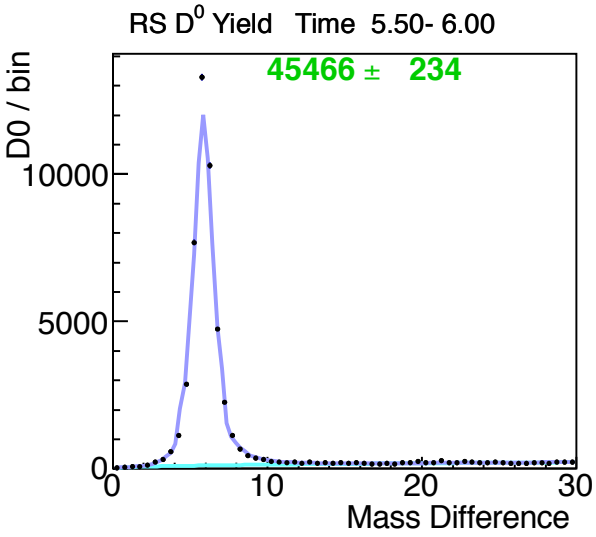

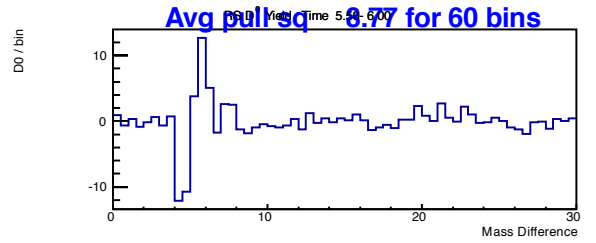

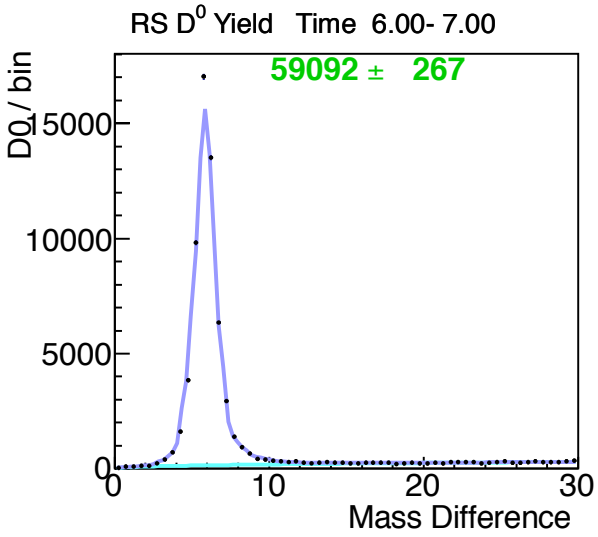

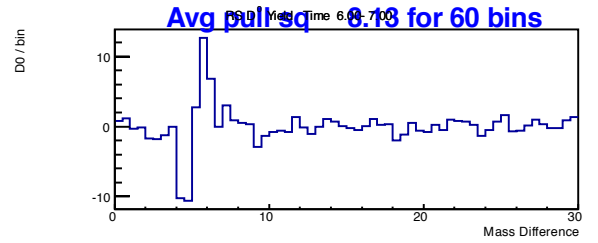

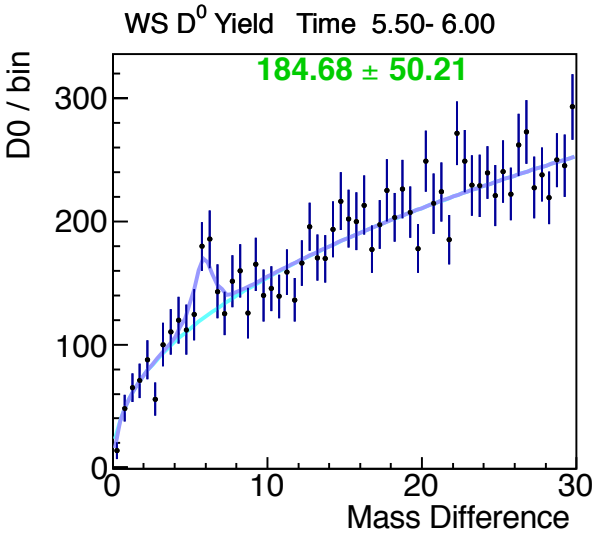

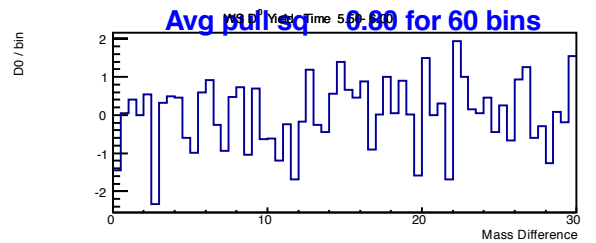

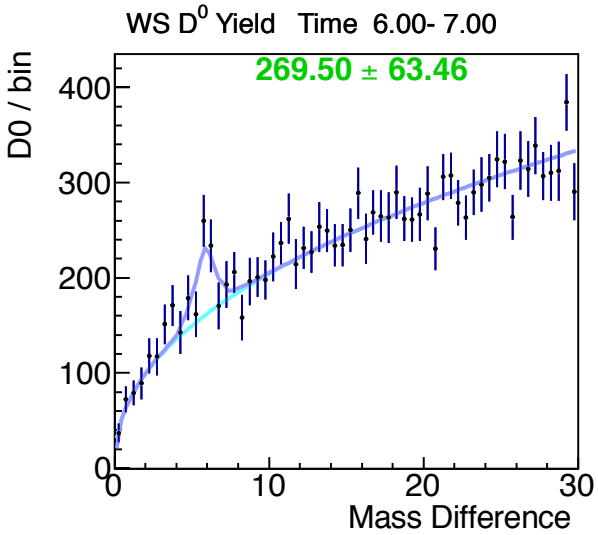

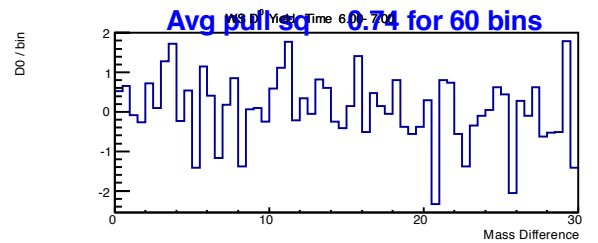

Appendix C: Δm Yield Fits $d_0 > 60\mu$m

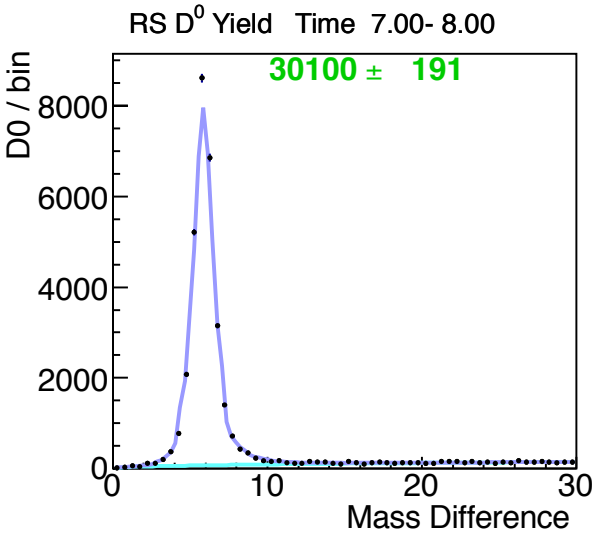

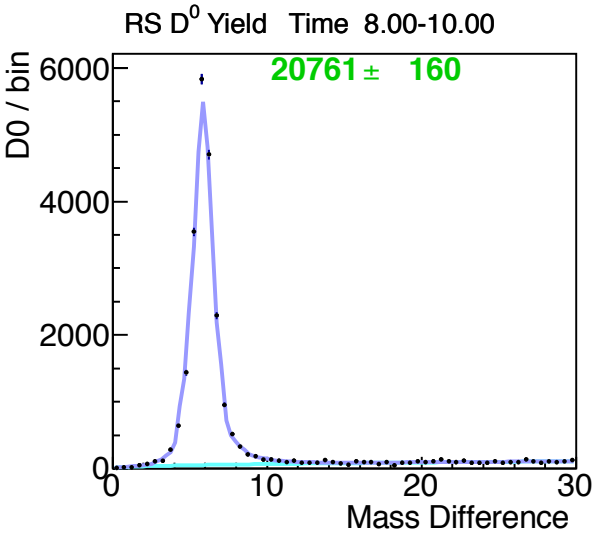

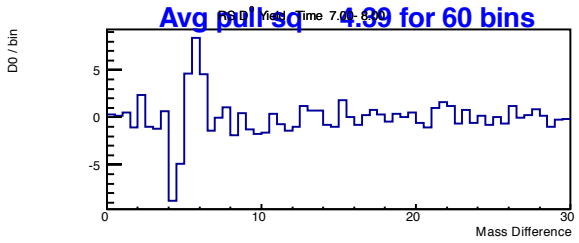

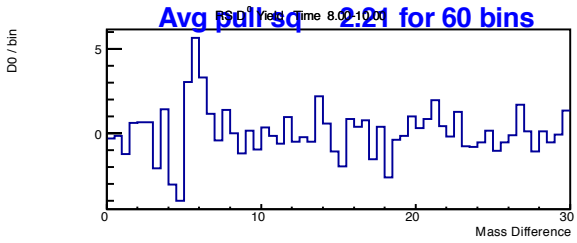

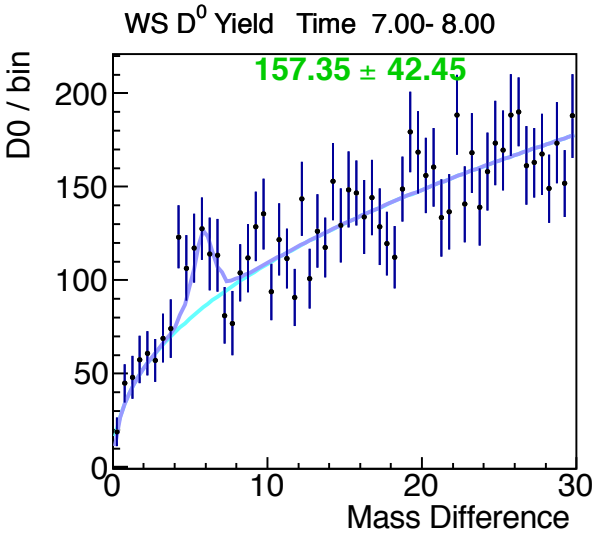

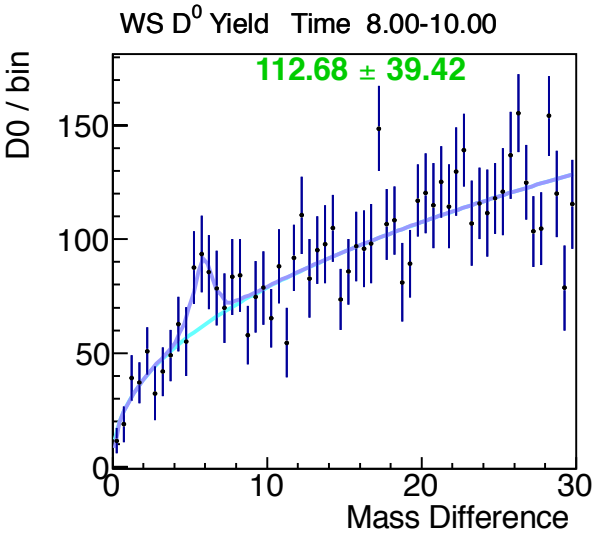

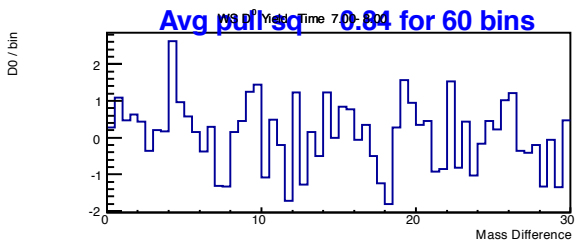

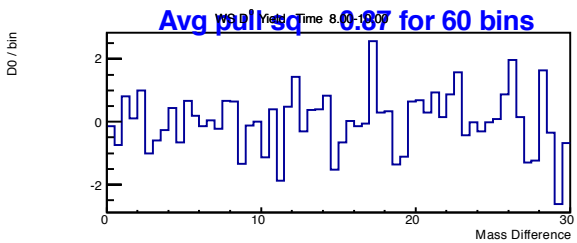

D Non-Prompt D^* Correction Details

This appendix shows the data fits for the time-binned $d0$ distributions We use RS D^* events, with $(K\pi)$ sideband-subtraction. The distribution for each time bin is fit with a double Gaussian for the prompt (signal) peak, and a double Gaussian for the non-prompt distribution. T Each plot covers the (unsigned) d_0 values from 0 to 500 microns.

The 16 time bin IP distributions were fit simultaneously, using the same prompt shape for all time bins. (The first and last two time bins were excluded, to have a simpler 83 parameter fit.) All parameters were floating. This fit is used to determine the prompt distribution shape.

After the prompt shape is determined, and the parameters fixed, all 20 time bin distributions are fit (one at a time), to determine the non-prompt shape. The non-prompt shape for each time bin is independent of the others, as are the amplitudes of the number of prompt and non-prompt D*. Those fits are shown over the next few pages. The blue curve is the non-prompt fit, the red curve is prompt plus non-prompt. For times less than 4 lifetimes, the fit range is limited, to avoid being biased by the low occupancy or empty bins.

After the fits are completed, we use the fit functions to calculate the fraction of the distributions that lies in two impact parameter regions: $|d_0| \leq 60\mu$m , and $0 < |d_0| \leq 500\mu$m. The amount of the prompt and non-prompt distributions in each IP region is summarized in Table 7. To estimate the uncertainty of those fractions, we vary the widths of the double Gaussian shape. The fits for the prompt and non-prompt shapes had uncertainties on the widths of the double Gaussian. We do four more sets of fits, fixing the shorter (longer) of the widths at its nominal value minus (plus) one sigma, and allowing the other parameters to float. The fraction of the new shape with $|d_0| \leq 60\mu$m is calculated, and compared to the nominal values. We use the second largest (absolute value) difference of the four as the uncertainty.

Appendix D: RS d_0 Distributions By Decay Time

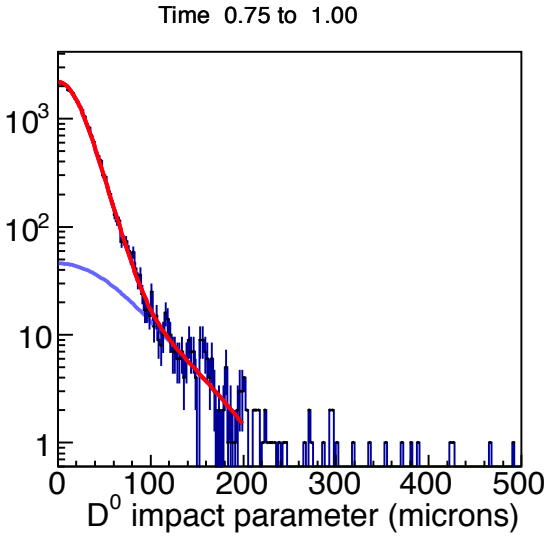

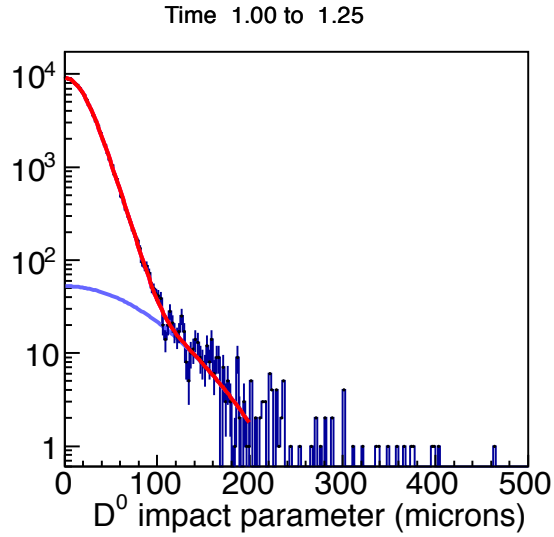

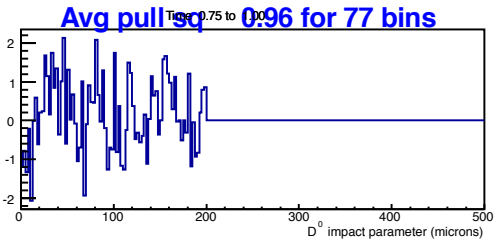

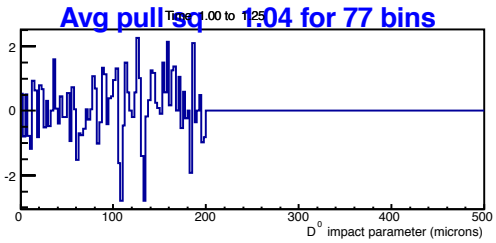

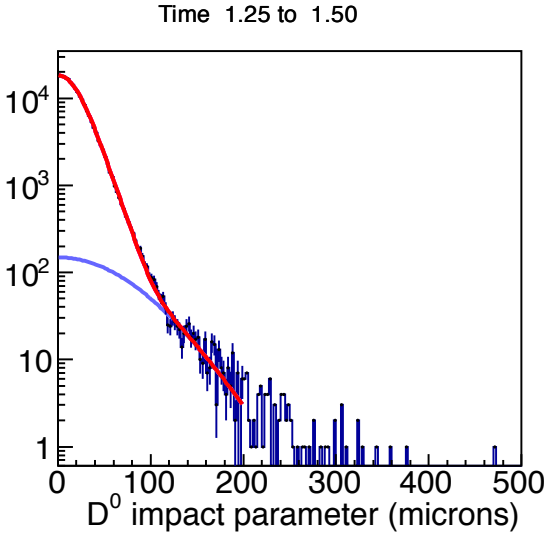

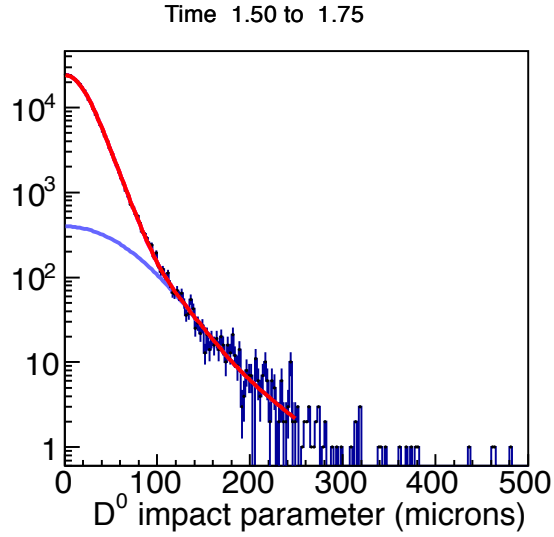

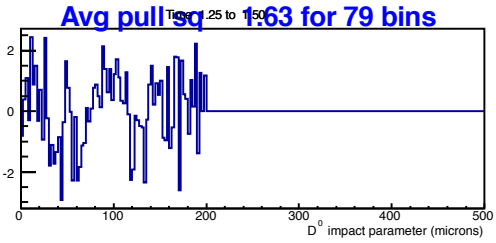

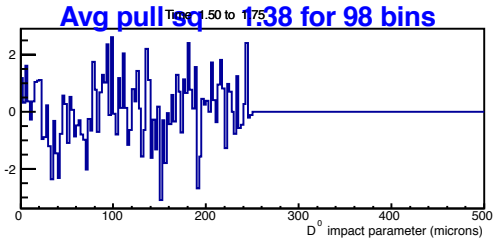

Appendix D: RS d_0 Distributions By Decay Time

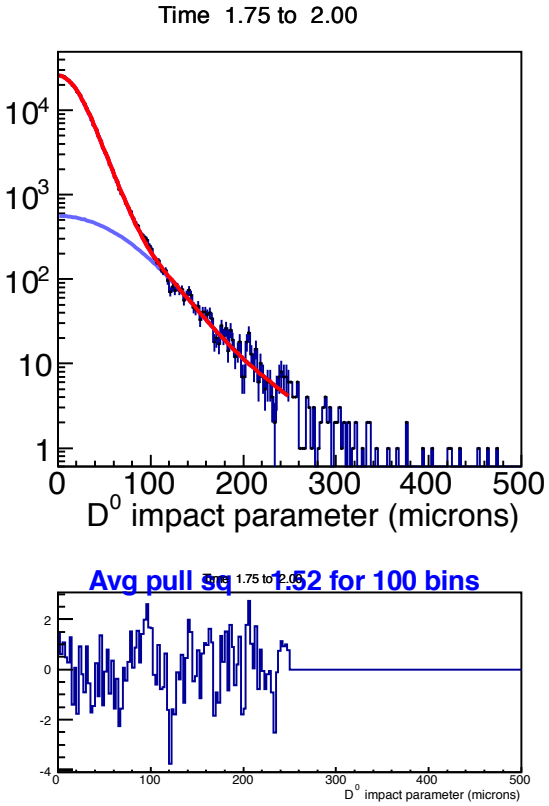

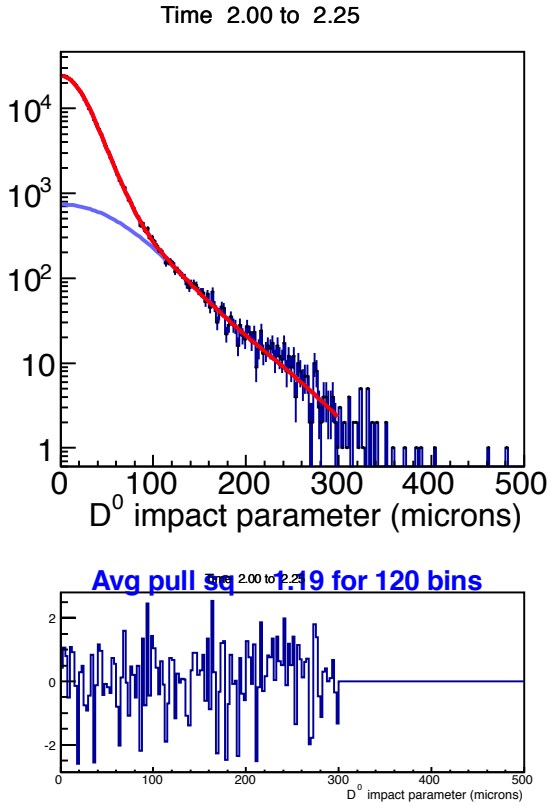

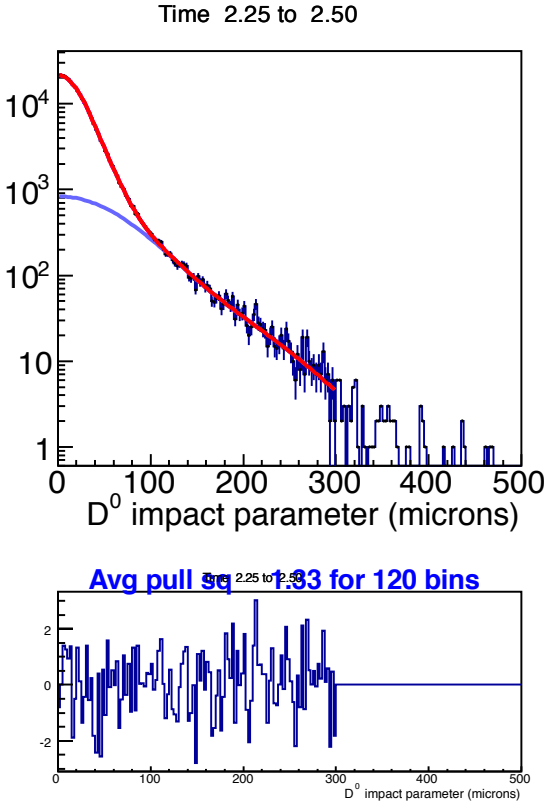

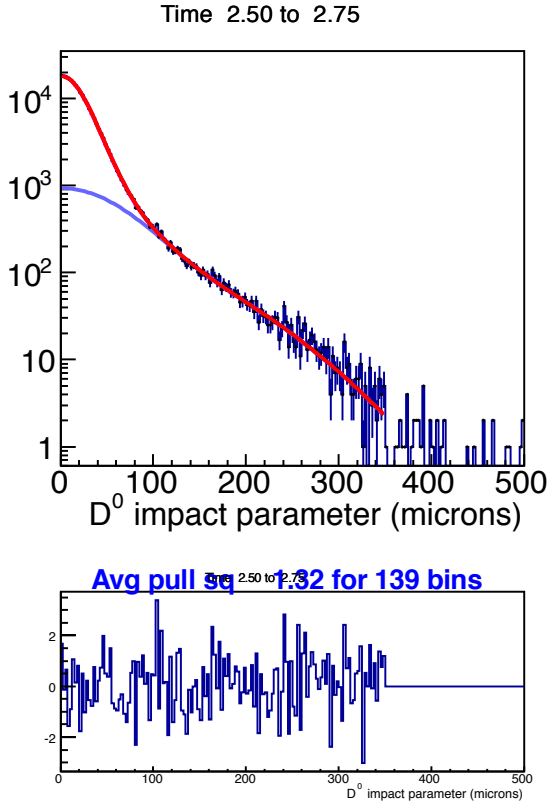

Appendix D: RS d_0 Distributions By Decay Time

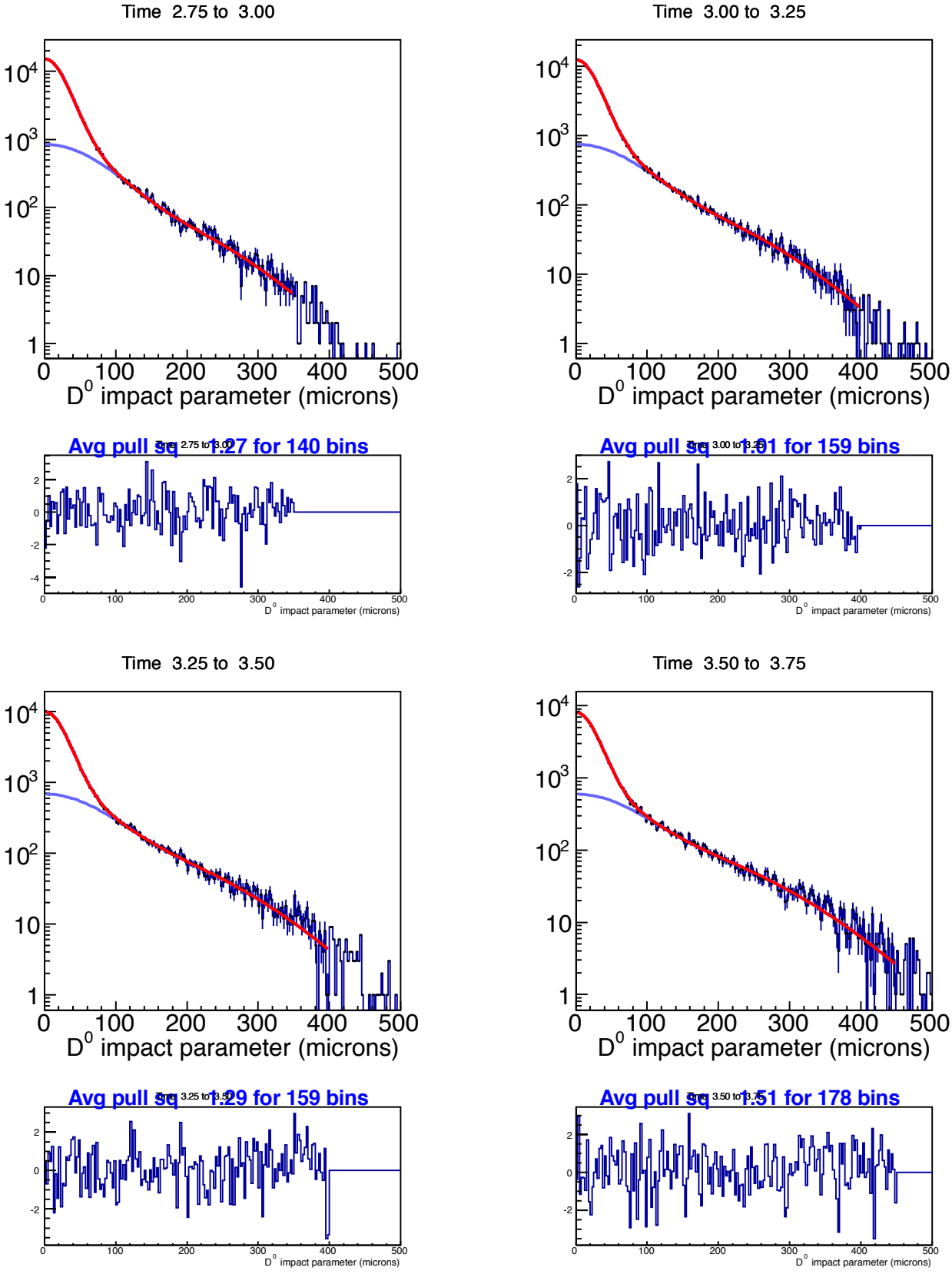

Appendix D: RS d_0 Distributions By Decay Time

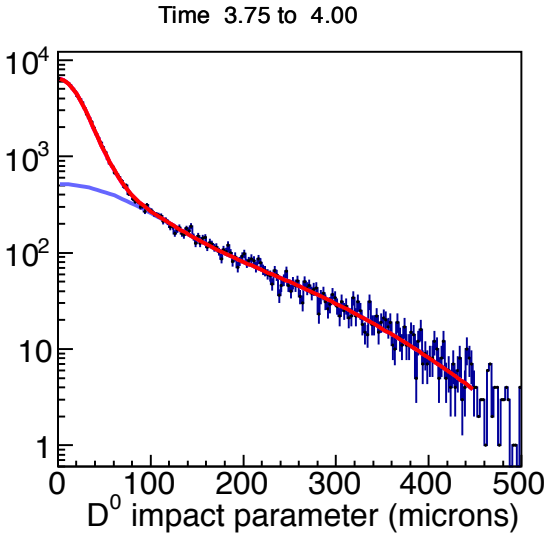

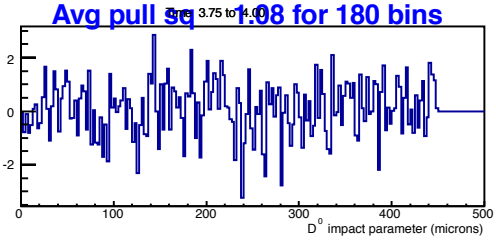

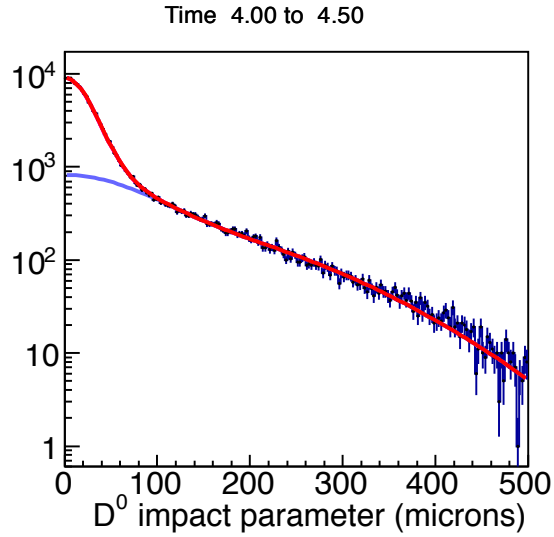

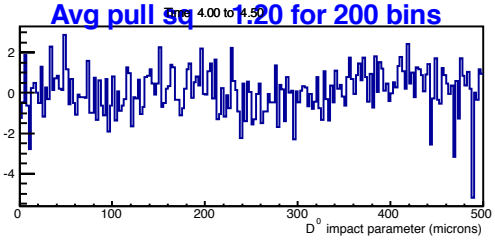

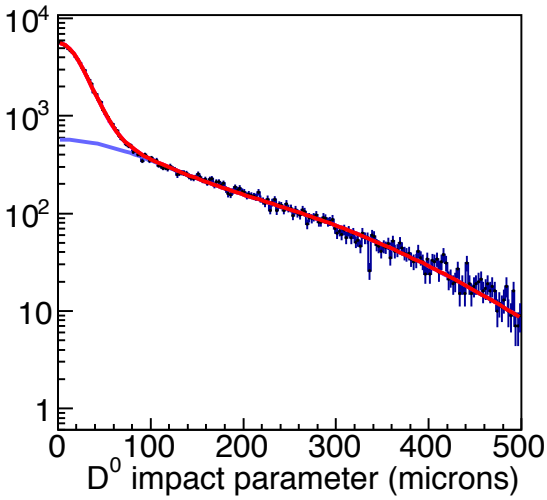

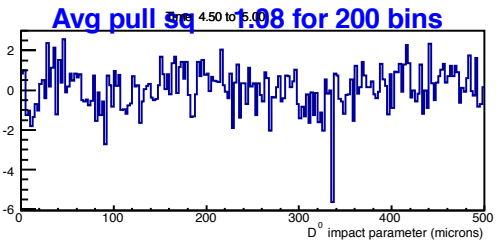

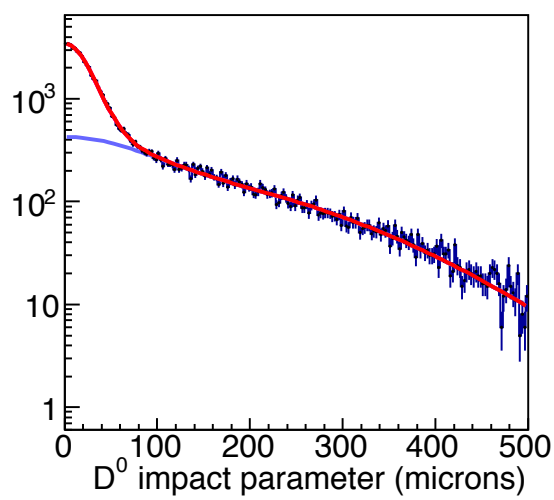

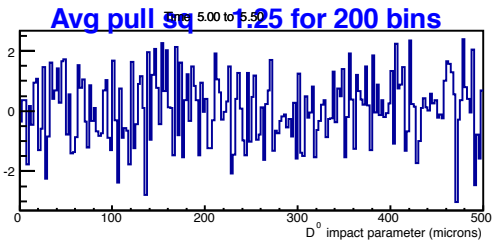

Appendix D: RS d_0 Distributions By Decay Time

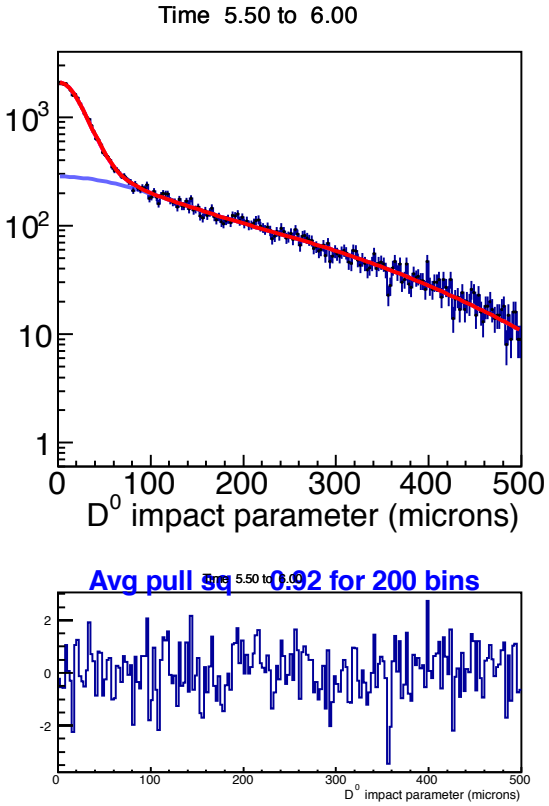

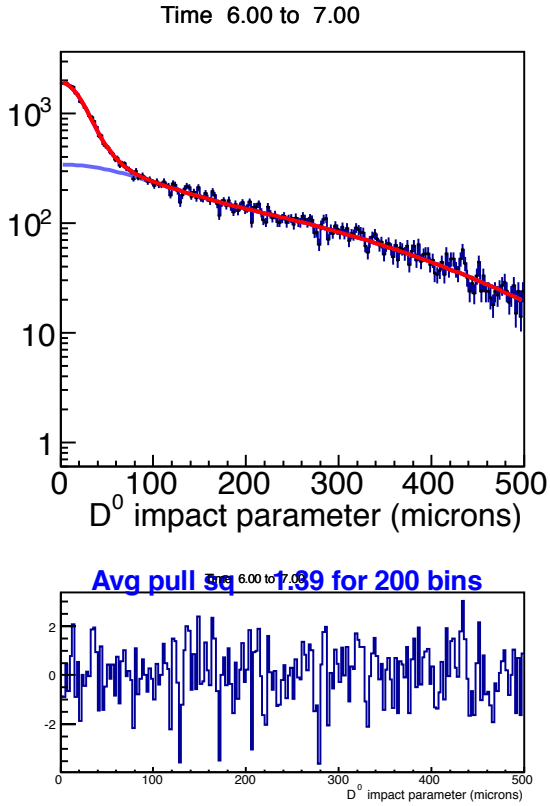

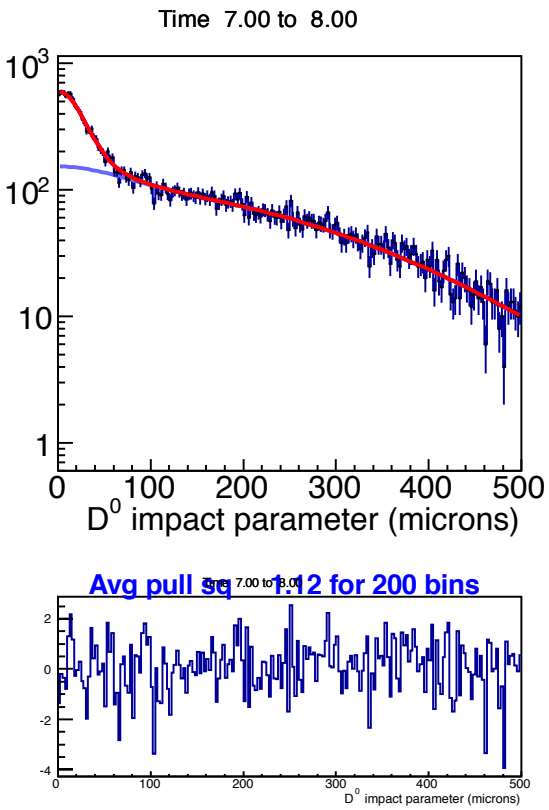

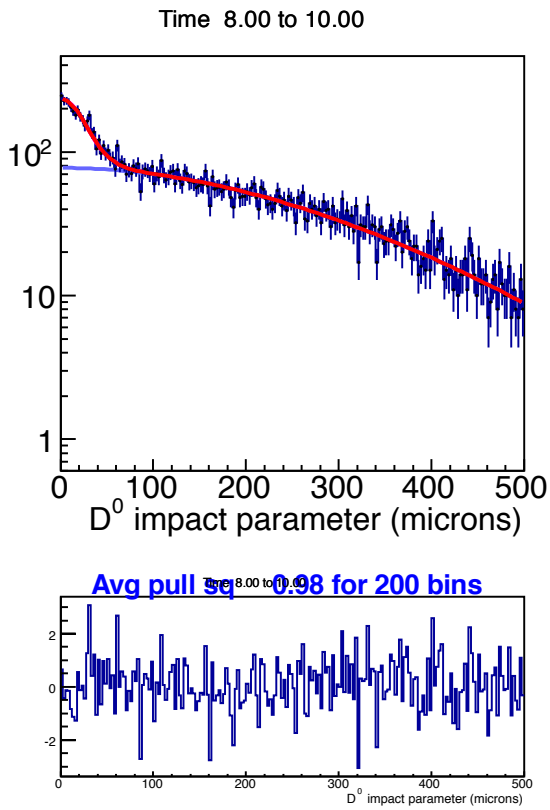

Time Bin	Fraction In (f_i)	σ_{f_i}
prompt distribution	0.9735	0.0007
0.75 - 1.00	0.6365	0.0293
1.00 - 1.25	0.5151	0.0625
1.25 - 1.50	0.5541	0.0114
1.50 - 1.75	0.6190	0.0062
1.75 - 2.00	0.6036	0.0071
2.00 - 2.25	0.5968	0.0051
2.25 - 2.50	0.5840	0.0047
2.50 - 2.75	0.5793	0.0045
2.75 - 3.00	0.5408	0.0047
3.00 - 3.25	0.5053	0.0046
3.25 - 3.50	0.4852	0.0045
3.50 - 3.75	0.4583	0.0046
3.75 - 4.00	0.4352	0.0047
4.00 - 4.50	0.3964	0.0033
4.50 - 5.00	0.3475	0.0042
5.00 - 5.50	0.3263	0.0041
5.50 - 6.00	0.2972	0.0037
6.00 - 7.00	0.2835	0.0028
7.00 - 8.00	0.2645	0.0020
8.00 - 10.0	0.2136	0.0095

Table 7: Prompt and non-prompt distribution fractions. f_i is the fraction of the distribution with $|d_0| \leq 60\mu$m, normalized to the events with $|d_0| \leq 500\mu$m. σ_{f_i} is the uncertainty on f_i.

References

[1] Mark Mattson and Paul Karchin, *Analysis of $D^0 - \bar{D}^0$ Mixing in the $K\pi$ Channel*, CDF-Note 7116, 2006.

[2] CDF Collaboration, A. Abulencia *et al.*, *Measurement of the Ratio of Branching Fractions $\mathcal{B}(D^0 \to K^+\pi^-)/\mathcal{B}(D^0 \to K^-\pi^+)$ using the CDF II Detector*, Phys. Rev. D **74**, 031109 (R) (2006).

[3] Mark Mattson, Paul Karchin, and Nagesh Kulkarni, *Time Dependent Analysis of $D^0 - \bar{D}^0$ Mixing*, CDF-Note 8879, 2007.

[4] CDF Collaboration, T. Aaltonen *et al.*, *Evidence for D0-D0bar Mixing Using the CDF II Detector*, Phys. Rev. Lett. **100**, 121802 (2008).

[5] Nagesh Kulkarni, Paul Karchin, and Mark Mattson, *Analysis of $D^0 - \bar{D}^0$ Mixing Using the CDF II Detector*, CDF-Note 9806, 2009.

[6] BaBar Collaboration, B. Aubert *et al.*, *Search for $D^0 - \overline{D}^0$ Mixing and a Measurement of the Doubly Cabibbo-suppressed Decay Rate in $D^0 \to K\pi$ Decays*, Phys. Rev. Lett. **91**, 171801 (2003), hep-ex/0304007.

[7] Marko Starič, *Search for $D^0 - \overline{D}^0$ mixing at Belle and BaBar*, talk at XLII Rencontres de Moriond, La Thuile, Italy (13 March, 2007).

[8] BaBar Collaboration, Kevin Flood, *Evidence for $D^0 - \overline{D}^0$ Mixing*, talk at XLII Rencontres de Moriond, La Thuile, Italy (13 March, 2007).

[9] Belle Collaboration, M. Starič *et al.*, *Evidence for $D^0 - \overline{D}^0$ Mixing*, Phys. Rev. Lett. **98**, 211803 (2007).

[10] BaBar Collaboration, B. Aubert *et al.*, *Evidence for $D^0 - \overline{D}^0$ Mixing*, Phys. Rev. Lett. **98**, 211802 (2007).

[11] Belle Collaboration, K. Abe *et al.*, *Measurement of $D^0 - \overline{D}^0$ mixing in $D^0 \to K^0_s\pi^+\pi^-$ decays*, arXiv:0704.1000v1 (7 April, 2007).

[12] BABAR, B. Aubert et al., *Measurement of $D^0 - \bar{D}^0$ mixing from a time- dependent amplitude analysis of $D^0 \to K^+\pi^-\pi^0$ decays*, (2008), 0807.4544.

[13] CLEO, R. Godang et al., *Search for $D^0 - \bar{D}^0$ Mixing*, Phys. Rev. Lett. **84**, 5038 (2000), hep-ex/0001060.

[14] FOCUS, J. M. Link et al., *Measurement of the branching ratio of the decay D0 –¿ pi- mu+ nu relative to D0 –¿ K- mu+ nu*, Phys. Lett. **B607**, 51 (2005), hep-ex/0410068.

[15] Heavy Flavor Averaging Group, E. Barberio et al., *Averages of b−hadron and c−hadron Properties at the End of 2007*, (2008), 0808.1297.

[16] F. Ruffini M. Morello, G. Punzi, *Measurement of Direct CP Violating Asymmetries in Charmless Decays of Strange Bottom Mesons and Bottom Baryons with 9.3 fb-1.*, CDF-Note 10726, 2012.

[17] http://www cdf.fnal.gov/htbin/twiki/bin/view/BStntuples/WebHome.

[18] Shin-Shan. Yu et al., *COT dE/dx Measurement and Corrections*, CDF-Note 6361, 2003.

[19] Saverio D'Auria et al., *Track-based calibration of the COT specific ionization*, CDF-Note 6932, 2004.

[20] CDF Statistics Committee Craig Blocker, *Uncertainties on Efficiencies*, CDF-Note 7168, 2004.

[21] Chen, Oldeman, and Kroll, *A Method to Measure the Direct and Secondary Charm Fraction in Two Track Data*, CDF-Note 5996, 2002.

[22] http://www cdf.fnal.gov/physics/statistics/statistics_recommendations.html, in particular, 'What is Systematics' by Giovanni Punzi, and 'Systematic Uncertainties' by Craig Blocker.

[23] S. Donati et al., *Measurement of branching fractions and direct CP asymmetries of B0(s) to h+h'- decays in 1/fb*, CDF-Note 8464, 2008.

[24] S. D'Auria et al., *Relative Branching Fractions and CP-violating Decay Rate Asymmetries in Cabibbo Suppressed Decays of the D^0 Meson*, CDF-Note 6391, 2004.